FUNCTIONAL CHARACTERIZATION OF BARDET-BIEDL SYNDROME PROTEINS

by

Junchul Kim
B.Sc., Yonsei University, 1996
M.Sc. Yonsei University, 1998

THESIS SUBMITTED IN PARTIAL FULFILLMENT OF
THE REQUIREMENTS FOR THE DEGREE OF

DOCTOR OF PHILOSOPHY

In the Department of
Molecular Biology and Biochemistry

SIMON FRASER UNIVERSITY

Summer 2005

APPROVAL

Name: **Junchul Kim**

Degree: **Doctor of Philosophy**

Title of Thesis: **Functional characterization of Bardet-Biedl syndrome proteins**

Examining Committee:

Chair: **Dr. Jenifer Thewalt**
Associate Professor, Department of Molecular Biology and Biochemistry/Physics

---

Dr. Michel R. Leroux
Senior Supervisor
Assistant Professor, Department of Molecular Biology and Biochemistry

---

Dr. Rosemary B. Cornell
Supervisor
Professor, Department of Molecular Biology and Biochemistry/Chemistry

---

Dr. Nicholas Harden
Supervisor
Associate Professor, Department of Molecular Biology and Biochemistry

---

Dr. Lynne Quarmby
Internal Examiner
Associate Professor, Department of Molecular Biology and Biochemistry

---

Dr. Jerome Rattner
External Examiner
Professor, Department of Cell Biology & Anatomy, University of Calgary

Date Approved: **July 5th, 2005**

SIMON FRASER UNIVERSITY

PARTIAL COPYRIGHT LICENCE

ABSTRACT

Bardet-Biedl syndrome (BBS) is a heterogeneous disorder characterized by complex symptoms, including retinitis pigmentosa, polydactyly, hypogonadism, renal anomaly, obesity, and diabetic mellitus. Despite the rare nature of the disease, BBS has been a subject of interest because patients manifest conditions that are commonly encountered in the general population, such as renal anomaly, obesity and diabetes. At least eight genes (*BBS1-8*) are known to be linked to the syndrome, and all have been cloned. Because mutations in any *BBS* gene give rise to a common set of symptoms that cannot distinguish which gene is affected, it has been hypothesized that all BBS proteins participate in the same cellular process. Recent studies with *C. elegans* showed that *BBS* genes are expressed exclusively in neuronal cells containing cilia but not in non-ciliated cells, suggesting that cellular activities related to ciliogenesis may be the underlying pathogenic mechanism of BBS. The regulation of the *C. elegans BBS* genes by a ciliogenic RFX-type transcription factor, DAF-19, further provides evidence that the *BBS* genes are involved in cilia biogenesis and/or function.

Here we show that two BBS proteins, BBS4 and BBS6, localize to the centrosome, an organelle involved in diverse cellular activities including cell division, microtubule organization, intracellular transport, and ciliogenesis. BBS4 localizes to the centriolar satellites of centrosomes and basal bodies (modified centrioles) of primary cilia. It interacts with p150Glued subunit of the dynein motor complex, and the silencing of the gene causes the mislocalization of a centrosomal protein, PCM1 suggesting that

BBS4 may function as an adaptor protein connecting the dynein motor complex and its protein cargo.

BBS6 localizes to the pericentriolar material (PCM), a proteinaceous tube structure surrounding centrosomes, and *BBS6* silencing leads to multi-nucleated and multi-centrosomal cells with defects in cytokinesis, a process that requires the transport of endosomal vesicles to the midbody. Both BBS4 and BBS6 are expressed exclusively within ciliated tissues in mice, suggesting that BBS proteins function in intracellular transport as well as intraflagellar transport in ciliated cells, and that the dysfunction of these ciliated cells during development likely gives rise to specific and pleiotropic symptoms in BBS patients.

DEDICATION

이 논문이 있기까지 힘든 과정속에서도 묵묵히 지원해준 가족과 부모님들께 이 논문을 바칩니다. 그 분들이 없었더라면 지금 이 노력의 결과는 가능하지 않았을것입니다. 제가 도움받은것 만큼 모든 분들께 앞으로 도움이 되는 삶을 살 수 있기를 기원합니다. 모두들 건강하세요.

To my family

ACKNOWLEDGEMENTS

It has been a great privilege for me to know and work with Dr. Michel Leroux and to be his first Ph.D student. I cannot thank enough for the encouragement, support, and openmindness that he showed. I would also like to express my sincere appreciation to my colleagues in Leroux lab and my supervisory committee members: Dr. Rosemary Cornell, Dr. Nick Harden for all the helpful comments and suggestions.

TABLE OF CONTENTS

LIST OF FIGURES

LIST OF TABLES

CHAPTER 1
GENERAL INTRODUCTION AND RESEARCH OBJECTIVES

1.1 History of Bardet-Biedl syndrome

In 1866, two ophthalmologists named John Z. Laurence (1829-1870) and Robert Moon (1844-1914) reported a case about a family with multiple symptoms, including retinitis pigmentosa, short stature, lack of intelligence, and hypogenitalism in males. Several years later in 1922, without knowing the finding of Laurence and Moon, George Bardet and Artur Biedl independently published their research about an illness characterized by polydactyly, obesity, and retinitis pigmentosa. In 1925, Solis-Cohen and Weiss rediscovered the paper by Laurence & Moon and concluded that the condition was the same as what George Bardet and Artur Biedl described. From that point on, the condition was named Laurence-Moon-Bardet-Biedl syndrome (LMBBS).

However, LMBBS was often split into the Laurence Moon syndrome (LMS) and Bardet Biedl syndromes (BBS) based on the slight differences in symptoms such as spastic paraplegia, polydactyly and obesity. Laurence-Moon syndrome (LMS) is characterised by retinitis pigmentosa, mental retardation, hypogenitalism and spastic paraplegia, but not obesity and polydactyly, whereas Bardet-Biedl syndrome (BBS) mainly features retinitis pigmentosa, obesity, postaxial polydactyly, mental retardation and hypogenitalism, but not paraplegia. Bardet Biedl syndrome is now the preferred term

amongst the medical and scientific community since it represents by far the majority of published cases, although the existence of two distinct syndromes is possible.

1.2 Prevalence of Bardet-Biedl syndrome

BBS is a rare genetic disease that occurs throughout the world with varying frequencies. Its population prevalence in North America and Europe ranges from 1:140,000 to 1:160,000 every live birth (Beales et al., 1997; Croft et al., 1995; Klein and Ammann, 1969). However, in genetically isolated populations such as in the Bedouin of Kuwait and in Newfoundland of Canada, estimated incidences (1: 13,500 and 1: 17,500, respectively) are ten times higher than in North American and Europe, likely due to a founder effect (Farag and Teebi, 1989; Green et al., 1989; O'Dea et al., 1996).

1.3 Clinical features of Bardet-Biedl syndrome

Generally, the diagnosis of BBS is first considered when a child is born with limb abnormality, and it is confirmed as BBS if a patient subsequently develops retinitis pigmentosa and obesity during early childhood and adolescence (Beales et al., 1999; Fralick et al., 1990). Since there are many other secondary or minor symptoms found in BBS patients, it has been an important issue to establish objective diagnostic criteria for BBS. Based on an extensive population survey of 109 BBS patients from the UK and their families, Beales et al proposed new revised diagnostic criteria for BBS in 1999 (Beales et al., 1999). In this report, they suggested that four primary features or three primary plus two secondary features should be present for a diagnosis of BBS to be made. The primary clinical features in the proposed diagnostic criteria include: retinitis

pigmentosa, polydactyly, obesity, mental retardation, hypogonadism in males and renal defects (Table 1-1).

1.3.1 Primary features

1.3.1.1 Retinitis pigmentosa

Retinitis Pigmentosa (RP) or pigmentary retinopathy is a group of inherited eye diseases that affect the retina. As the name indicates, the hallmark of RP is the presence of dark pigmented spots in the retina. By affecting the light sensitive photoreceptors such as rod and cone cells, RP causes the loss of visual field, and eventually blindness. The first symptom of RP is night blindness, which is usually noted in early childhood. RP then causes progressive loss of peripheral vision, which is often referred as tunnel vision, before it affects the central vision. Its symptoms progress rapidly and usually lead to severe visual impairment by early adulthood (de Olivera-Dias and Rosemberg, 1977).

As a heterogeneous disorder, RP is caused by mutations in many different genes. To date, thirty two genes including rhodopsin, RP1 and retinitis pigmentosa GTPase-regulator (RPGR) are known to be associated with RP though 60% RP cases still have no known genetic cause (Wang et al., 2005). Beales et al showed in their studies with 109 BBS patients that RP was the most commonly observed symptom of BBS (93% of BBS patients) (Beales et al., 1999). Night blindness and complete blindness were noted at a mean age of 8.5 years (range 1-34 years) and 15.5 years (range 8-43 years) respectively. Their analysis suggested that RP in BBS patients starts earlier and progresses more rapidly with a mean of seven years from diagnosis to blindness than in isolated typical retinitis pigmentosa (Beales et al., 1999).

1.3.1.2 Limb abnormality

Limb abnormalities found in BBS include post-axial polydactyly (extra fingers/toes near the fifth digit), brachydactyly (short and broad fingers/toes), syndactyly (fused fingers/toes) and clinodactyly (curved finger/toes).

According to Beales et al, 69% of BBS patients had polydactyly. 21% of them had polydactyly in all four limbs, 8% of them showed polydactyly only on the hands, and 21% only on the feet. In addition to polydactyly, brachydactyly and syndactyly were reported in 46% and 8% of patients, respectively (Beales et al., 1999).

1.3.1.3 Obesity

Obesity in BBS patients usually begins in early childhood and progresses with age although patients can control their weight through caloric restriction and exercise. In adult patients, obesity is usually limited to the trunk and proximal limbs and is less frequently present on the face (Fan et al., 2004b).

By measuring the body mass index (BMI=weight/height^2), Beales et al (1999) found that BBS patients had begun to develop obesity at around 2-3 years. Overall, 72% of post-pubertal BBS patients were overweight (BMI >25 kg/m^2). 52% had a BMI >30 kg/m^2 (defined as obese) and 16% had a BMI >40 kg/m^2 (defined as morbidly obese) (Beales et al., 1999). The reason for the obesity is not known yet, but may be a combination of hyperphagia (binge eating) and an inadequate consumption of calories through exercise.

1.3.1.4 Mental retardation

The degree of mental retardation in BBS patients ranges from mild cognitive disabilities to severe mental retardation. In many early studies, IQ tests were used to assess this phenotype. However, its accuracy has been a subject of debate because of the effect of visual impairment on the test performance. Generally, patients show a deficit in short term memory which is often counterbalanced by excellent long term memory. Studies by Beales at al showed that the majority of children with BBS were able to remain in mainstream education in the early years, provided that adequate classroom assistance and/or visual aids were available. However, almost half required placement in special schools (Beales et al., 1999).

1.3.1.5 Hypogonadism

Hypogonadism is more common among male patients than females. Puberty is not significantly delayed, although the undescended testis is often noted and in most case, patients develop a micropenis that is buried in the adipose tissue. Following the onset of menstruation, irregular cycles are observed in the majority of females. However, in contrast to male patients that are potentially all infertile, many reports showed that female patients successfully gave birth to healthy children.

1.3.1.6 Renal defects

Renal defects are one of the major causes of early mortality in BBS patients (Hurley et al., 1975). According to Beales et al, a renal defect develops in 46% of patients and a wide range of renal defects have been reported, including cystic tubular disease, urinary tract malformation and chronic glomerulonephritis (Beales et al., 1999). In many

cases (67% of patients), BBS patients show excess thirst and urine production, which reflect the underlying inability to concentrate the urine. Renal imaging on patients often reveals the abnormal kidney shape as well as the presence of communicating cysts and cystic dilatation of collecting ducts and calyces. These renal defects generally cause chronic renal failure and urinary tract infections (Beales et al., 1999; Dippell and Varlam, 1998).

1.3.2 Secondary features

Various secondary features with lower frequency have been reported and play important roles for the diagnosis of BBS. The reported secondary features include anosmia, asthma, speech disorder, strabismus/cataracts/astigmatism, brachydactyly/syndactyly, developmental delay, polyuria/polydipsia (nephrogenic diabetes insipidus), ataxia/poor coordination/imbalance, mild spasticity (especially lower limbs), diabetes mellitus, dental crowding/ hypodontia/small roots/high arched palate, left ventricular hypertrophy/congenital heart disease and hepatic fibrosis.

1.4 Genetic heterogeneity of Bardet-Biedl Syndrome

In 1975, Bergsma et al noted through segregation analysis on a large study of Bardet-Biedl syndrome patients in Switzerland that there is a great degree of heterogeneity of ophthalmologic and endocrinologic symptoms among BBS patients, and that the inheritance of BBS differs from that of the simple monogenic, autosomal recessive disorders (Bergsma and Brown, 1975). Based on these findings, they proposed that Bardet-Biedl syndrome may be transmitted by polygenic inheritance. About twenty years after the hypothesis of the genetic heterogeneity of BBS was proposed, the first

BBS locus (*BBS2*) was mapped by Kwitek-Black et al in 1993. Authors demonstrated by genetic linkage analysis on a large inbred Bedouin family that the first *BBS* gene is located on the long arm of chromosome 16(q21) (Kwitek-Black et al., 1993). Later on, five additional *BBS* loci were identified by similar approaches (*BBS1*, 11q13; *BBS3*, 3p12-q13; *BBS4*, 15q22.3-q23; *BBS5*, 2q31; *BBS6*, 20p12) (Carmi et al., 1995; Kwitek-Black et al., 1993; Leppert et al., 1994; Sheffield et al., 1994; Slavotinek et al., 2000; Young et al., 1999).

In 2000, Slavotinek et al cloned the first *BBS* gene by a conventional positional cloning approach (Slavotinek et al., 2000). The authors first noticed that the reduced critical interval in the *BBS6* locus encompasses a chaperonin-like gene (*MKKS*). Interestingly, mutations in this gene were previously reported to be associated with McKusick-Kaufman syndrome, which shows many overlapping phenotypes with BBS, including polydactyly, cardiomyopathy, and hydrometrocolpos (Slavotinek and Biesecker, 2000; Slavotinek et al., 2000). Based on both the mapping information and clinical similarities between these two syndromes, Slavotinek et al screened the *MKKS* gene and identified mutations in five Newfoundland and two European-American BBS pedigrees, therefore demonstrating that *MKKS* also represents the *BBS6* gene. A sequence similarity search with the conceptual translation of the *BBS6* gene suggested that *BBS6* gene likely encodes a novel member of a protein family called chaperonins (see also chapter 3 introduction for further information), which form large protein complexes that assist the proper folding of newly synthesized proteins in the cell (Leroux and Hartl, 2000; Stirling et al., 2003). Given this finding, the researchers hypothesized that other *BBS* genes might also be members of the chaperonin family, or were the protein substrates of BBS6

chaperonin. If other BBS proteins were substrates acting in the same cellular pathway or process, their deficient folding by the putative BBS6 chaperonin would therefore give rise, expectedly, to the same phenotype. However, the hypothesis that other BBS proteins were related to chaperonins turned out to be incorrect since none of the seven *BBS* genes cloned subsequently were found to be homologous to chaperonin proteins.

BBS2 gene was positionally cloned in 2001 by Nishimura et al (Nishimura et al., 2001). BLAST analysis showed that it has no significant similarity to other known genes. However, computational domain analysis revealed that BBS2 has a putative beta propeller domain structure, which is involved in a wide range of cellular activities, including protein-protein interactions and the regulation of enzymatic activity.

In the same year, *BBS4* gene was identified by Mykytyn et al. Initial sequence analysis conducted by Mykytyn et al did not identify significant similarities to any proteins of known function (Mykytyn et al., 2001). However, the more comprehensive domain analysis by Kim et al in 2004 (see also the chapter 2) revealed that BBS4 likely consists of 13 consecutive tetratricopeptide repeat (TPR) motifs flanked by short N- and C-terminal regions. TPRs are composed of degenerate stretches of 34 amino acids that fold into characteristic helix-turn-helix structures and typically occur as single or multiple triplet arrays. These usually in turn mediate protein-protein interactions by cradling a specific linear peptide sequence (Blatch and Lassle, 1999).

BBS1 gene was positionally cloned by the same group in 2002 (Mykytyn et al., 2002). The authors of this paper found that mutations in *BBS1* allele are involved in about one-third of all BBS cases, indicating that mutation in *BBS1* is the most common cause of BBS. Sequence analysis showed that BBS1 protein contains no signal sequence,

conserved domain or predicted transmembrane regions. Interestingly, however, they noted that BBS1 and BBS2 have 40% of amino acid similarity, which suggested the hypothesis that identifying more distantly related members of one BBS protein might help identifying other BBS proteins.

Based on the hypothesis that other *BBS* genes might be distantly related members of *BBS2*, Badano et al attempted to search the EST database with the human and a zebrafish BBS2 peptide sequence (Badano et al., 2003). By assembling a number of EST sequences showing 25-40% similarity to BBS2, the authors identified two ORFs, namely *BBS2L1* and *BBS2L2* (*BBS1*). Interestingly, *BBS2L1* was located at 4q27, a chromosome position not overlapping with any *BBS* locus that had been identified. Despite this unpredicted result, the authors hypothesized that *BBS2L1* might be in a novel *BBS* locus, *BBS7*. Screening the sequence of *BBS2L1* in BBS patients of European ancestry revealed a number of pathogenic mutations, demonstrating that *BBS2L1* is *BBS7*.

Following the success in cloning *BBS7* gene by a phylogenetic/genomic approach using distant paralogues of known BBS proteins, Ansley et al applied the same approach and identified *BBS8* gene in a screen for *BBS4*-like genes (Ansley et al., 2003). Most interestingly, the authors also found that the *C. elegans* orthologues of human *BBS1, 2, 7* and *8* are exclusively expressed in a limited number of neuronal cells that possess cilia, but not in any non-ciliated cells. The finding that the expression of multiple *C. elegans bbs* genes are cilia-specific provided a very important clue as to the function of BBS proteins as well as a potential new way of identifying *BBS* genes using *C. elegans* by screening for genes bearing a similar expression profile.

Based on the hypothesis that *BBS* genes exist only in the genomes of ciliated organisms, Li et al (2004) took a comparative genomics approach to identify a new *BBS* gene. The authors subtracted the genome of *Arabidopsis thaliana*, which is devoid of cilia, from the shared genomes of the ciliated organisms *Chlamydomonas* and *Homo sapiens*. As a result, they identified a proteome enriched for ciliary/flagellar proteins and proteins found at the basal body, which gives rise to cilia/flagella; this so-called FABB proteome contains 688 genes. Results showed that the identified FABB proteome contains orthologs of all known *BBS* genes except for *BBS6*. Interestingly, the authors found that two genes, namely FLJ11457 (NM_024753) and DKFZp762I194 (NM_152384) encoding IFT139 and a novel protein of unknown function respectively, are located at 2q31, where the *BBS5* locus maps to. Subsequent sequencing analysis of two genes from a BBS patient revealed several pathogenic mutations in DKFZp762I194, verifying that it represents the sought-after *BBS5* gene (Li et al., 2004).

Based on the previous finding that all known *C. elegans bbs* genes are expressed exclusively in ciliated cells, owing to the presence of a DAF-19 RFX transcription factor binding site (X box) in their promoters, which are known to direct the expression of genes exclusively in ciliated cells in the nematode (Ansley et al., 2003) (see also chapter 4), Fan et al (2004) hypothesized that the *C. elegans* orthologue of human *BBS3* also contains this regulatory element. Genome-wide screening to identify genes with X-boxes revealed that the *C. elegans* genome has approximately 368 X-box containing genes, 168 of which had a bona fide human orthologue. The authors found that three of them existed in the critical interval of human *BBS3* loci, namely ESRRBL1 (human orthologue of *C. elegans* ciliary protein CHE-13), the hypothetical protein DKFZp761H07, and ARL6, a

member of ARL (ADP Ribosylation factor-like) family. Sequencing analysis of the complete reading frames and exon-intron boundaries of the three genes from BBS patients from a Newfoundland and a Saudi Arabian family revealed multiple pathogenic mutations in ARL6, demonstrating that ARL6 is BBS3 (Fan et al., 2004a). The brief summary of recent progress in identifying BBS genes and their predicted domain structures is provided in Table 1-2 below.

1.5 Structure and function of the centrosome

In animal cells, centrosomes serve numerous functions, including spindle formation, transport of cytoplasmic organelles, morphogenesis, regulation of cell division and determination of cell shape (Zimmerman et al., 1999). The centrosome acts as a microtubule organizing center (MTOC) by nucleating and anchoring microtubules, in a manner similar to that of the spindle pole body in yeast and the blepharoplast in lower plants (Zimmerman et al., 1999). Overwheliming amount of evidence indicates that the γ-tubulin containing-ring complex (γTuRC) in pericentriolar material (PCM, see below) acts as an efficient template structure for the initiation of microtubule growth at the centrosome where γ-tubulins are proposed to interact laterally with each other and to bind to α/β-tubulin dimmers at the minus (slow growing) end of growing micrtubules.

Ultrastructural studies have determined that centrosomes consist of a pair of centrioles which are nearly surrounded by a tube of amorphous material termed pericentriolar material (PCM) (Kubo et al., 1999; Ou et al., 2003; Zimmerman and

Doxsey, 2000). Additionally, electron-dense granules referred to as massules or centriolar satellites are peripherally associated with centrosomes (Rattner, 1992).

Centrioles are thought to organize the PCM and confer stability to the centrosome (Bobinnec et al., 1998). They are conserved microtubule-based structures that localize within centrosomes as well as in at the basal bodies of cilia or flagella. The process by which a mother centriole is converted into a basal body that gives rise to a primary cilium in mammalian cells appears to be regulated in a cell type-specific and developmentally regulated manner (Beisson and Wright, 2003).

Although exact number of proteins existing at the centrosome is hard to establish due to technical difficulty of obtaining pure centrosomes, it has been proposed that at least 100 proteins associate with centrosome at some stage of cell cycle in different species. Most of them are thought to be structural components of centrosome including α, β, and γ-tubulin, centrin, pericentrin, ninein, PCM-1, Nude1, and various centriole associated proteins such as CPAP and centriolin. Some proteins that are proposed to play regulatory roles in centrosome duplication and segregation include various cell cycle dependent kinases (Cdk), Aurora kinase, Nima-related kinase, and Protein phosphatase 2A. Other motor related proteins have been also identified to be centrosomal proteins such as dynein and dynactin complex (Zimmerman et al., 1999).

In contrast to centrioles, the composition of centriolar satellites is poorly defined. One component is Pericentriolar Material 1 (PCM1), a 228 kDa protein identified in patient antiserum capable of cross-reacting with centrosomes (Balczon et al., 1994; Kubo et al., 1999). PCM1 shows a dynamic cellular distribution, localizing with centrosomal satellites throughout the cell cycle except during metaphase and anaphase, when it

becomes cytosolic (Balczon et al., 1994; Dammermann and Merdes, 2002). PCM1 acts as a scaffold for several proteins, including centrin, pericentrin, kendrin, and ninein, and is transported to the centrosome in a microtubule-dependent manner by the dynein-dynactin molecular motor (Zimmerman and Doxsey, 2000).

The cellular localization of PCM1 indicates that the material surrounding centrosomes and basal bodies are molecularly related. PCM1 is postulated to be important for recruiting proteins necessary for centrosome replication, and for organizing/anchoring microtubules emanating from the MTOC (Dammermann and Merdes, 2002; Zimmerman and Doxsey, 2000). PCM1 is also a component of fibrous granules, electron dense particles that form during ciliogenesis and basal body replication, leading to the notion that fibrous granules and centriolar satellites are equivalent non-membranous organelles (Kubo et al., 1999). Together, these observations suggest that PCM1 participates in the biogenesis, function and maintenance of both centrosomes and cilia (Kubo et al., 1999; Zimmerman and Doxsey, 2000).

1.6 Research objectives

Bardet Biedl syndrome is a very rare genetic disease—in the United States and Europe, it occurs once out of every 150,000 births, although higher incidence has been reported in the confined ethnic groups of Newfoundland (1: 13 000) and Kuwait (1: 17 000) (Katsanis, 2004). Nonetheless, studying the pathogenicity of BBS is particularly meaningful because it may help to improve a greater understanding of the many ailments that are commonly observed in the general public, such as obesity, diabetes, renal

anomaly, and congenital heart disease, for example. In addition, BBS may serve as an excellent model disease to study how living organisms develop healthy organs such as digits, eyes, heart, and kidney, which are organs that are affected in BBS patients. Lastly, as will be described below, it appears as though BBS proteins are essential for the proper function of centrosomes and cilia, and likely for the function of protein trafficking in general. The characterization of BBS proteins will therefore help to shed light on these fundamental biological processes.

The goal of my Ph.D. research was to elucidate the molecular cause of BBS by characterizing two known BBS proteins, BBS4 (see chapter 2) and BBS6 (see chapter 3). Because patients affected by mutations in different *BBS* genes are phenotypically indistinguishable, the proteins are believed to function in same cellular pathway. Therefore, it can be surmised that learning the functions of these two proteins will also provide information about the functions of BBS proteins on the whole, and eventually, provide insight into the molecular etiology of BBS.

Both BBS4 and 6 are novel proteins whose functions are unknown. Thus, many experiments can be proposed to characterize the proteins. However, my study will be focused on addressing the following three main questions. 1) Where in the cell are BBS4 and BBS6 are localized? 2) What are the possible cellular functions of BBS4 and BBS6? 3) In which cell types or tissues in a living organism are BBS4 and 6 expressed, and therefore act?

A combination of bioinformatic, genetic, biochemical and cell biological approaches was employed to tackle these questions. For example, amino acid sequences of BBS4 and 6 weree analyzed using a domain prediction program to identify what

functional protein motifs BBS4 and 6 may contain. Based on those results, which domains in the proteins are required for interacting with their binding partners and which domains are involved in their subcellular localization were characterized. Most importantly, siRNA experiment with mammalian cultured cells as a model system can shed light on the cellular functions of BBS4 and 6, and the subsequent immunohistochemistry can suggest in which body parts of living organism BBS proteins carry out such functions. Chapter 2 describes the results of our analyses that were conducted with BBS4 to address the above three questions, and chapter 3 describes the results obtained from the molecular characterization of BBS6. Finally, in chapter 4, locating transcription factor binding sites on the promoter sequence of *BBS* genes will suggest how the expression of *BBS* genes may be regulated at the transcription level.

1.7 Table

Table 1-1 Modified diagnostic criteria (Beales et al., 1999)

Primary clinical features	Secondary clinical features
Retinitis pigmentosa Polydactyly Obesity Mental retardation Hypogonadism in males Renal defects	Speech disorder/delay Strabismus/cataracts/astigmatism Brachydactyly/syndactyly Developmental delay Polyuria/polydipsia (nephrogenic diabetes insipidus) Ataxia/poor coordination/imbalance Mild spasticity (especially lower limbs) Diabetes mellitus Dental crowding/ hypodontia/small roots/high arched palate Left ventricular hypertrophy/congenital heart disease Hepatic fibrosis

Table 1-2 Summary of identified human *bbs* genes and their predicted domain structures

	Size	Loci	Cloned in	Predicted domain structure
BBS1	65kDa	11q13	2002	β-propeller
BBS2	80kDa	16q21	2001	β-propeller
BBS3 (*ARL6)	21kDa	3p12-q13	2004	GTP binding
BBS4	58kDa	15q22.3-q23	2001	*TPR
BBS5	39kDa	2q31	2004	N/A
BBS6	62kDa	20p12	2000	chaperonin
BBS7	80kDa	4q27	2003	β-propeller
BBS8	57kDa	14q32.1	2003	TPR

* *ARL6: ADP-ribosylation factor-like 6*
* *TPR: Tetratrico peptide repeat*

1.8 References

Ansley, S. J., Badano, J. L., Blacque, O. E., Hill, J., Hoskins, B. E., Leitch, C. C., Kim, J. C., Ross, A. J., Eichers, E. R., Teslovich, T. M., et al. (2003). Basal body dysfunction is a likely cause of pleiotropic Bardet-Biedl syndrome. Nature 425, 628-633.

Badano, J. L., Ansley, S. J., Leitch, C. C., Lewis, R. A., Lupski, J. R., and Katsanis, N. (2003a). Identification of a novel Bardet-Biedl syndrome protein, BBS7, that shares structural features with BBS1 and BBS2. Am J Hum Genet 72, 650-658.

Balczon, R., Bao, L., and Zimmer, W. E. (1994). PCM-1, A 228-kD centrosome autoantigen with a distinct cell cycle distribution. J Cell Biol 124, 783-793.

Beales, P. L., Elcioglu, N., Woolf, A. S., Parker, D., and Flinter, F. A. (1999). New criteria for improved diagnosis of Bardet-Biedl syndrome: results of a population survey. J Med Genet 36, 437-446.

Beales, P. L., Warner, A. M., Hitman, G. A., Thakker, R., and Flinter, F. A. (1997). Bardet-Biedl syndrome: a molecular and phenotypic study of 18 families. J Med Genet 34, 92-98.

Beisson, J., and Wright, M. (2003). Basal body/centriole assembly and continuity. Curr Opin Cell Biol 15, 96-104.

Bergsma, D. R., and Brown, K. S. (1975). Assessment of ophthalmologic, endocrinologic and genetic findings in the Bardet-Biedl syndrome. Birth Defects Orig Artic Ser 11, 132-136.

Blatch, G. L., and Lassle, M. (1999). The tetratricopeptide repeat: a structural motif mediating protein-protein interactions. Bioessays 21, 932-939.

Bobinnec, Y., Khodjakov, A., Mir, L. M., Rieder, C. L., Edde, B., and Bornens, M. (1998). Centriole disassembly in vivo and its effect on centrosome structure and function in vertebrate cells. J Cell Biol 143, 1575-1589.

Carmi, R., Elbedour, K., Stone, E. M., and Sheffield, V. C. (1995). Phenotypic differences among patients with Bardet-Biedl syndrome linked to three different chromosome loci. Am J Med Genet 59, 199-203.

Croft, J. B., Morrell, D., Chase, C. L., and Swift, M. (1995). Obesity in heterozygous carriers of the gene for the Bardet-Biedl syndrome. Am J Med Genet 55, 12-15.

Dammermann, A., and Merdes, A. (2002). Assembly of centrosomal proteins and microtubule organization depends on PCM-1. J Cell Biol 159, 255-266.

de Olivera-Dias, G., and Rosemberg, J. A. (1977). [Obtaining cellular mass from Chlorella sp. on a solid medium]. Rev Latinoam Microbiol 18, 151-153.

Dippell, J., and Varlam, D. E. (1998). Early sonographic aspects of kidney morphology in Bardet-Biedl syndrome. Pediatr Nephrol 12, 559-563.

Fan, Y., Esmail, M. A., Ansley, S. J., Blacque, O. E., Boroevich, K., Ross, A. J., Moore, S. J., Badano, J. L., May-Simera, H., Compton, D. S., et al. (2004a). Mutations in a member of the Ras superfamily of small GTP-binding proteins causes Bardet-Biedl syndrome. Nat Genet 36, 989-993.

Fan, Y., Rahman, P., Peddle, L., Hefferton, D., Gladney, N., Moore, S. J., Green, J. S., Parfrey, P. S., and Davidson, W. S. (2004b). Bardet-Biedl syndrome 1 genotype and obesity in the Newfoundland population. Int J Obes Relat Metab Disord 28, 680-684.

Farag, T. I., and Teebi, A. S. (1989). High incidence of Bardet Biedl syndrome among the Bedouin. Clin Genet 36, 463-464.

Fralick, R. A., Leichter, H. E., and Sheth, K. J. (1990). Early diagnosis of Bardet-Biedl syndrome. Pediatr Nephrol 4, 264-265.

Green, J. S., Parfrey, P. S., Harnett, J. D., Farid, N. R., Cramer, B. C., Johnson, G., Heath, O., McManamon, P. J., O'Leary, E., and Pryse-Phillips, W. (1989). The cardinal manifestations of Bardet-Biedl syndrome, a form of Laurence-Moon-Biedl syndrome. N Engl J Med 321, 1002-1009.

Hurley, R. M., Dery, P., Norady, M. B., and Drummond, K. N. (1975). The renal lesion of the Laurence-Moon-Biedl syndrome. J Pediatr 87, 206-209.

Katsanis, N. (2004). The oligogenic properties of Bardet-Biedl syndrome. Hum Mol Genet 13 Spec No 1, R65-71.

Klein, D., and Ammann, F. (1969). The syndrome of Laurence-Moon-Bardet-Biedl and allied diseases in Switzerland. Clinical, genetic and epidemiological studies. J Neurol Sci 9, 479-513.

Kubo, A., Sasaki, H., Yuba-Kubo, A., Tsukita, S., and Shiina, N. (1999). Centriolar satellites: molecular characterization, ATP-dependent movement toward centrioles and possible involvement in ciliogenesis. J Cell Biol 147, 969-980.

Kwitek-Black, A. E., Carmi, R., Duyk, G. M., Buetow, K. H., Elbedour, K., Parvari, R., Yandava, C. N., Stone, E. M., and Sheffield, V. C. (1993). Linkage of Bardet-Biedl syndrome to chromosome 16q and evidence for non-allelic genetic heterogeneity. Nat Genet 5, 392-396.

Leppert, M., Baird, L., Anderson, K. L., Otterud, B., Lupski, J. R., and Lewis, R. A. (1994). Bardet-Biedl syndrome is linked to DNA markers on chromosome 11q and is genetically heterogeneous. Nat Genet 7, 108-112.

Leroux, M. R., and Hartl, F. U. (2000). Protein folding: versatility of the cytosolic chaperonin TRiC/CCT. Curr Biol 10, R260-264.

Li, J. B., Gerdes, J. M., Haycraft, C. J., Fan, Y., Teslovich, T. M., May-Simera, H., Li, H., Blacque, O. E., Li, L., Leitch, C. C., et al. (2004). Comparative genomics identifies a flagellar and basal body proteome that includes the *BBS5* human disease gene. Cell 117, 541-552.

Mykytyn, K., Braun, T., Carmi, R., Haider, N. B., Searby, C. C., Shastri, M., Beck, G., Wright, A. F., Iannaccone, A., Elbedour, K., et al. (2001). Identification of the

gene that, when mutated, causes the human obesity syndrome BBS4. Nat Genet 28, 188-191.

Mykytyn, K., Nishimura, D. Y., Searby, C. C., Shastri, M., Yen, H. J., Beck, J. S., Braun, T., Streb, L. M., Cornier, A. S., Cox, G. F., et al. (2002). Identification of the gene (*BBS1*) most commonly involved in Bardet-Biedl syndrome, a complex human obesity syndrome. Nat Genet 31, 435-438.

Nishimura, D. Y., Searby, C. C., Carmi, R., Elbedour, K., Van Maldergem, L., Fulton, A. B., Lam, B. L., Powell, B. R., Swiderski, R. E., Bugge, K. E., et al. (2001). Positional cloning of a novel gene on chromosome 16q causing Bardet-Biedl syndrome (BBS2). Hum Mol Genet 10, 865-874.

O'Dea, D., Parfrey, P. S., Harnett, J. D., Hefferton, D., Cramer, B. C., and Green, J. (1996). The importance of renal impairment in the natural history of Bardet-Biedl syndrome. Am J Kidney Dis 27, 776-783.

Ou, Y. Y., Zhang, M., Chi, S., Matyas, J. R., and Rattner, J. B. (2003). Higher order structure of the PCM adjacent to the centriole. Cell Motil Cytoskeleton 55, 125-133.

Rattner, J. B. (1992). Ultrastructure of centrosome domains and identification of their protein components. in the Centrosome (ed Kalnins, VI) (Academic, San Diego,), 45-69.

Sheffield, V. C., Carmi, R., Kwitek-Black, A., Rokhlina, T., Nishimura, D., Duyk, G. M., Elbedour, K., Sunden, S. L., and Stone, E. M. (1994). Identification of a Bardet-Biedl syndrome locus on chromosome 3 and evaluation of an efficient approach to homozygosity mapping. Hum Mol Genet 3, 1331-1335.

Slavotinek, A. M., and Biesecker, L. G. (2000). Phenotypic overlap of McKusick-Kaufman syndrome with bardet-biedl syndrome: a literature review. Am J Med Genet 95, 208-215.

Slavotinek, A. M., Stone, E. M., Mykytyn, K., Heckenlively, J. R., Green, J. S., Heon, E., Musarella, M. A., Parfrey, P. S., Sheffield, V. C., and Biesecker, L. G. (2000). Mutations in MKKS cause Bardet-Biedl syndrome. Nat Genet 26, 15-16.

Stirling, P. C., Lundin, V. F., and Leroux, M. R. (2003). Getting a grip on non-native proteins. EMBO Rep 4, 565-570.

Wang, D. Y., Chan, W. M., Tam, P. O., Baum, L., Lam, D. S., Chong, K. K., Fan, B. J., and Pang, C. P. (2005). Gene mutations in retinitis pigmentosa and their clinical implications. Clin Chim Acta 351, 5-16.

Young, T. L., Penney, L., Woods, M. O., Parfrey, P. S., Green, J. S., Hefferton, D., and Davidson, W. S. (1999). A fifth locus for Bardet-Biedl syndrome maps to chromosome 2q31. Am J Hum Genet 64, 900-904.

Zimmerman, W., and Doxsey, S. J. (2000). Construction of centrosomes and spindle poles by molecular motor-driven assembly of protein particles. Traffic 1, 927-934.

Zimmerman, W., Sparks, C. A., and Doxsey, S. J. (1999). Amorphous no longer: the centrosome comes into focus. Curr Opin Cell Biol 11, 122-128.

CHAPTER 2
THE FAMILIAL OBESITY PROTEIN BBS4 TARGETS CARGO TO THE PERICENTRIOLAR REGION AND IS REQUIRED FOR MICROTUBULE ANCHORING AND CELL CYCLE PROGRESSION

The following chapter has been published in *Nature Genetics*. 2004, 36 462-70. The authors of the paper were as follows:.

Jun Chul Kim[1,6], Jose L Badano[2,6], Sonja Sibold[3,6], Muneer A Esmail[1], Josephine Hill[3], Bethan E Hoskins[3], Carmen C Leitch[2], Kerrie Venner[4], Stephen J Ansley[2], Alison J Ross[3], Michel R Leroux[1], Nicholas Katsanis[2,5] & Philip L Beales[3]

[1] Department of Molecular Biology and Biochemistry, Simon Fraser University, 8888 University Dr., Burnaby BC, V5A 1S6, Canada.
[2] Institute of Genetic Medicine, Johns Hopkins University, 600 North Wolfe Street, Baltimore, Maryland 21287, USA.
[3] Molecular Medicine Unit, Institute of Child Health, University College London, London WC1N 1EH, UK.
[4] Department of Electron Microscopy, Institute of Neurology, Queens Square, London, UK.
[5] Wilmer Eye Institute, Johns Hopkins University, 600 North Wolfe Street, Baltimore, Maryland 21287, USA.
[6] These authors contributed equally to this work.
Correspondence should be addressed to Michel R Leroux leroux@sfu.ca or Nicholas Katsanis katsanis@jhmi.edu

As the first author, I carried out most of the laboratory work for this manuscript and interpreted most of the results. Jose Badano and Sonja Sibold conducted the yeast two hybrid experiment and coimmunoprecipitation experiments (Figure 2-2, Figure 2-6b). Philip Beales conducted an electron microscopy experiment. Muneer Esmail conducted the sucrose gradient sedimentation experiments (Figure 2-2b). Carmen Leitech conducted the immunohistochemistry experiment (Figure 2-9).

2.1 Abstract

BBS4 is one of several proteins causing Bardet-Biedl syndrome (BBS), a multisystemic disorder of significant genetic and clinical complexity. Here we show that BBS4 localizes to the centriolar satellites of centrosomes and basal bodies of primary cilia, where it functions as an adaptor of the $p150^{glued}$ subunit of the dynein transport machinery to recruit PCM1 (Pericentriolar Matrix 1 protein) and its associated cargo to the satellites. *BBS4* silencing induces PCM1 mislocalization and concomitant de-anchoring of centrosomal microtubules, arrest in cell division, and apoptotic cell death. An equivalent effect on PCM1 and microtubules is observed upon expression of two truncated forms of BBS4 that are similar to those found in some BBS patients. Our findings indicate that defective targeting and/or anchoring of pericentriolar proteins, and microtubule disorganization, contribute to the phenotype of BBS and provide novel insights into possible causes of familial obesity, diabetes and retinal degeneration.

2.2 Introduction

Bardet-Biedl syndrome (BBS-OMIM: 209900) is a heterogeneous disorder characterized by retinal dystrophy, renal dysfunction, obesity, polydactyly as well as numerous developmental and behavioral defects (Beales et al., 1999). It is typically inherited in an autosomal recessive fashion, although in some families three mutations in two genes are required for pathogenesis (Katsanis et al., 2001). At least eight *BBS* genes have been cloned to date, encoding proteins of unknown function: BBS1, BBS2, BBS3, BBS4, BBS5, BBS6, BBS7 and BBS8 (Badano et al., 2003; Katsanis et al., 2000; Li et al., 2004; Mykytyn et al., 2001; Mykytyn et al., 2002; Nishimura et al., 2001; Slavotinek

et al., 2000; Fan et al., 2004). The resemblance of various BBS phenotypes to disorders caused by improper cilia function has led to the proposal that BBS might be of the same etiology (Rosenbaum, 2002). Notably, the recent identification and expression studies of mammalian *BBS8* and of four *C. elegans bbs* orthologues have suggested that BBS may be caused by defects in centrosomes, basal bodies/cilia, or both (Ansley et al., 2003). However, the functions of BBS proteins, and thus the molecular basis of BBS, have remained elusive.

Here we provide the first direct evidence for the cellular mechanism of BBS pathogenesis. We show that the BBS4 protein localizes to the centriolar satellites of centrosomes and basal bodies and is necessary for the recruitment of PCM1 to centrosomal satellites by acting as an adaptor between PCM1 and the dynein-dynactin motor complex (see Fig 2-10). Disruption of BBS4 function results in PCM1 mislocalization and loss of microtubule anchoring at the centrosome, defects in cytokinesis and apoptosis. Our data model both the null mutations observed in some patients with BBS4 mutations as well as the effect of truncating mutations observed in other patients and suggest that at least some of the molecular defects of this phenotype arise from improper targeting of PCM1 and its associated proteins to centriolar satellites, as well severe microtubule disorganization that disrupts the proper function of both centrosomes and basal bodies.

2.3 Materials and methods

2.3.1 Yeast two hybrid screen

Both the cytotrap and Gal-4 Yeast two-hybrid screens were performed as described (Ansley et al., 2003). The complete open reading frame (ORF) of BBS4 was amplified from cDNA by PCR using forward and reverse primers tagged with Sal I and Not I and cloned into the pSOS vector (bait) (Stratagene) or pGBDU. We used a fetal brain library (Stratagene) for the cytotrap and a kidney library (Clontech) in the Gal-4 screen.

2.3.2 DNA constructs

cDNAs encoding full-length or truncated BBS4 proteins were generated by PCR using different sets of 5' and 3' primer containing *Sal* I and *Not* I restriction sites, respectively, and subcloned into the expression vector pCMV-Myc (Clontech). BBS4 deletion constructs encode the amino acids corresponding to those detailed in Figure 2-1. The Myc-tagged p50-dynamitin expression vector was a kind gift from Dr. Richard Vallee.

2.3.3 Antibodies

Polyclonal antibodies were generated by co-immunization of rabbits with two human BBS4 peptides (QFPVSTESQKPRQKK and VESSPTETSEQIREK). Immune serum was affinity-purified by passing through a Sepharose bead column conjugated to the respective peptides (CovalAb, Cambridge). Other antibodies used were: mouse monoclonal anti-Myc (ClonTech), anti-HA (ROCHE), and anti-porin (Molecular probes), anti-acetylated tubulin (Sigma), anti-α-tubulin (Sigma), rabbit monoclonal or polyclonal

anti-γ-tubulin (Sigma), and rabbit polyclonal anti-GFP (Clontech). Secondary antibodies used were Alexa Fluor 488 and 594 conjugated anti-rabbit and anti-mouse antibodies (Molecular Probes). The rabbit polyclonal anti-PCM-1 antibody was a kind gift from Dr. Andreas Merdes.

2.3.4 Mammalian cell culture and synchronization

HeLa, HEK 293, NIH 3T3 and COS-7 cells were maintained in DMEM (Gibco BRL) supplemented with 10% FBS at 37°C in 5% CO_2. Mouse kidney collecting duct epithelial cells (IMCD-3) were maintained in 1:1 mixture of DMEM and Ham's F12 medium (Gibco BRL) with 10% fetal bovine serum at 37°C in 5% CO_2. For cell synchronization, HeLa cells were grown in 2 mM thymidine (Sigma) for 18 h washed with PBS, and grown in fresh medium without thymidine for 8 h. Subsequently, cells were incubated with 2 mM thymidine for 18 h, transferred to fresh medium, and fixed at various time points to monitor cell cycle progression.

2.3.5 Sucrose density gradient centrifugation

HEK 293 cells were harvested into 10 ml cold PBS, pelleted and washed in PBS and cold TES buffer [20mM Tris pH 7.4, 5mM EDTA, 250mM Sucrose, 1X protease inhibitor without EDTA (Roche Diagnostics)]. The final cell pellet was resuspended in 700 µl TES buffer lacking or containing 1% Triton X-100. Cells were lysed mechanically on ice by passing through a 27 gauge needle 60 times. Cells in Triton-containing buffer were vortexed and incubated on ice for 30 min. 300 µl of each cell lysate was loaded on top of discontinuous sucrose gradients comprising 10 steps of 300 µl each, prepared in 20mM Tris pH 7.4, 10% glycerol, and appropriate amount of sucrose). Samples were

centrifuged at 100000 *g* for 16 hr at 4°C. Fractions (300 µl) collected from the top were subjected to Western blot analysis.

2.3.6 Coimmunoprecipitations

The ORF of BBS4 and a partial cDNA fragment encoding the last 450 amino acids of PCM1 (from amino acid 1574 to 2024) were cloned into the pCMV-Myc and pCMV-HA expression vectors (Invitrogen) and confirmed by sequencing. HEK 293 cells were transfected by calcium phosphate and harvested 48 h after transfection in co-immunoprecipitation (co-IP) buffer (150 mM NaCl, 50 mM TRIS-HCl pH 7.5, 1% NP-40) supplemented with protease inhibitor (Roche) and 500 µl of 100 mM sodium orthovanadate. Cell lysates were incubated overnight with 10 µg anti-Myc monoclonal antibody immobilized on sepharose beads (Covance). IPs were washed 3x with co-IP buffer, resuspended in loading buffer and western blotted. Immunoblot PVDF membranes were blocked with 0.2 % Tween 20 in PBS and 5% milk, and probed with appropriate antibodies. Detection was performed by ECL (Amersham).

2.3.7 Fluorescence microscopy

Cells grown on glass coverslips were rinsed in PBS, fixed in –20°C methanol for 10 min and blocked in PBS with 5.5% FBS for 60 min at room temp. Cells were then incubated for 60 min at room temp with the relevant 1° antibody diluted in PBS. Antibody binding was visualized with Alexa-fluor 488 and 594 conjugated 2° antibodies. Nuclei were counterstained with DAPI. Slides were mounted in Prolong™ anti-fade reagent (Molecular Probes) and observed by fluorescence microscopy using standard epifluorescence, Leica TCS SP confocal, or Deltavision microscope systems.

2.3.8 Transmission electron microscopy

Following 1° labeling of cells with affinity-purified BBS4 antibody, HEK 293 cells were secondarily labeled with 1 nm particle-size gold conjugated goat anti-rabbit IgG (BBInternational, UK). Cells were silver-enhanced (Silver Enhancing Kit, BBInternational, UK) and fixed in 3% glutaraldehyde (EM grade, Agar Scientific) in 0.1 M sodium cacodylate and 5 mM $CaCl_2$. Post-fixing was performed with 1% aqueous OsO_4, and dehydration through ascending grades of ethanol. Cells were then impregnated in Araldite resin mixture: ethanol in 50:50 ratio (Araldite CY212 20 ml, DDSA 25 ml, DMP30 0.8 ml; Agar Scientific). The preparation was polymerized at 60°C for 2 days. The resultant thin resin-cell films were cut and mounted onto resin blanks prior to ultrathin sectioning using a diamond knife on a Reichert Ultracut microtome and collected on 400 mesh copper grids. These were stained using 25% uranyl acetate in methanol (Analar) followed by Reynolds Lead Citrate. Sections were viewed with a JEOL 120 EX transmission electron microscope.

2.3.9 Knockdown of *BBS4* expression by RNA interference

2.3.9.1 Oligonucleotide-based method

DNA oligonucleotides (21-mers) specific to BBS4 were designed with an online tool (www.ambion.com/techlib/misc/silencer_siRNA_template.html). These corresponded to human BBS4 nucleotides 27-48 (CTCAATTTCCTGTATCTAC – Si27), 566-587 (GTCTACAAGAAAGCAGTGG- Si566), 831-852 (TGTGTTTCTTTGGCAAGAA – Si831), and 2025-2046 (ATATATTAGATTAATAATCCA – Si2025). Each oligo was used to synthesize specific siRNAs according manufacturer's instructions (*Silencer* siRNA Construction Kit

– Ambion Inc). Prior to transfection, HeLa cells were grown overnight in DMEM/10% FBS (antibiotic-free) on chamber glass slides and transfected with Lipofectamine2000 (Invitrogen) in a 250 µl OPTIMEM/DMEM mix (1:5) (Life Technologies) at a final concentration of 1 nM siRNA in cells plated at a density of $1x10^4$ over a glass substrate area of 1.8 cm^2. After 4h, the medium was expanded with DMEM and FBS (10% final concentration). Chambers were incubated for 48h before fixing and processing for immunofluorescence.

2.3.9.2 pSUPER vector method

Sense and antisense primers corresponding to human BBS4 (5'-GGCACAAGACCAGTTGCAC) were cloned into a mammalian expression vector (pSUPER) as described (Brummelkamp et al., 2002). HeLa cells seeded on 6-well plates were co-transfected with 0.1µg of a neomycin containing plasmid (pcDNA3.1, Invitrogen) and 1µg of either pSUPER-BBS4 or pSUPER empty vector. 24h post transfection, the HeLa cells were split onto coverslips at a 1:5 ratio into growth media with 500 µg activity/ml G-418 (Gibco). Transfected cells were maintained in culture for 4-5 days in G-418 before harvesting.

2.3.9.3 pSilencer vector method

pSilencer™ 2.1-U6 neo siRNA expression vector (Ambion) was used to generate siRNA against *BBS4* by ligating annealed oligonucleotides into *Hin*dIII and *Bam*HI sites: Forward: 5'-GATCCCGGCACAAGACCAGTTGCACTTCAAGAGAGTGCAACTGGTCTTGTGCCTTTTTTGGAAA-3', reverse: 5'-

AGCTTTTCCAAAAAAGGCACAAGACCAGTTGCACTCTCTTGAAGTGCAACTGGTCTTGTG CCGG-3'. The resulting construct was introduced into COS-7 cells, which were subjected to neomycin selection (500 μg activity/ml) for 9 days.

2.3.10 Microtubule regrowth assays

HeLa cells transfected with pSUPER-BBS4 or pSUPER empty vector were treated with 25 μM nocodazole at 37°C for 1 hr. After removal of the drug, cells were incubated for various times to allow microtubules to regrow, as visualized by immunofluorescence microscopy using an anti-α-tubulin antibody.

2.3.11 Fluorescence-assisted cell sorting (FACS) analyses

COS-7 cells were transfected with pSilencer-BBS4 constructs and cultured in DMEM with 500 g/ml G418 for 9 days, removed from plates by trypsin digestion, and fixed in 75 % ethanol. Fixed cells were stained in PBS containing 3.8 mM sodium citrate 50 μg/ml propidium iodide and 500 ng/ml RNase A. Samples were analyzed with the FACSCalibur® system (Becton Dickinson).

2.3.12 TUNEL assay

HeLa cells were untreated, treated with *BBS4* siRNA or a control scrambled siRNA. Following fixation in 4% paraformaldehyde (30 min), blocking with 3% H_2O_2 in methanol (10 mins) and permeabilisation with 0.1% Triton X-100, DNA strand breaks were identified by labelling free 3'-OH termini with a fluoroscein-conjugated nucleotide (dUTP) using terminal deoxynucleotidyl transferase (TdT) (In Situ Cell Death Detection Kit, Roche). Apoptosis was scored by counting the number of typical apoptotic cells per

high power field (60X) under fluorescence microscopy. The mean of 10 fields per cell preparation was calculated.

2.4 Results

2.4.1 Domain composition of BBS4

Sequence analyses of human and mouse BBS4 protein sequences have not revealed significant similarity to proteins of known function. To investigate the domain structure of BBS4, we performed homology searches and scanned the SMART protein domain database (Schultz et al., 2000). We detected as many as 13 tandem tetratricopeptide repeat (TPR) motifs flanked by short N- and C-terminal regions (Figure 2-1). TPRs are composed of degenerate stretches of 34 amino acids that fold into characteristic helix-turn-helix structures and typically occur as single or multiple triplet arrays; these in turn usually mediate protein-protein interactions by cradling a specific linear peptide sequence (Blatch and Lassle, 1999).

2.4.2 BBS4 interacts with the C-terminus of PCM1

Since BBS4 consists mostly of TPRs, we reasoned that it might function in a multisubunit complex and that the identification of other members of this complex might illuminate its function. We therefore performed a yeast two-hybrid screen with full-length BBS4 cDNA as bait and a fetal brain cDNA library as prey. From an initial screen of 106 yeast colonies, we selected five that fulfilled our selection criteria. Sequencing revealed that two clones contained different but overlapping fragments of PCM1, a 2024 amino acid (228 kDa) pericentriolar protein that recruits several centrosomal components (Dammermann and Merdes, 2002). One clone encoded a C-terminal portion of PCM1

between residues 1574 to 2024, whereas the other encoded a smaller region (1744-2024). We confirmed the specificity of the yeast two-hybrid interaction by performing a series of control experiments (Figure 2-2A). A second independent yeast two-hybrid screen of a human kidney cDNA library with BBS4 as bait also identified independent clones containing coding regions of PCM1 (1845- and 1913-2024) (data not shown). These data suggested that BBS4 can bind to the C-terminal 112 amino acids of PCM1.

We next sought to corroborate the BBS4-PCM1 interaction by co-immunoprecipitations in mammalian cells. We first determined the biochemical behavior of BBS4 using discontinuous sucrose gradient fractionation. We observed that endogenous and Myc-tagged BBS4 sediment in a similar manner at a high-molecular weight position (Figure 2-2B, fractions 10 and 11). Given that PCM1 is a pericentrosomal protein, we also compared the sedimentation behavior of BBS4 to that of γ-tubulin, an established centrosomal marker. We observed that the bulk of both endogenous and Myc-tagged BBS4 from mechanically-lyzed cell extracts sedimented to a position similar to γ-tubulin (fractions 10 and 11). Triton X-100 lysis led to the pelleting of most of the BBS4 and also of the detergent-insoluble centrosomal γ-tubulin (fractions 10 and 11; γ-tubulin contained in fraction 3 complexes with the chaperonin CCT (Moudjou et al., 1996) and the γ-tubulin in fractions 8 and 9 is associated with soluble cellular components (Dictenberg et al., 1998)). Since some of the Myc-BBS4 (Figure 2-2B, Fraction 3) and HA-tagged PCM1 (Figure 2-2C) is solubilized in the presence of detergent, we used the supernatant of this extract as the starting material for immunoprecipitations.

The entire BBS4 open reading frame and the C-terminal 450 amino acids of PCM1 were cloned into pCMV-Myc and pCMV-HA mammalian expression vectors, respectively, and transfected into HEK 293 cells. Immunoprecipitations with an anti-Myc monoclonal antibody showed that Myc-BBS4 can be co-precipitated with the HA-tagged PCM1 protein fragment (Figure 2-2C). The immunoprecipitation with the anti-Myc antibody was specific, since the HA-PCM1 fragment was not recovered by immunoprecipitating extracts of cells co-expressing pCMV-HA-PCM1 and an empty pCMV-Myc vector (Figure 2-2C) and the two proteins could also be co-immunoprecipitated with the tags reversed (data not shown). More importantly, we also observed semi-native interaction between the expressed Myc-tagged BBS4 protein and endogenous PCM1 using a polyclonal anti-PCM1 antibody (Figure 2-2C).

2.4.3 BBS4 is a pericentriolar protein that co-localizes with PCM1

We next sought to determine whether the interaction between BBS4 and PCM1 is physiologically relevant. Since BBS4 and PCM1 mRNAs are coexpressed in numerous cell types (Kubo et al., 1999; Mykytyn et al., 2001), we generated an affinity-purified polyclonal antibody against BBS4 to probe whether it co-localizes with PCM1, which is found within the centriolar satellites of centrosomes and ciliary basal bodies (Kubo et al., 1999). In a Western blot prepared with extracts from HeLa or HEK 293 cells, the antibody cross-reacts with a single protein species of the expected molecular weight (Figure 2-2D). Using this antibody, we found that endogenous BBS4 localized to the pericentriolar region of various mammalian cells, including HeLa, HEK 293, NIH 3T3, IMCD3 and COS-7, based on its close proximity to centrosomal γ-tubulin (Figure 2-3A).

Consistent with our earlier sucrose gradient data, the localization of epitope-tagged BBS4 expression constructs was identical to that of the endogenous protein (Figure 2-3C).

We determined the ultrastructural localization of BBS4 by immunogold labeling of cultured HEK 293 cells immunostained with the BBS4 antibody. Silver enhanced, resin-embedded cells visualized by transmission electron microscopy confirmed the localization of BBS4 as distinct aggregates adjacent to, but not directly associated with, the two centrosomal centrioles. The aggregates are not membrane-bound and are often found as pairs, typically spaced between 0.5-1 μm apart (Figure 2-3B).

Importantly, we also observed signal overlap for endogenous PCM1 and BBS4 in several cell types (such as HeLa and HEK 293; Figure 2-3C). Together, these data indicate that BBS4 is a novel component of centriolar satellites.

Given that one of a pair of centrosomal centrioles is recruited to the cell apex to serve as a basal body in ciliated cells, we investigated whether BBS4 also co-localizes to the basal body of primary cilia, like PCM1 (Dammermann and Merdes, 2002; Kubo et al., 1999), by performing immunofluorescence microscopy in ciliated mouse kidney epithelial cells, IMCD3 with γ-tubulin as a centrosomal marker and acetylated tubulin to stain the cilium. In these experiments, a significant proportion of cells had widely-spaced mother and daughter centrioles; co-staining experiments revealed that BBS4 was specifically associated with both the basal body and the daughter centriole (Figure 2-3D).

We next examined whether BBS4 exhibits a cell-cycle dependent behavior by co-staining synchronized HeLa cells with antibodies to BBS4 and to γ-tubulin. In contrast to PCM1, endogenous BBS4 remains associated with the centrosome throughout the cell cycle (Figure 2-3E), even during metaphase and anaphase when PCM1 disperses

(Balczon et al., 1994; Dammermann and Merdes, 2002). This raised the possibility that BBS4 localizes to the pericentriolar region in a PCM1-independent manner.

2.4.4 Truncated BBS4 mutants exert a dominant-negative effect on PCM1 localization

To further investigate the function of BBS4 and explore its relationship with PCM1, we determined which regions of BBS4 are required for localization to the centrosome and for binding to PCM1. We constructed and expressed in HeLa cells a panel of nine Myc-tagged BBS4 deletion mutants lacking one or both of the terminal regions, and up to 9 of the 13 predicted TPR motifs (Figure 2-4A, B). Immunofluorescence analysis with an anti-Myc antibody showed that deletion of either or both of the terminal regions of BBS4 had no effect on its pericentriolar localization (Figure 2-4C). In contrast, proteins lacking the N-terminal region and the first predicted TPR (construct 2-13-C) and additional TPRs (constructs 3-13-C, 4-13-C, 7-13-C and 10-13-C) consistently failed to localize near the centrosome. Similarly, the BBS4 deletion mutant N-1-9, which is missing the C-terminal region and the last four predicted TPRs, was also found scattered in the cytoplasm as punctate spots (Figure 2-4C).

We then probed whether the BBS4 truncation mutants could interact effectively with PCM1. Using HeLa cells transiently expressing the Myc-BBS4 deletion mutants, we tested for an overlap in immunoflurescence signal with endogenous PCM1 and found that BBS4 mutants containing the third predicted TPR motif (2-13-C, 3-13-C and N-1-9) failed to localize and co-mislocalized with endogenous PCM1 (Figure 2-5A) to cytoplasmic granules similar in morphology and distribution to non-membranous

granular organelles termed "PCM1-granules" (Kubo and Tsukita, 2003). Because endogenous BBS4 was present in these cells, the truncated forms of the protein likely acted in a dominant-negative manner in preventing proper PCM1 localization. Consistent with this observation, immunoprecipitations indicated that only the BBS4 deletion mutants that co-mislocalized with PCM1 (constructs 2-13-C, 3-13-C and N-1-9) retained an appreciable ability to interact with PCM1 (Figure 2-5B). In contrast, other mislocalized BBS4 mutants that interacted weakly or not at all with PCM1 (constructs 4-13-C, 7-13-C and 10-13-C; Figure 2-5B), had no appreciable effect on the localization of PCM1 near the centrosome (Figure 2-5A), likely due to the presence of endogenous BBS4.

2.4.5 Dynein is necessary for the transport of BBS4 to the centrosome

Previous studies have reported that PCM1 depends on the molecular motor dynein-dynactin for their retrograde transport along microtubules (Balczon et al., 1994; Dammermann and Merdes, 2002), whereas other centrosomal proteins, such as γ-tubulin, do not (Zimmerman and Doxsey, 2000). We therefore queried whether BBS4 function is also dynein-dependent. We examined whether BBS4 is targeted to centriolar satellites in a dynein-dependent manner by determining its cellular location in cells overexpressing p50-dynamitin, which antagonizes dynactin function (Vaughan and Vallee, 1995). First, we confirmed that HeLa cells overexpressing Myc-tagged p50-dynamitin displayed mislocalized PCM1 but not γ-tubulin (Figure 2-6A, top and middle panels, respectively). We then observed that as with PCM1, cells transfected with p50-dynamitin showed loss of the BBS4 perinuclear signal (Figure 2-6A, bottom panels).

In parallel, yeast two-hybrid experiment also identified the p150glued subunit of the dynactin complex as an interacting partner of BBS4 (Fig. 2-6B). We substantiated this finding by observing that BBS4 and p150glued expressed in HEK 293 cells could be co-immunoprecipitated specifically (Figure 2-6C). Sequence analysis of yeast constructs expressing partial p150 protein fragments indicated that the C-terminus of p150glued (amino acids 1022-1170) is sufficient to mediate interaction with BBS4. This is important, since p150glued physically links dynein to dynactin and is a key factor in modulating the function and cargo binding of the dynein molecular motor (Vale, 2003). Since the region of interaction with BBS4 lies outside those regions of p150glued required for binding microtubules (amino acids 39-150; (Waterman-Storer et al., 1995) and dynein intermediate chain (200-811; ref (Vaughan and Vallee, 1995)), this interaction suggests that BBS4 is transported to the pericentriolar region by the dynein-dynactin complex.

2.4.6 Loss of BBS4 function results in PCM1 dispersal, defective microtubule anchoring, cell division arrest and apoptotic cell death

To probe the function of BBS4 further, we depleted BBS4 from mammalian cells by RNA interference (RNAi). To ensure maximum specificity of targeting, we adopted two different approaches: (i) transfection of the vectors pSUPER (and a neomycin-resistance marker) or pSilencer™ (includes the marker), which resulted in the endogenous production of siRNAs; (ii) direct transfection of synthetic double-stranded siRNAs. To further ensure that any observed consequences of siRNA silencing would be specific to BBS4 knockdown, we also generated three different, non-overlapping BBS4-specific sequences which we used for both types of RNAi protocols (see Experimental Procedures).

Transfection of HeLa cells with BBS4 antisense sequences resulted in loss of BBS4 message on a northern blot at both 48h and 72h after transfection (Figure 2-7A). Real-time RT-PCR with human BBS4-specific primers also indicated a 30-fold reduction in BBS4 mRNA abundance (data not shown). The successful knockdown of BBS4 was further confirmed by immunocytochemistry with the anti-BBS4 antibody (Figure 2-7B). By observing >100 cells in multiple independent experiments, we estimate that most pSUPER-BBS4 or pSilencer-BBS4 transfected cells (≥90%) gave no perceptible immunofluorescence signal compared to control cells (Figure 2-7B). The targeting was specific to BBS4 because scrambling the oligo sequence gave no loss of BBS4 message and targeting other genes by RNAi, including *BBS2*, did not affect *BBS4* expression as judged by real-time RT-PCR (data not shown). We transfected pSUPER-BBS4 into HeLa cells and assessed the cellular phenotype. In agreement with our hypothesis, we observed that in the absence of BBS4, PCM1 became completely dispersed in the cytosol (Figure 2-7C). This was confirmed, and found to be specific, by analyzing COS-7 cells transfected with three different pSilencer-BBS4 vectors (encoding different siRNA sequences), and by observing HeLa and HEK 293 cells transfected with three different synthesized siRNA sequences (data not shown). Negative controls, which had no effect on the localization of PCM1, included empty vectors or scrambled (control) sequences.

Given the interaction of BBS4 with PCM1, and the involvement of PCM1 in the proper anchoring of microtubules at the centrosome, we also addressed whether the organization of the microtubule network is disrupted in BBS4 knockdown cells by immunostaining with an anti-α-tubulin antibody. In addition to HeLa or HEK 293 cells (Figure 2-7D, left panel), we also examined COS-7 cells because they possess a distinct,

radiating microtubule array. When transformed with three different pSilencer-BBS4 knockdown vectors, but not a control vector, COS-7 cells displayed a striking microtubule staining pattern consistent with a failure to anchor at the centrosome; in all cells showing loss of BBS4 signal and therefore PCM1 mislocalization, the microtubule network either showed a disorganized array emanating crudely from the outer edges of the nucleus, or was more extensively dispersed and formed bundles close to the cell periphery (Figure 2-7D, two middle panels). This phenotype is due to defective microtubule anchoring, not nucleation, since regrowth of microtubules in control cells (Figure 2-7E, top three panels) and BBS4-depleted cells (Figure 2-7E, bottom three panels) was essentially identical following transient treatment with nocodazole.

HeLa cells transfected with pSUPER-BBS4 fail to divide, a defect also observed upon transfection of synthetic BBS4 siRNA oligonucleotides in various cell types. This implicates BBS4 in cell cycle processes. Furthermore, individual BBS4-depleted COS-7, HeLa and HEK 293 cells often display two or more nuclei of variable sizes (Figure 2-7F). Notably, such multinucleated cells always contain replicated centrioles, as we consistently observed greater than two distinct γ-tubulin staining spots (Figure 2-8A).

To investigate this phenotype further, we performed fluorescence-activated cell sorting (FACS) cell cycle analyses on COS-7 control cells, nocodazole- and mimosine-treated cells, and cells transfected with two different pSilencer-BBS4 vectors, measuring their DNA content (n) with propidium iodide (Figure 2-7G and Figure 2-8B). Control cells showed a normal cell cycle profile with a majority of cells in the G1 phase (2n DNA content), and smaller cell populations undergoing DNA replication (S phase) and in the G2/M phase (4n DNA content); treatment with nocodazole presented the expected profile

of cells arrested in the G2 phase. A small proportion of nocodazole-treated cells were also apoptotic (<2n DNA content) or were exhibited greater than 4n DNA content—an indication of two rounds of DNA replication without cytokinesis. BBS4 knockdown cells showed a significant decrease in the number of G1 phase cells and a concomitant increase in the number of apoptotic cells and cells with a DNA content > 4n, suggesting that a proportion of BBS4-depleted cells fail to undergo cell division.

We confirmed that BBS4-depleted cells were prone to undergo apoptosis by using the TdT-mediated dUTP nick end-labeling (TUNEL) assay, where we found that siRNA-treated cells had a significantly greater proportion of apoptotic cells (12.5% and 7.6% for si27 and si831 siRNAs, respectively), compared to untreated cells (0.4%) or to cells transfected with a scrambled siRNA sequence (0.2%) (Figure 2-7H).

2.4.7 BBS4 and PCM1 localize to tissues relevant to BBS

The severe effect of disrupting the function of BBS4 in cultured mammalian cells might suggest that null mutations are not compatible with viability in humans, but this is not the case. But the BBS4-PCM1 interaction may be found in only a subset of differentiated cell types whose malfunction would not compromise organismal viability but may account for the specific, yet pleiotropic, BBS phenotype. To investigate this, we determined the relative localization of BBS4 and PCM1 by staining consecutive sections of various mouse organs and embryos with antibodies to BBS4 and PCM1. Each protein was expressed in only a subset of tissues, and BBS4 and PCM1 colocalized in some, but not all, cell types. For example, we detected identical staining in the cell bodies of neurons in the adult hippocampus and dentate gyrus (Figure 2-9A, B). Consistent with the predicted involvement of both proteins with ciliogenesis and ciliary function, we

observed identical localization in several ciliated tissues, including the ciliated border of bronchioles (Figure 2-9C, D) and olfactory epithelium (Figure 2-9I, J). In the retina, BBS4 was expressed in several layers, but the two proteins colocalized only in the inner photoreceptor segment and not in the outer nuclear layer (Figure 2-9E, F). Such specific colocalization was also found in other tissues, such as the developing pericardium and interdigital epithelium, but not in chondrocytes (Figure 2-9G, H, K, L).

2.5 Discussion

In this study, we show that BBS4, one of at least eight proteins involved in the pathogenesis of Bardet-Biedl syndrome (BBS), is a pericentriolar protein that plays a central role in recruiting cargo to centriolar satellites and allowing for the formation of a functional centrosomal microtubule organizing center (MTOC). From our data, we propose a model that describes the normal cellular role of BBS4, as well as the effects caused by a loss of BBS4 function in patients with the syndrome (Figure 2-10). According to this model, BBS4 forms a stable complex with PCM1, and both proteins co-localize to the centriolar satellites of centrosomes. Depletion of BBS4 by siRNA-mediated silencing results in the dispersal of PCM1 to the cytosol, loss of microtubule radiation from the centrosome, alteration of cell cycle dynamics, and an increased incidence of apoptotic cell death. Given that PCM1 is necessary for recruiting several proteins (e.g., centrin, pericentrin and ninein) to the centrosome and that it is also required for microtubule anchoring and cell cycle progression (Balczon et al., 1999; Dammermann and Merdes, 2002; Kubo et al., 1999; Young et al., 2000), we propose that at least some of the cellular defects in BBS4-deficient cells are due to a loss of a functional interaction between BBS4 and PCM1.

Thus, in normal cells, BBS4 modulates the recruitment of PCM1 (and probably its associated proteins) to the pericentriolar region, permitting the proper anchoring and radiation of centrosomal microtubules (Figure 2-8A). BBS4 also interacts with the $p150^{glued}$ subunit of the dynactin-dynein microtubule-based molecular motor, suggesting that BBS4 is directly involved in the transport of PCM1 to the centrosomal satellites by acting as an adaptor protein. Evidence for this hypothesis comes from our observation that disrupting dynein function prevents BBS4 and PCM1 from coalescing near the centrosome. Alternatively, or in addition, both proteins are trafficked independently and the specific interaction of BBS4 with PCM1 may be needed for retaining PCM1 in its correct cellular location.

Based on the severe effect of disrupting the function of BBS4 in cultured mammalian cells, one might expect that such mutations would not be compatible with viability in humans, which is clearly not the case. One possibility is that in humans, BBS proteins are only produced and required in a subset of differentiated cell type(s) whose malfunction would not compromise viability but would account for the specific, yet, pleiotropic, BBS phenotype. Support for this notion comes from our finding that *C. elegans bbs* genes (*bbs-1*, *bbs-2*, *bbs-7* and *bbs-8*) are expressed exclusively in cells that harbor cilia, a finding that is remarkably consistent with the limited expression pattern of *BBS8* in mammalian tissue (Ansley et al., 2003). Alternatively, some BBS4 null cell types might escape by activating alternative pathways capable of rescuing the phenotype, either by enabling PCM1 docking to the pericentriolar region or facilitating microtubule anchoring in the cytoplasm.

BBS is a multisystemic disorder of significant interest because of its clinical overlap with a wide spectrum of complex traits that are prevalent in the general population, including obesity, kidney dysfunction, diabetes and blindness. To our knowledge, BBS is the first pleiotropic phenotype attributed to pericentriolar dysfunction, providing the opportunity to investigate the role of BBS4 and other centriole-associated proteins in complex traits that represent major health problems and are currently poorly understood.

2.6 Figures

Figure 2-1 BBS4 consists mostly of TPR repeats flanked by small N- and C-terminal regions.

a

regions	sequence	amino acids	motifs
N	MAEERVATRTQFPVSTESQKPRQKKAPEFPI	1-31	N-terminal region
1	LEKQNWLIHLHYIRKDYEACKAVIKEQLQETQGLC	32-66	TPR? (14/34)
2	EYAIYVQALIFRLEGNIQESLELFQTCAVLSPQS	67-100	TPR (15/34)
3	ADNLKQVARSLFLLGKHKAAIEVYNEAAKLNQKD	101-134	TPR (22/34)
4	WEISHNLGVCYIYLKQFNKAQDQLHNALNLNRHD	135-168	TPR (17/34)
5	-LTYIMLGKIHLLEGDLDKAIEVYKKAVEFSPEN	169-201	TPR (23/34)
6	TELLTTLGLLYLQLGIYQKAFEHLGNALTYDPTN	202-235	TPR (19/34)
7	YKAILAAGSMMQTHGDFDVALTKYRVVACAVPES	236-269	TPR? (19/34)
8	PPLWNNIGMCFFGKKKYVAAISCLKRANYLAPFD	270-303	TPR (21/34)
9	WKILYNLGLVHLTMQQYASAFHFLSAAINFQPKM	304-337	TPR (13/34)
10	GELYMLLAVALTNLEDTENAKRAYAEAVHLDKCN	338-371	TPR (19/34)
11	PLVNLNYAVLLYNQGEKKNALAQYQEMEKKVSLLKDNSSLEF	372-413	TPR? (14/34)
12	DSEMVEMAQKLGAALQVGEALVWTKPVKDPKSKHQ	414-448	TPR? (10/34)
13	TTSTSKPASFQQPLGSNQALGQAMSSAAAYRTLP	449-482	TPR? (11/34)
C	SGAGGTSQFTKPPSLPLEPEPAVESSPTETSEQIREK	483-519	C-terminal region
	spsatslGpsatptucaccAlcsap+ALclsPss TPR consensus		

b

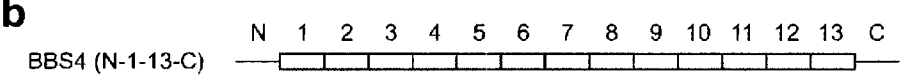

(a) Amino acid sequence of human BBS4 and alignment of its 13 putative TPR motifs. Residues are highlighted in gray if they match the corresponding consensus residue present in 50% of a TPR motif as defined by the SMART database (Schultz et al., 2000). Regions predicted to be TPR motifs are labeled "TPR", and those not predicted but may be *bona fide* TPRs are labeled "TPR?", followed by the number of residues (out of 34) matching the consensus. The consensus TPR motifs represent actual amino acids (uppercase) or denote charged (c; amino acids DEHKR), aliphatic (l; ILV), aromatic (a; FWYH), polar (p; CDEHKNQRST), positive (+; HKR), small (s; ACDGNPSTV), tiny (u; AGS) or turnlike (t; ACDEGHKNQRST). Bold, underlined residues in the alignment and consensus sequence are predicted to form α-helices according to the secondary structure prediction algorithm JPRED. **(b) Schematic of BBS4 domain architecture.**

Figure 2-2 BBS4 interacts with PCM1.

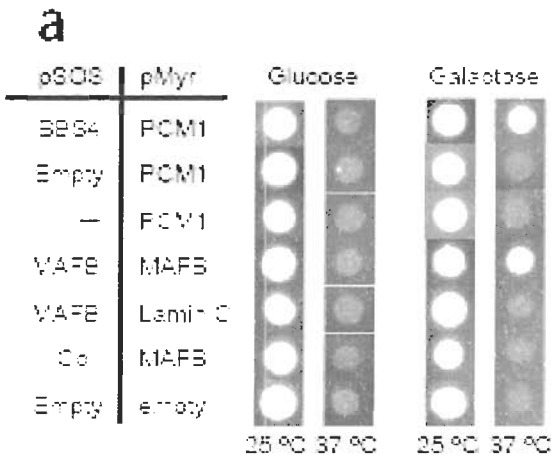

(a) BBS4 interacts specifically with PCM1 by yeast two-hybrid. Colonies expressing both full-length BBS4 bait fused to pSOS and pMyr-PCM1 (amino acids 1574 to 2024) fused at its N-terminus with a myristylation sequence can survive on galactose at a non-permissive temperature. Positive (MAFB, which homodimerizes) and negative (MAFB and Lamin C, or Coll and MAFB) controls are also shown. This experiment was conducted by Jose Badano and Sonja Sibold

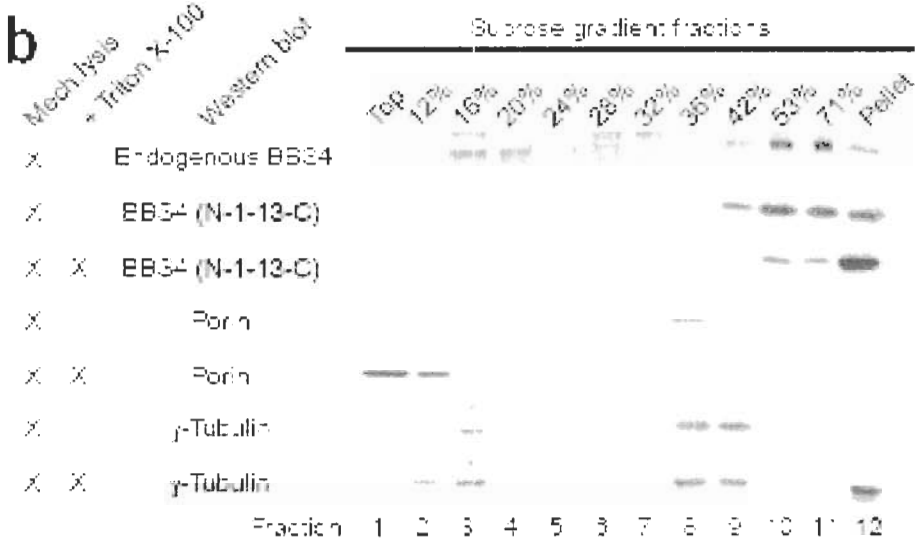

(b) BBS4 and γ-tubulin are cofractionated in discontinuous sucrose gradient. BBS4 is present in high-molecular weight fractions coinciding with the centrosomal fractions of γ-tubulin (fractions 10 and 11). Porin is a mitochondrial protein that is released to a soluble form (top of gradient) in detergent, a behavior that is different from that of BBS4 and γ-tubulin. This experiment was conducted by Muneer Esmail.

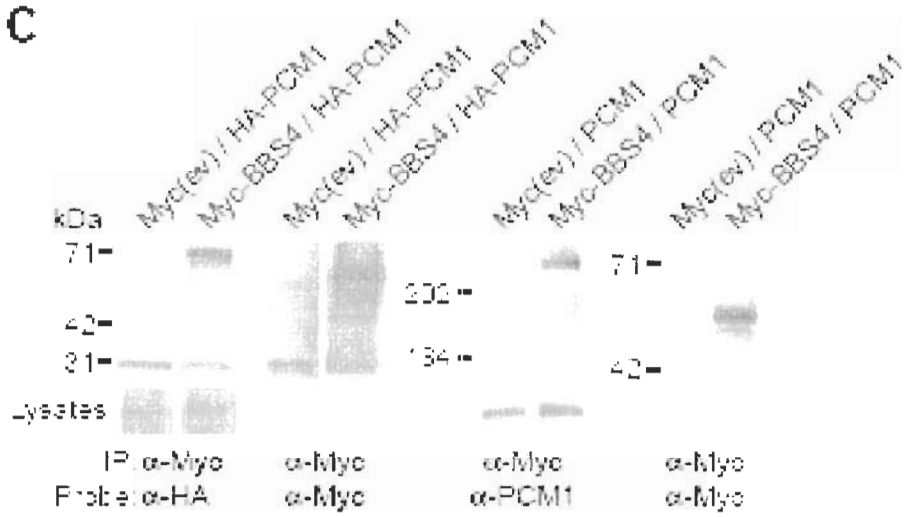

(c) **BBS4 interacts with PCM1.** Two panels on the left: approximately 2.2 mg of protein from supernatant of HEK 293 cell lysates transiently expressing constructs (as indicated) were immunoprecipitated with an anti-Myc monoclonal antibody and Western blotted with an anti-HA antibody. Myc-BBS4 but not Myc-empty vector (ev) co-immunoprecipitates PCM1 (HA-PCM1, ~70 kDa protein species). The control lanes show Myc-BBS4 (58 kDa) expression using the anti-Myc. Two panels on the right: to detect the interaction between BBS4 and endogenous PCM1, approximately 10 mg of protein from lysates of cells transfected with Myc-BBS4 were immunoprecipitated with the anti-Myc monoclonal antibody and western-blotted with a polyclonal anti-PCM1 antibody; a band corresponding to the endogenous 220 kDa PCM1 protein was detected only in cells transfected with Myc-BBS4. The control Myc-BBS4 expression is also shown.

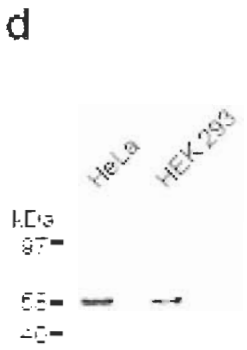

(d) Western blot analysis of total HeLa and HEK 293 protein extracts with affinity-purified polyclonal antibody against the human BBS4 protein.

Figure 2-3 BBS4 is a pericentriolar protein associated with centrosomes and basal bodies.

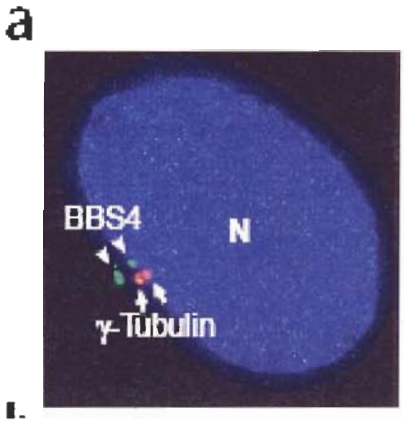

(a) BBS4 localizes at a pericentriolar region. Co-immunofluorescence staining in HeLa cells using an antibody against endogenous BBS4 (green) and a γ-tubulin-specific antibody (red) which marks the centrosome.

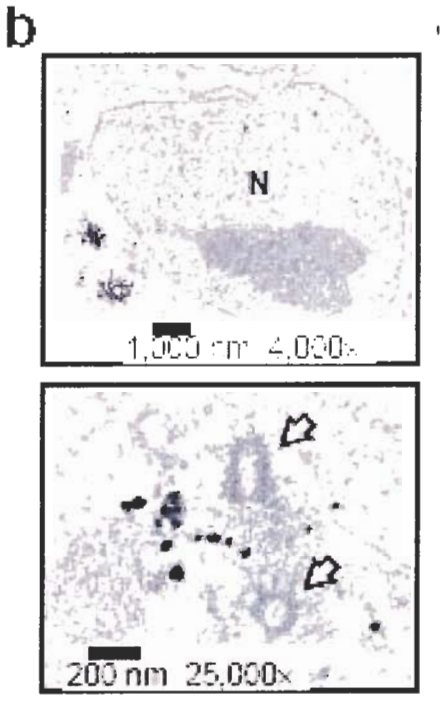

(b) Transmission Electron Micrographs (TEMs) of immunogold-stained BBS4 shows electron-dense spots at perinuclear (top panel) and pericentriolar (bottom panel) positions. Arrows denote centrioles and N represents the nucleus. (This experiment was conducted through the collaboration with Dr. Philip Beales).

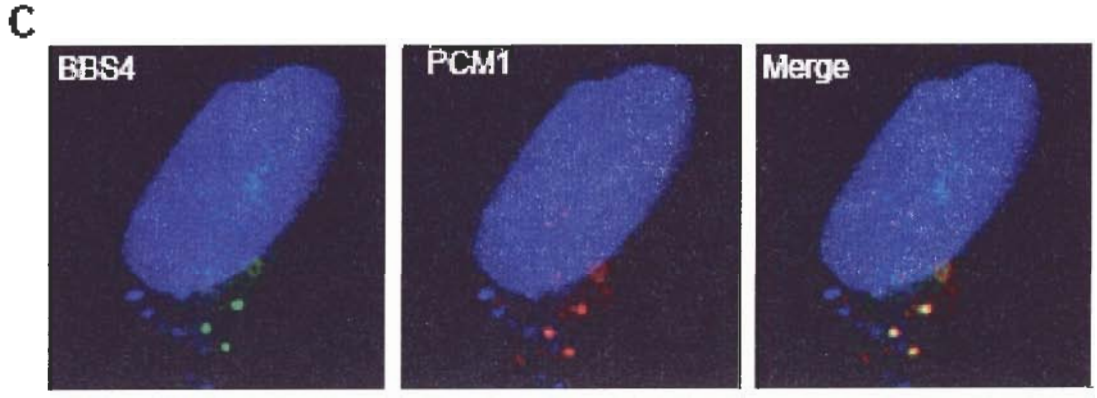

(c) BBS4 and PCM1 are colocalized in the cell. Higher-resolution deconvolution images showing that the signal from BBS4 (green, left panel) and PCM1 (red, middle panel) overlap in HeLa cells (yellow, right panel).

d

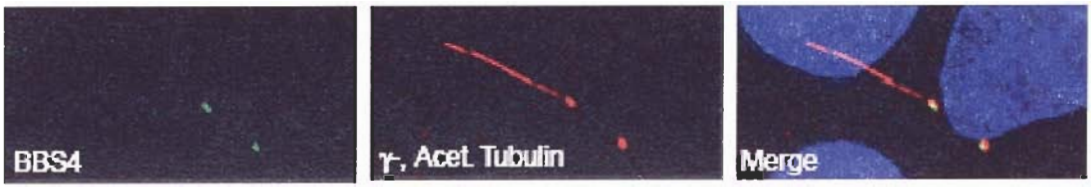

(d) BBS4 specifically localizes near the basal body in IMCD3 cells. The BBS4 signals (green, left panel) overlap those of the mother centriole (basal body emanating a primary cilium) and daughter centriole (middle and right panels). The centrioles are detected with an anti-γ-tubulin antibody, and the cilium is stained with an antibody against acetylated tubulin (both are red).

e

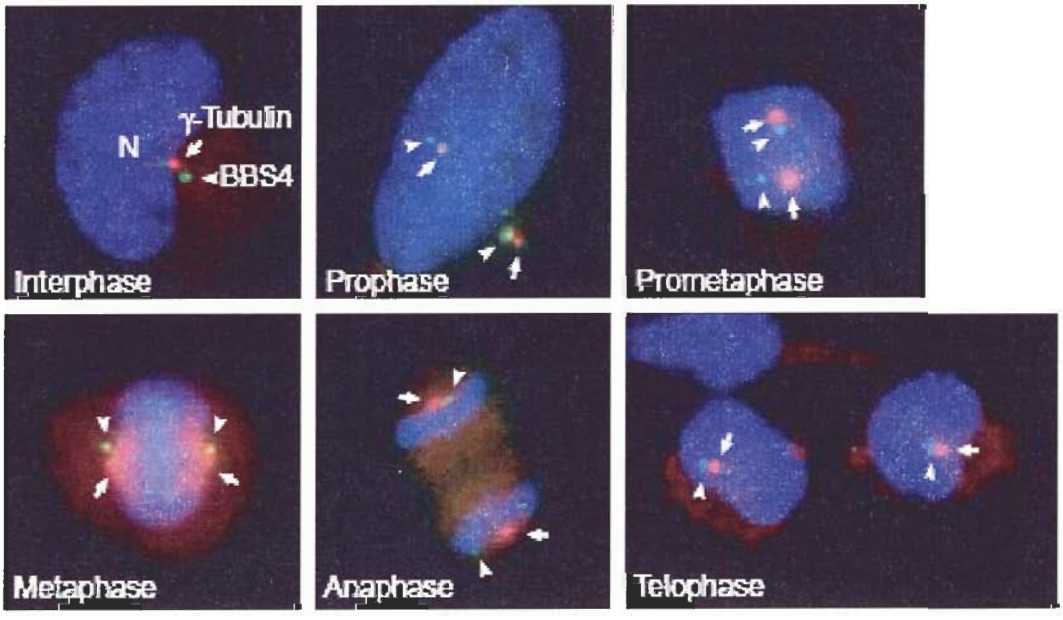

(e) BBS4 retains its pericentrosomal association during all phases of the cell cycle. HeLa cells were synchronized and co-stained with antibodies against BBS4 and γ-tubulin. Arrowheads mark BBS4 signals (green), and arrows denote γ-tubulin staining (red). Cell cycle stages are indicated in each panel.

Figure 2-4 BBS4 localization to centrosomal satellites depends on both N- and C-terminal TPRs

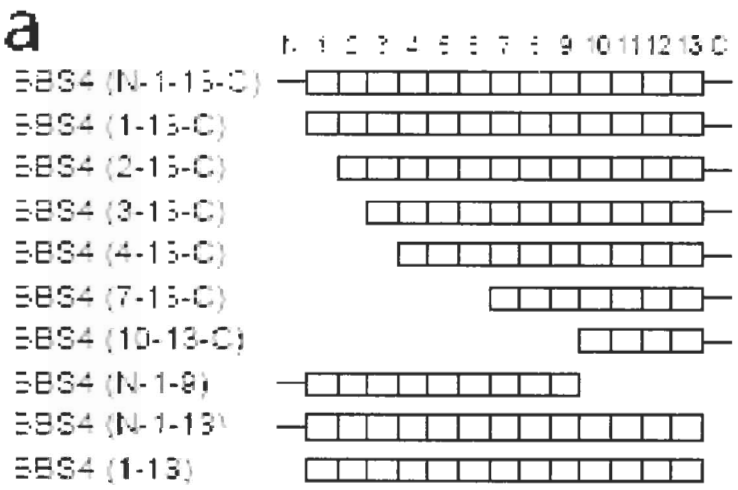

(a) Schematic representation of Myc-tagged full-length BBS4 and of nine truncation mutants. The nomenclature of the constructs and the sequences of the different BBS4 segments is detailed in Figure 2-1.

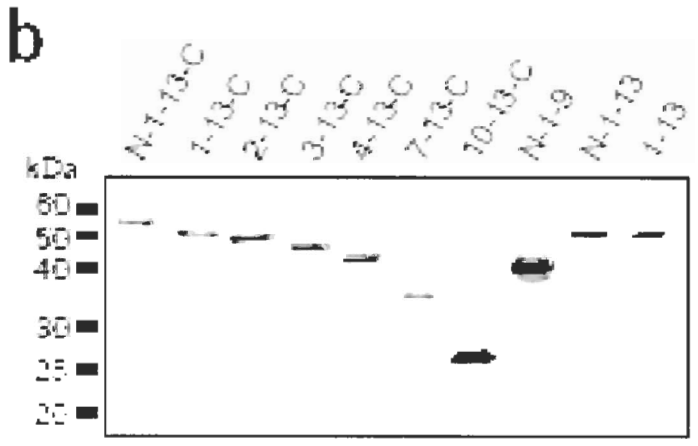

(b) Transient expression of Myc-tagged BBS4 trancation mutants. Western blot (using an anti-Myc antibody) of extracts from HeLa cells expressing Myc-tagged full-length and truncation BBS4 constructs shows that the proteins produced are of the predicted size.

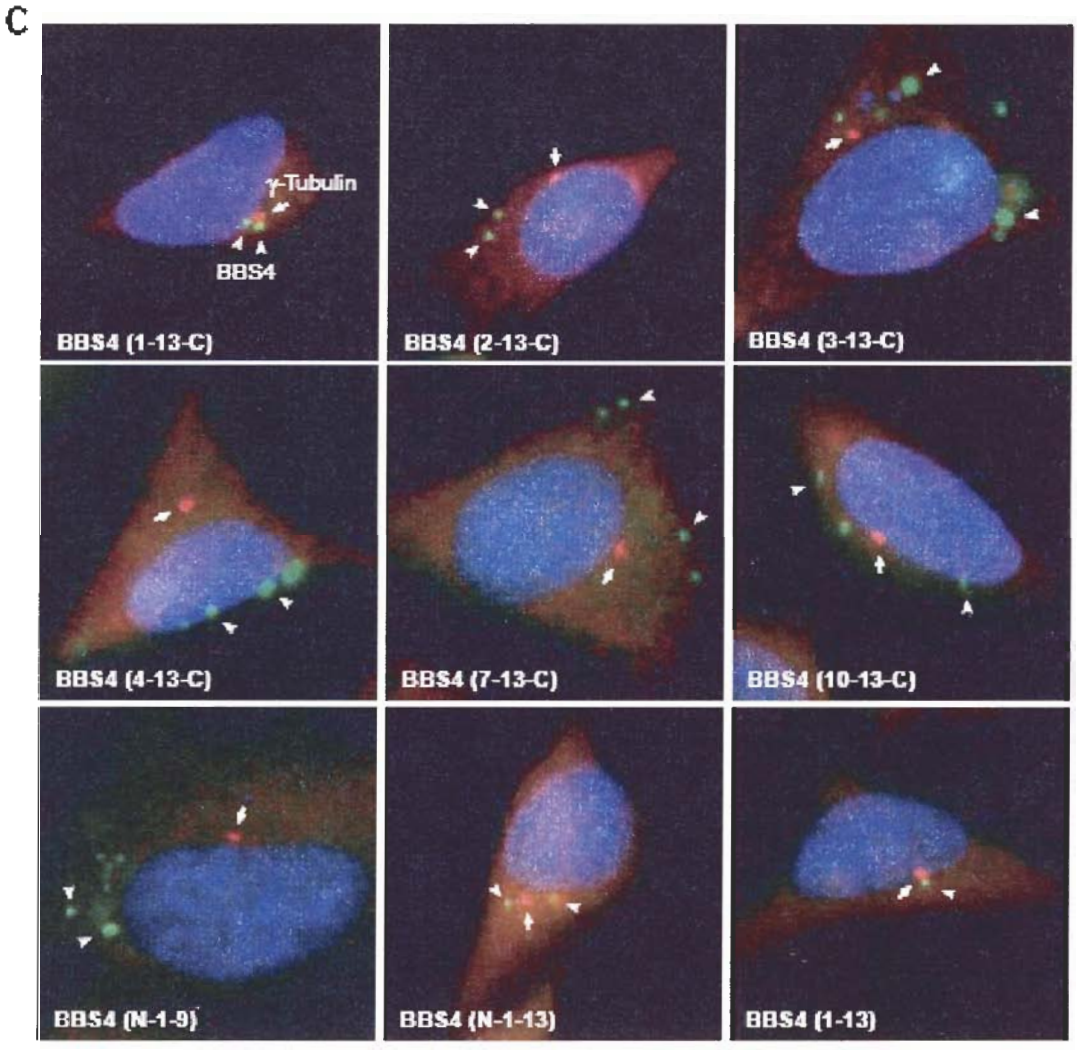

(c) Immunolocalization of the Myc-tagged BBS4 truncation constructs in HeLa cells. BBS4 was detected using an anti-Myc antibody, and cells were co-stained with γ-tubulin. Arrowheads point to BBS4 signals (green), and arrows denote γ-tubulin signals (red).

Figure 2-5 Incorrect BBS4 localization affects the behavior of PCM1.

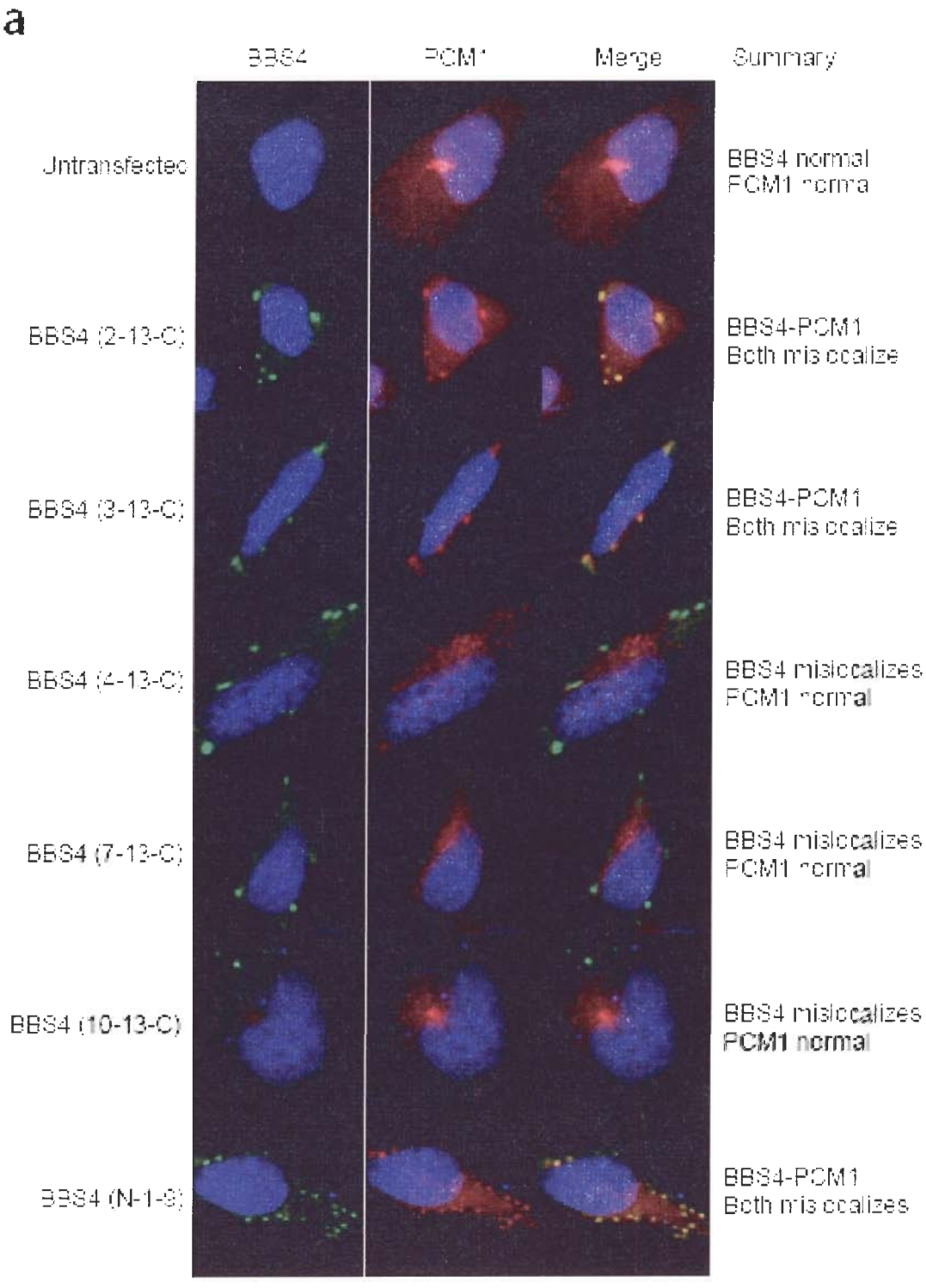

(a) PCM1 localization to the pericentrosomal region is affected when some Myc-tagged truncated BBS4 constructs are expressed in HeLa cells. Co-staining with antibodies against the Myc tag (left panels, green) and endogenous PCM1 (middle panels, red) shows proper PCM1 localization in untransfected cells and cells expressing BBS4 (4-13-C, 7-13-C, 10-13-C), or co-mislocalization with BBS4 in cells expressing BBS4 (2-13-C, 3-13-C and N-1-9).

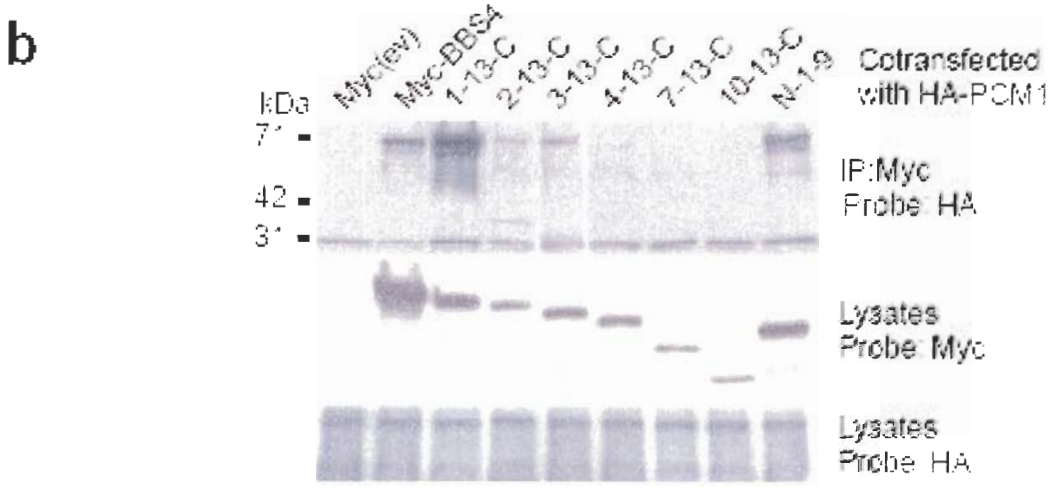

(b) Interaction of truncated BBS4 proteins with PCM1 as detected by co-immunoprecipitations. HEK 293 cells were transfected with each Myc-tagged truncated BBS4 construct. Equal amounts (~2.5mg) of protein extracts were immunoprecipitated with an anti-Myc antibody and Western blotted with anti-HA antibody to detect HA-PCM1 (~70 kDa). Note that deletion of the third TPR domain in BBS4 significantly weakens the BBS4-PCM1 interaction (i.e., compare 3-13-C with 4-13-C), whereas deletion of additional TPRs abolishes all detectable interaction.

Figure 2-6 BBS4 dependence and interaction with the dynein complex.

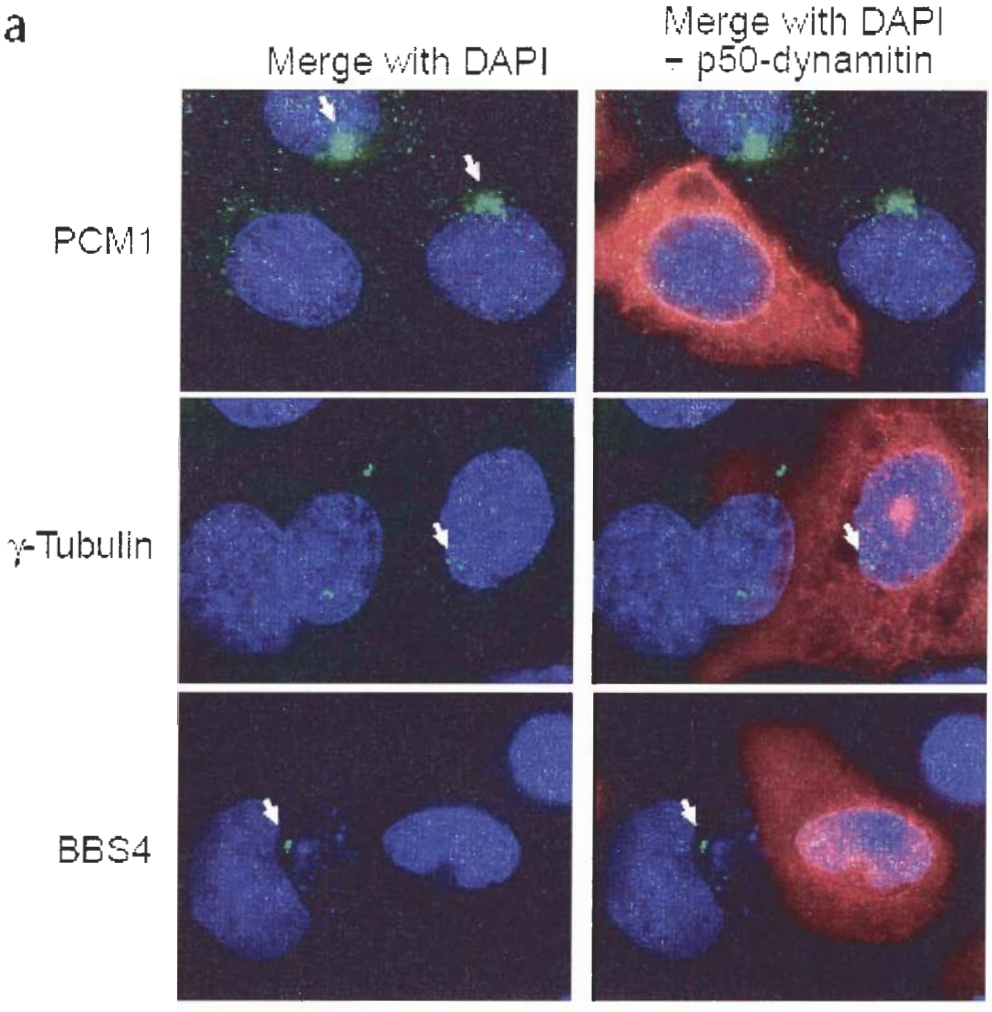

(a) BBS4 is delivered to the centrosome by the dynein motor dependent manner. HeLa cells were transfected with a Myc-tagged p50-dynamitin construct to inhibit dynein function, and were co-stained with different antibodies. The top two panels show correct PCM1 localization (green) in untransfected cells (left panel), but a diffuse cytosolic staining pattern in p50-dynamitin-transfected cells (red, right panel). The middle two panels show a control experiment, wherein γ-tubulin localization (red, shown with an arrow in the left panel) is not affected by p50-dynamitin overexpression (green, right panel). The bottom two panels show the correct perinuclear location of BBS4 in untransfected cells (left panel; arrowhead) and the loss of perinuclear signal in p50-dynamitin transfected cells (right panel).

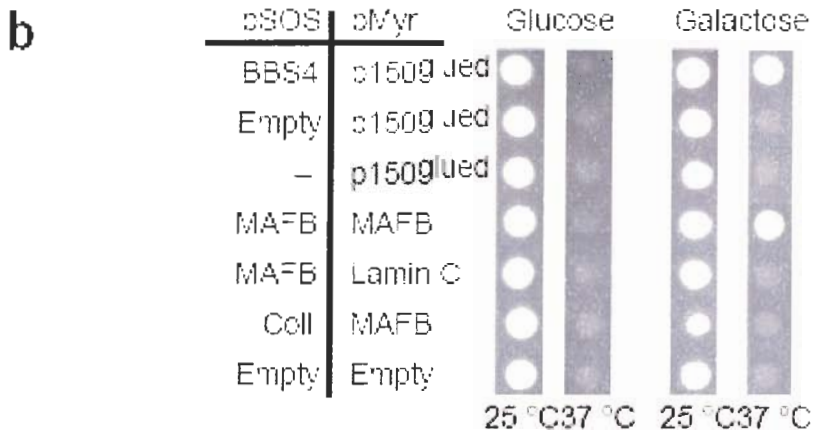

(b) BBS4 interacts with p150^{glued}. Colonies expressing both full-length BBS4 bait fused to pSOS and pMyr- p150^{glued} (amino acids 1022-1170) fused at its N-terminus with a myristylation sequence can survive on galactose at a non-permissive temperature. Positive and negative controls are also shown. This experiment was conducted by Jose Badano and Sonja Sibold.

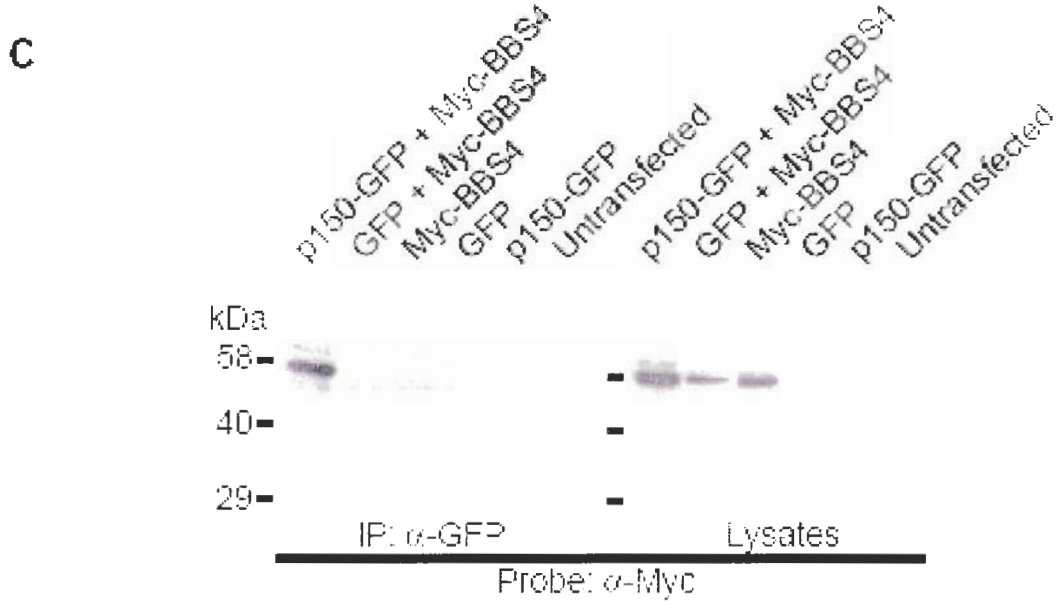

(c) BBS4 and p150^{glued} are co-immunoprecipitated. Western blotting of cell extracts expressing p150-GFP, Myc-BBS4 or empty vectors show specific interaction between BBS4 and p150^{glued}, since Myc-BBS4 can only be detected in the presence of GFP-p150.

Figure 2-7 Loss of BBS4 function leads to PCM1 dispersal, microtubule de-anchoring from centrosomes, cell division arrest and induction of apoptosis.

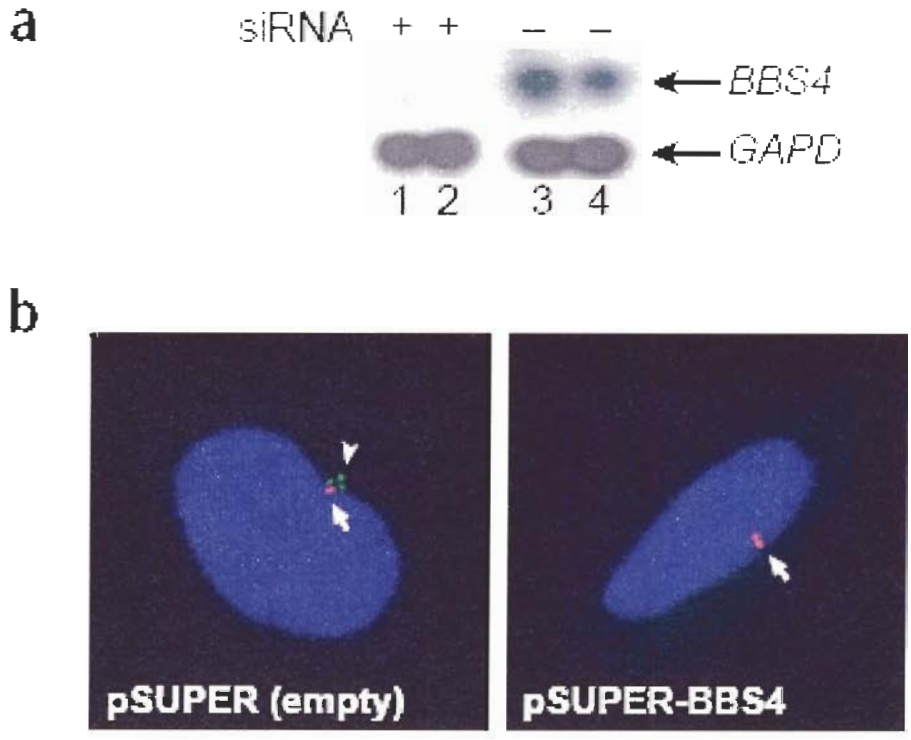

(**a**) Northern blot analysis of HeLa cells untrasfected and transfected with siRNA oligos at 24h (lanes 1 and 3) and 72h (lanes 2 and 4) after transfection. In cells transfected with antisense siRNA oligos, *BBS4* mRNA is undetectable at both timepoints.

(**b**)Expression of pSUPER-BBS4 vector in HeLa cells causes loss of the BBS4 signal near the centrosome. Cells were transfected with empty pSUPER vector (left panel), or with pSUPER-BBS4 (right panel), and immunocytochemistry was performed using antibodies against endogenous BBS4 (green; shown as arrowhead) and γ-tubulin (red; marked with arrow). Note the absence of a BBS4 signal in cells expressing the BBS4 siRNA.

c

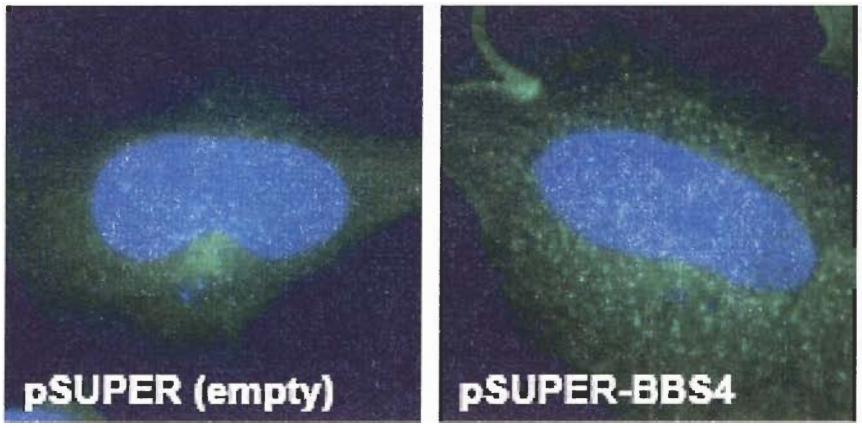

(c) Loss of BBS4 function leads to PCM1 dispersal. HeLa cells transfected with the control pSUPER vector show proper perinuclear localization of PCM1 (green, left panel), but those transfected with pSUPER-BBS4 show a dispersion of the PCM1 signal to the cytosol (right panel).

d

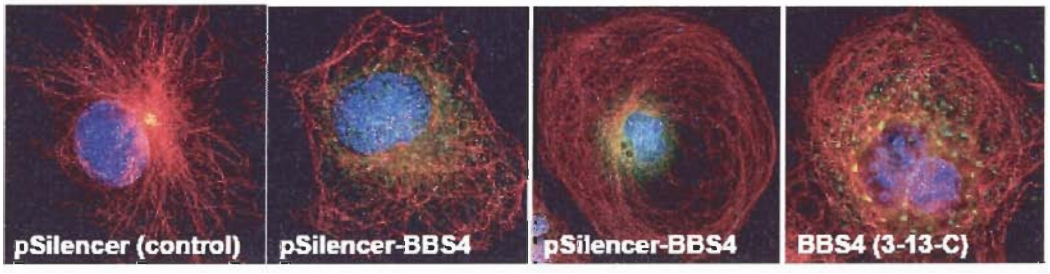

(d) Loss of BBS4 function leads to PCM1 dispersal and concomitant microtubule de-anchoring from centrosomes. Compared to COS-7 cells transfected with a pSilencer(control) vector, which have a very characteristic tubulin network radiating from the centrosome, COS-7 cells expressing a pSilencer-BBS4 knockdown vector (two middle panels, showing PCM1 staining in green) or expressing the Myc-tagged BBS4 (3-13-C) construct (green, right panel) have disorganized tubulin staining patterns, as detected by immunofluorescence staining with an anti-α-tubulin antibody (red). Cells are co-stained using an anti-PCM1 antibody (left and middle panels) and an anti-Myc antibody (right panel).

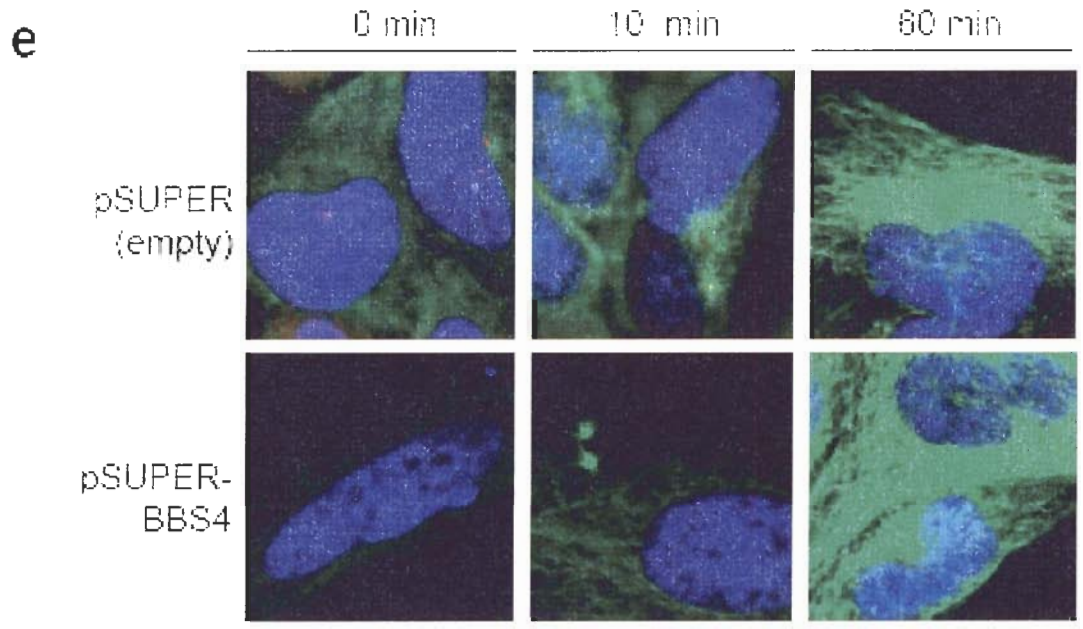

(e) Loss of BBS4 function does not affect the microtubule nucleation activity. Microtubule nucleation and regrowth after nocodazole treatment is as efficient in HeLa cells depleted of BBS4 (lower panels) compared to untransfected cells (upper panels). Microtubules were immunostained with an anti-α-tubulin antibody at the time points shown.

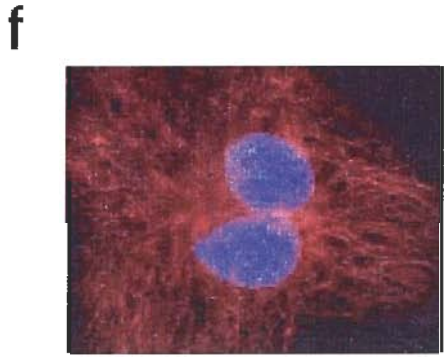

(f) *BBS4*-silenced cells are often binucleated. COS-7 cell expressing pSilencer-BBS4 construct was stained with DAPI and an anti-α-tubulin antibody.

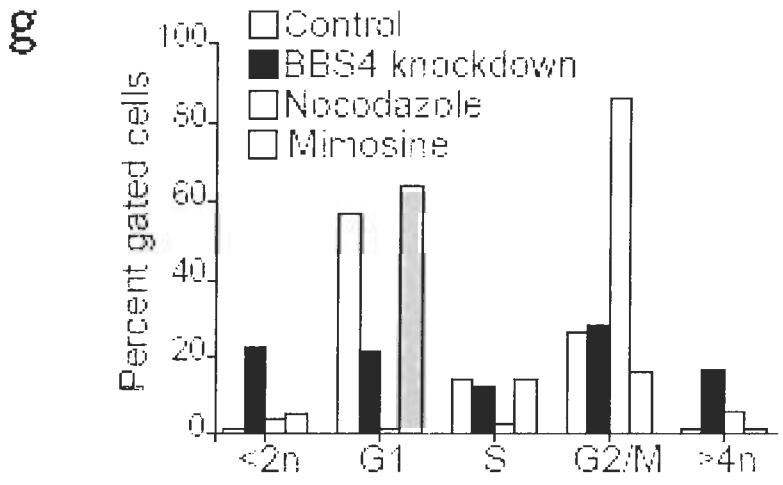

(g) BBS4 knock-down induces aberrant cell cycle distribution. Graph showing the results from FACS analyses performed on COS-7 control cells (white bars), cells expressing pSilencer-BBS4 vector (black), and cells treated with nocodazole (light gray) or mimosine (dark gray). The Y axis represents the percent of cells showing DNA staining intensities corresponding to <2n, G1, S and G2/M cell cycle phases, and >4n, as shown on the X axis. Raw FACS plots are shown in Figure 2-8B.

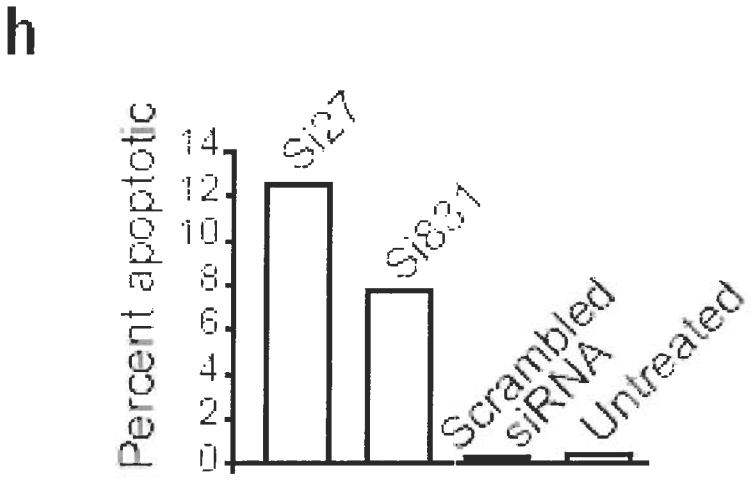

(h) BBS4 knock-down induces apoptosis. Graph of the results from TUNEL assays performed on untreated HeLa cells, or cells transfected with siRNA oligonucleotides (si27 and si831) or a scrambled siRNA sequence. The Y axis displays the percent apoptotic cells in each category of cells. (This experiment was conducted through the collaboration with Dr. Philip Beales).

Figure 2-8 Cytokinesis defects in BBS4-depleted cells.

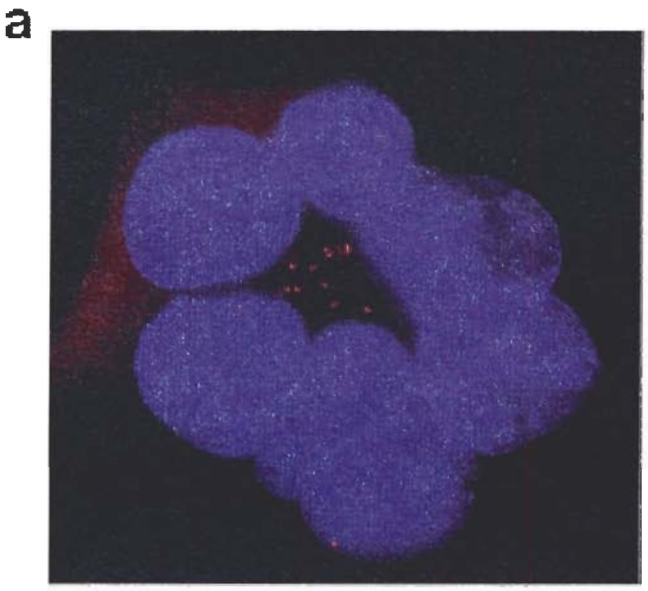

(a) BBS4 knock-down cells show multinuclear and abnormal centrosome duplication phenotypes. Typical multinucleated cell in which centrioles have replicated (stained with γ-tubulin) but plasma membranes have not formed. Nuclei were stained with DAPI (blue) and centrosome with γ-tubulin antibody (red)

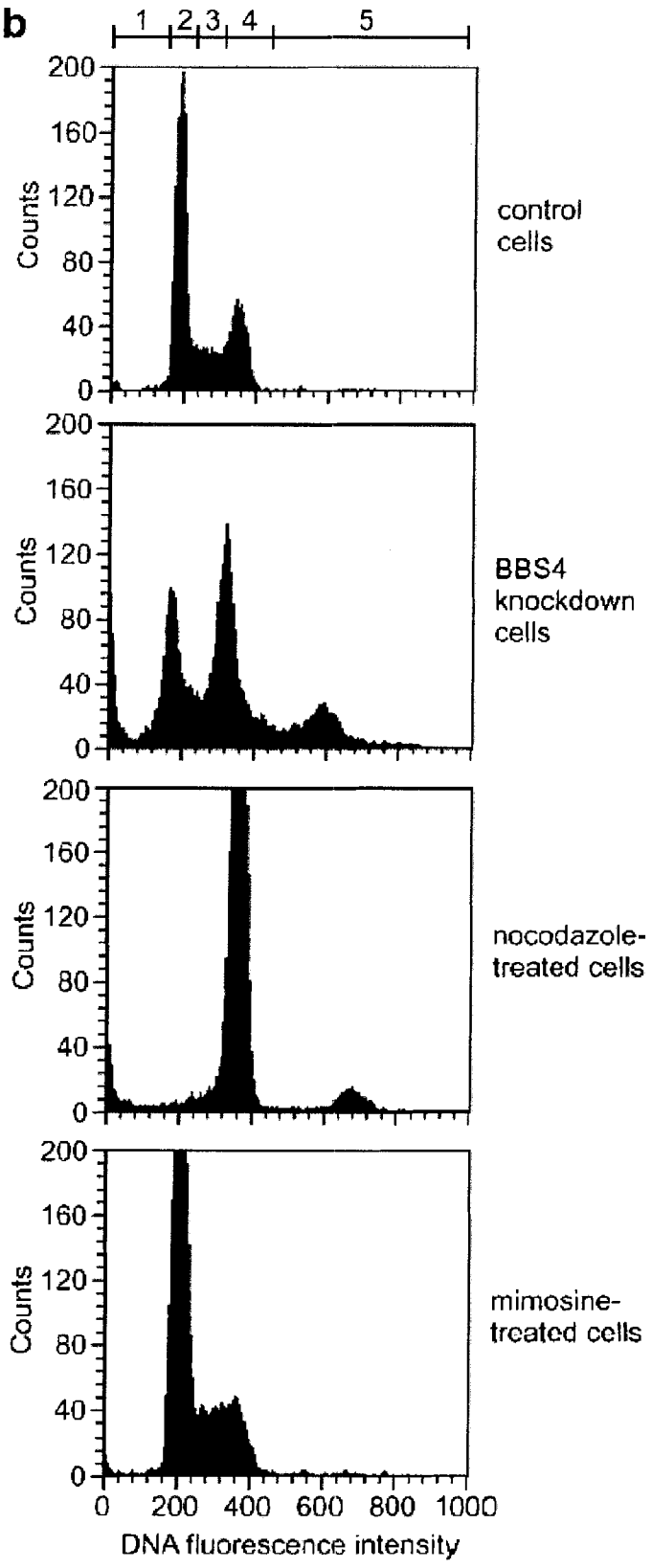
b
1
2
3
4
5
Counts
200
160
120
80
40
0
control cells
BBS4 knockdown cells
nocodazole-treated cells
mimosine-treated cells
0
200
400
600
800
1000
DNA fluorescence intensity

(b) BBS4 knock-down cells fail to undergo cell division. FACS analysis of control, BBS4-depleted cells, and cells treated with the microtubule depolymerization drug nocodazole, and mimosine, which cause cell cycle arrests at the G2/M and G1/S boundaries, respectively. Results are shown as graphs of total cell count on the Y axis and relative DNA fluorescence intensity on the X axis. Cells were classified according to five categories (shown on top of the graphs), based on DNA content: 1, <2n; 2, 2n (G1 phase); 3, between 2n and 4n (S phase); 4, 4n (G2/M phase); 5, > 4n. (This experiment was conducted by the collaboration with Muneer Esmail at Dr. Michel Leroux laboratory).

Figure 2-9 Histological localization of BBS4 and PCM1.

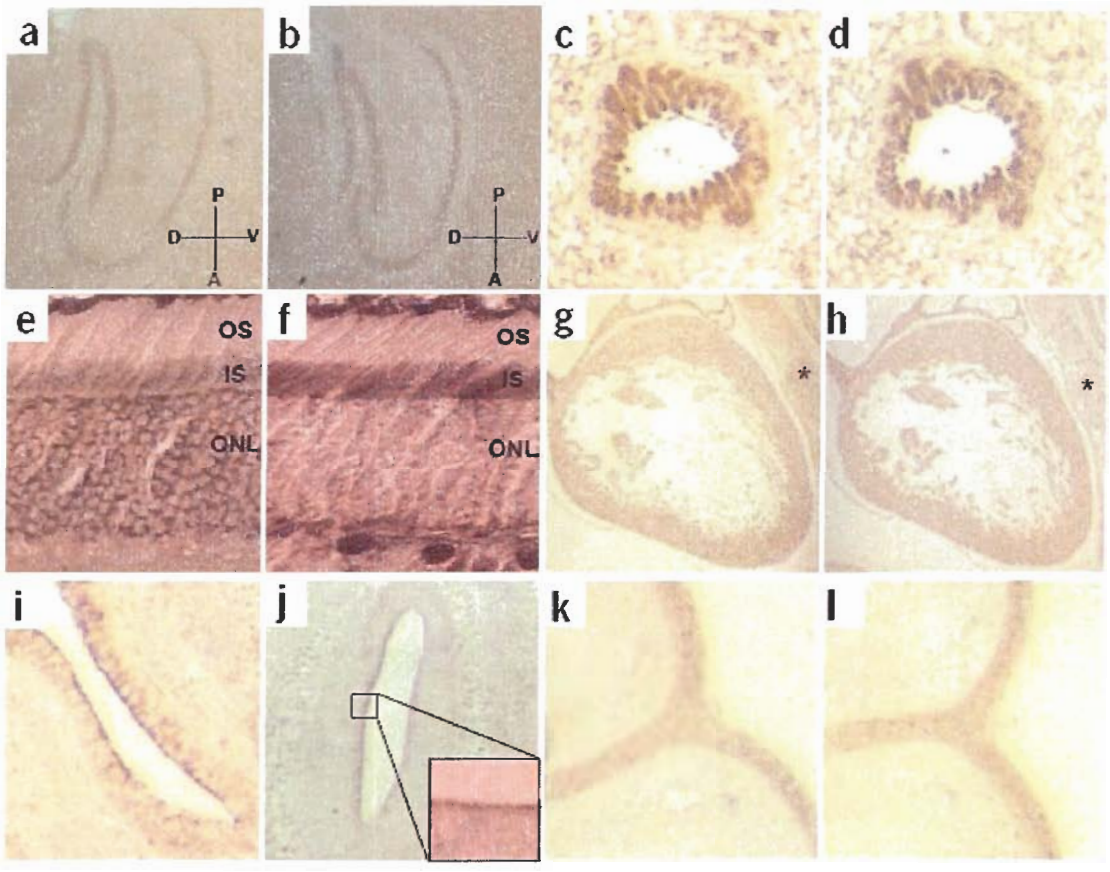

(a-i) BBS4 and PCM1 localize to tissues relevant to BBS. BBS4 (a) and PCM1 (b) have identical localization throughout the adult mouse hippocampus and dentate gyrus. The cross indicates dorsoventral (DV) and anteroposterior (AP) orientation. (c,d) In the adult mouse lung, both proteins are found in columnar epithelial cells of bronchioles. (e) Adult mouse retina showing BBS4 in the outer nuclear layer (ONL) and the inner segment (IS). By contrast, PCM1 is detected in the inner segment but not the outer nuclear layer (f). OS, outer segment. (g,h) BBS4 and PCM1 are both detectable in the pericardium of an E16 mouse embryo, but only BBS4 can be detected in chondrocytes (asterisk). (i,j) Both proteins are prominent in the olfactory epithelium. Inset, a magnified image of the boxed area, with most of the signal concentrated at the ciliated border. (k,l) Strong expression of BBS4 and PCM1 in the epidermal layer surrounding the digits of an E16 mouse embryo. All images are at 10× magnification, except e, f and the inset in j, which are at 64× magnification. This experiment was conducted by Carmen Leitech.

Figure 2-10 Model of BBS4 (dys)function.

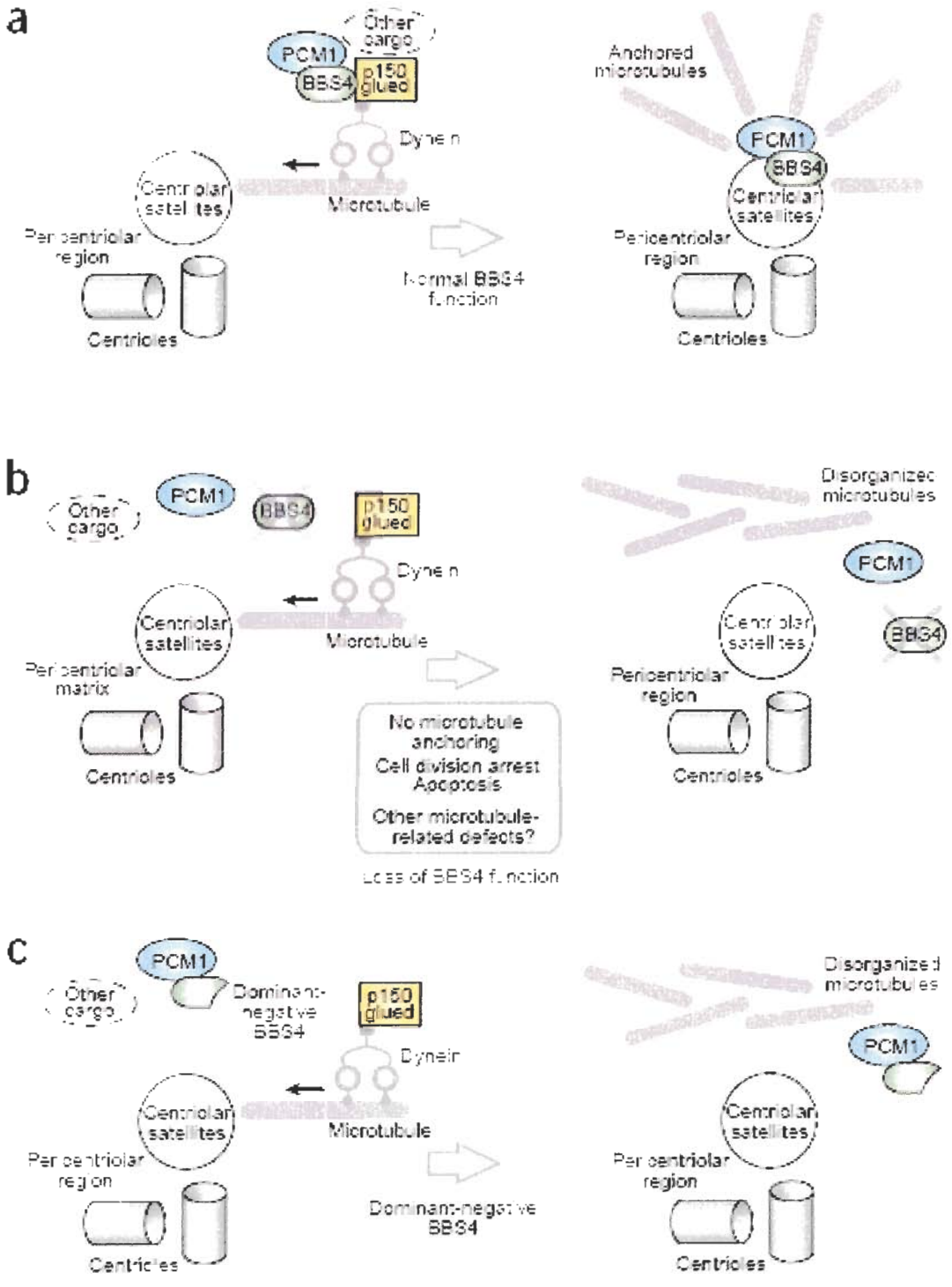

(a) Normal BBS4 function: BBS4 recruits PCM and associated cargo to the centriolar satellites in a dynein-dependent manner through its interactions with $p150^{glued}$. **(b)** In the absence of BBS4, PCM1 and possibly its cargo do not localize to the centriolar satellites, leading to several cellular phenotypes. **(c)** Some BBS4 truncation mutants have an equally detrimental effect by inhibiting PCM1 localization to the centriolar satellites.

2.7 Reference list

Ansley, S. J., Badano, J. L., Blacque, O. E., Hill, J., Hoskins, B. E., Leitch, C. C., Kim, J. C., Ross, A. J., Eichers, E. R., Teslovich, T. M., et al. (2003). Basal body dysfunction is a likely cause of pleiotropic Bardet-Biedl syndrome. Nature 425, 628-633.

Badano, J. L., Ansley, S. J., Leitch, C. C., Lewis, R. A., Lupski, J. R., and Katsanis, N. (2003). Identification of a novel Bardet-Biedl syndrome protein, BBS7, that shares structural features with BBS1 and BBS2. Am J Hum Genet 72, 650-658.

Balczon, R., Bao, L., and Zimmer, W. E. (1994). PCM-1, A 228-kD centrosome autoantigen with a distinct cell cycle distribution. J Cell Biol 124, 783-793.

Balczon, R., Varden, C. E., and Schroer, T. A. (1999). Role for microtubules in centrosome doubling in Chinese hamster ovary cells. Cell Motil Cytoskeleton 42, 60-72.

Beales, P. L., Elcioglu, N., Woolf, A. S., Parker, D., and Flinter, F. A. (1999). New criteria for improved diagnosis of Bardet-Biedl syndrome: results of a population survey. J Med Genet 36, 437-446.

Beisson, J., and Wright, M. (2003). Basal body/centriole assembly and continuity. Curr Opin Cell Biol 15, 96-104.

Blatch, G. L., and Lassle, M. (1999). The tetratricopeptide repeat: a structural motif mediating protein-protein interactions. Bioessays 21, 932-939.

Bobinnec, Y., Khodjakov, A., Mir, L. M., Rieder, C. L., Edde, B., and Bornens, M. (1998). Centriole disassembly in vivo and its effect on centrosome structure and function in vertebrate cells. J Cell Biol 143, 1575-1589.

Dammermann, A., and Merdes, A. (2002). Assembly of centrosomal proteins and microtubule organization depends on PCM-1. J Cell Biol 159, 255-266.

Dictenberg, J. B., Zimmerman, W., Sparks, C. A., Young, A., Vidair, C., Zheng, Y., Carrington, W., Fay, F. S., and Doxsey, S. J. (1998). Pericentrin and gamma-tubulin form a protein complex and are organized into a novel lattice at the centrosome. J Cell Biol 141, 163-174.

Fan, Y., Esmail, M. A., Ansley, S. J., Blacque, O. E., Boroevich, K., Ross, A. J., Moore, S. J., Badano, J. L., May-Simera, H., Compton, D. S., et al. (2004). Mutations in a member of the Ras superfamily of small GTP-binding proteins causes Bardet-Biedl syndrome. Nat Genet 36, 989-993.

Katsanis, N., Ansley, S. J., Badano, J. L., Eichers, E. R., Lewis, R. A., Hoskins, B. E., Scambler, P. J., Davidson, W. S., Beales, P. L., and Lupski, J. R. (2001). Triallelic inheritance in Bardet-Biedl syndrome, a Mendelian recessive disorder. Science 293, 2256-2259.

Katsanis, N., Beales, P. L., Woods, M. O., Lewis, R. A., Green, J. S., Parfrey, P. S., Ansley, S. J., Davidson, W. S., and Lupski, J. R. (2000). Mutations in MKKS

cause obesity, retinal dystrophy and renal malformations associated with Bardet-Biedl syndrome. Nat Genet 26, 67-70.

Kubo, A., Sasaki, H., Yuba-Kubo, A., Tsukita, S., and Shiina, N. (1999). Centriolar satellites: molecular characterization, ATP-dependent movement toward centrioles and possible involvement in ciliogenesis. J Cell Biol 147, 969-980.

Kubo, A., and Tsukita, S. (2003). Non-membranous granular organelle consisting of PCM-1: subcellular distribution and cell-cycle-dependent assembly/disassembly. J Cell Sci 116, 919-928.

Moudjou, M., Bordes, N., Paintrand, M., and Bornens, M. (1996). gamma-Tubulin in mammalian cells: the centrosomal and the cytosolic forms. J Cell Sci 109 (Pt 4), 875-887.

Li, J. B., Gerdes, J. M., Haycraft, C. J., Fan, Y., Teslovich, T. M., May-Simera, H., Li, H., Blacque, O. E., Li, L., Leitch, C. C., et al. (2004). Comparative genomics identifies a flagellar and basal body proteome that includes the BBS5 human disease gene. Cell 117, 541-552.

Mykytyn, K., Braun, T., Carmi, R., Haider, N. B., Searby, C. C., Shastri, M., Beck, G., Wright, A. F., Iannaccone, A., Elbedour, K., et al. (2001). Identification of the gene that, when mutated, causes the human obesity syndrome BBS4. Nat Genet 28, 188-191.

Mykytyn, K., Nishimura, D. Y., Searby, C. C., Shastri, M., Yen, H. J., Beck, J. S., Braun, T., Streb, L. M., Cornier, A. S., Cox, G. F., et al. (2002). Identification of the gene (BBS1) most commonly involved in Bardet-Biedl syndrome, a complex human obesity syndrome. Nat Genet 31, 435-438.

Nishimura, D. Y., Searby, C. C., Carmi, R., Elbedour, K., Van Maldergem, L., Fulton, A. B., Lam, B. L., Powell, B. R., Swiderski, R. E., Bugge, K. E., et al. (2001). Positional cloning of a novel gene on chromosome 16q causing Bardet-Biedl syndrome (BBS2). Hum Mol Genet 10, 865-874.

Ou, Y. Y., Zhang, M., Chi, S., Matyas, J. R., and Rattner, J. B. (2003). Higher order structure of the PCM adjacent to the centriole. Cell Motil Cytoskeleton 55, 125-133.

Rattner, J. B. (1992). Ultrastructure of centrosome domains and identification of their protein components. in the Centrosome (ed Kalnins, VI) (Academic, San Diego,), 45-69.

Rosenbaum, J. (2002). Intraflagellar transport. Curr Biol 12, R125.

Schultz, J., Copley, R. R., Doerks, T., Ponting, C. P., and Bork, P. (2000). SMART: a web-based tool for the study of genetically mobile domains. Nucleic Acids Res 28, 231-234.

Slavotinek, A. M., Stone, E. M., Mykytyn, K., Heckenlively, J. R., Green, J. S., Heon, E., Musarella, M. A., Parfrey, P. S., Sheffield, V. C., and Biesecker, L. G. (2000). Mutations in MKKS cause Bardet-Biedl syndrome. Nat Genet 26, 15-16.

Vale, R. D. (2003). The molecular motor toolbox for intracellular transport. Cell 112, 467-480.

Vaughan, K. T., and Vallee, R. B. (1995). Cytoplasmic dynein binds dynactin through a direct interaction between the intermediate chains and p150Glued. J Cell Biol 131, 1507-1516.

Waterman-Storer, C. M., Karki, S., and Holzbaur, E. L. (1995). The p150Glued component of the dynactin complex binds to both microtubules and the actin-related protein centractin (Arp-1). Proc Natl Acad Sci U S A 92, 1634-1638.

Young, A., Dictenberg, J. B., Purohit, A., Tuft, R., and Doxsey, S. J. (2000). Cytoplasmic dynein-mediated assembly of pericentrin and gamma tubulin onto centrosomes. Mol Biol Cell 11, 2047-2056.

Zimmerman, W., and Doxsey, S. J. (2000). Construction of centrosomes and spindle poles by molecular motor-driven assembly of protein particles. Traffic 1, 927-934.

Zimmerman, W., Sparks, C. A., and Doxsey, S. J. (1999). Amorphous no longer: the centrosome comes into focus. Curr Opin Cell Biol 11, 122-128.

CHAPTER 3
MKKS/BBS6, A DIVERGENT CHAPERONIN-LIKE PROTEIN LINKED TO THE OBESITY DISORDER BARDET-BIEDL SYNDROME, IS A NOVEL CENTROSOMAL COMPONENT REQUIRED FOR CYTOKINESIS

The following chapter has been published in *Journal of Cell Science*. 2005, 118:1007-20 with the following co-authors:

Jun Chul Kim[1], Young Y. Ou[2], Jose L. Badano[3], Muneer A. Esmail[1], Carmen C. Leitch[3], Elsa Fiedrich[1], Philip L. Beales[4], John M. Archibald[5], Nicholas Katsanis[3], Jerome B. Rattner[2] and Michel R. Leroux[1,*]

[1] Department of Molecular Biology and Biochemistry, Simon Fraser University, 8888 University Drive, Burnaby, BC, V5A 1S6, Canada
[2] Department of Cell Biology and Anatomy, University of Calgary, 3330 Hospital Drive NW, Calgary, AB, T2N 4N1, Canada
[3] Institute of Genetic Medicine and Wilmer Eye Institute, Johns Hopkins University, North Wolfe Street, Baltimore, MD 21287, USA
[4] Molecular Medicine Unit, Institute of Child Health, University College London, London, WC1 1EH, UK
[5] Department of Biochemistry and Molecular Biology, Dalhousie University, 5850 College Street, Halifax, NS, B3H 1X5, Canada
[*] Author for correspondence (e-mail: leroux@sfu.ca)

As the first author, I carried out most of the laboratory work for this manuscript and interpreted the results. John Archibald conducted the phylogenetic analysis (Figure 3-1). Young Ou conducted the high resolution mapping microscopy experiment (Figure 3-5). Carmen Leitch conducted the immunohistochemistry experiment (Figure 3-11).

3.1 Abstract

Chaperonins are multisubunit, cylinder-shaped molecular chaperones involved in folding newly-synthesized polypeptides. Here we show that MKKS/BBS6, one of several proteins associated with Bardet-Biedl Syndrome (BBS), is a Group II chaperonin-like protein that has evolved recently in animals from a subunit of the eukaryotic chaperonin CCT/TRiC, and diverged rapidly to acquire distinct functions. Unlike other chaperonins, cytosolic BBS6 does not oligomerize, and the majority of BBS6 resides within the pericentriolar material (PCM), a proteinaceous tube surrounding centrioles. During interphase, BBS6 is confined to the lateral surfaces of the PCM but during mitosis it relocalizes throughout the PCM and is found at the intercellular bridge. Its predicted substrate-binding apical domain is sufficient for centrosomal association, and several patient-derived mutations in this domain cause mislocalization of BBS6. Consistent with an important centrosomal function, silencing of the *BBS6* transcript by RNA interference in different cell types leads to multi-nucleate and multi-centrosomal cells with cytokinesis defects. The restricted tissue distribution of BBS6 further suggests that it may play important roles in ciliated epithelial tissues, consistent with the likely functions of BBS proteins in basal bodies (modified centrioles) and cilia. Our findings provide the first insight into the nature and cellular function of BBS6, and shed light on the potential causes of several ailments, including obesity, retinal degeneration, kidney dysfunction, and congenital heart disease.

3.2 Introduction

Chaperonins represent a ubiquitous and essential family of sequence- and structurally-related molecular chaperones required for assisting the folding of newly-synthesized, non-native polypeptides (Hartl and Hayer-Hartl, 2002). In bacteria, the chaperonin GroEL is implicated in folding ~10% of all cytoplasmic proteins. Together with endosymbiotically-derived mitochondrial Hsp60 and chloroplast cpn60, chaperonins of bacterial origin are classified as Group I (Horwich and Willison, 1993). Their distant relatives, termed Group II chaperonins, are found in the cytosols of eukaryotes and archaea (Gutsche et al., 1999). The eukaryotic cytosolic chaperonin, known as CCT, TRiC or c cpn, interacts with a range of substrates comparable to that of GroEL, but has also evolved the ability to fold proteins found only in eukaryotes, including actins and tubulins (Leroux and Hartl, 2000; Valpuesta et al., 2002). Both Group I and II chaperonin monomers exhibit a bilobed structure consisting of an ATPase equatorial domain that is joined, via a small intermediate domain, to a substrate-binding apical domain; these in turn typically form double-stacked ring complexes where the apical domains face outward (Carrascosa et al., 2001).

The three primary distinguishing features of chaperonins are their number of subunits per ring, subunit composition, and requirement for a co-chaperone. All Group I chaperonins display 7-fold symmetry and are homo-oligomeric, except for plastid cpn60, which is built from α and β subunits. Their activities depend on a bowl-shaped co-chaperone (GroES) that displaces non-native substrates from the opening of the cavity and encloses them inside a hydrophilic cavity conducive for folding (Hartl and Hayer-Hartl, 2002). Group II chaperonins possess 8 different subunits per ring with the

exception of some archaeal chaperonins, which have 9 (Archibald et al., 1999; Gutsche et al., 1999). The 8 subunits of CCT display ~30% amino acid sequence identity to each other, at least as much to archaeal chaperonins, and significantly less (~15%) to Group I chaperonins (Kubota et al., 1995). The different CCT apical domains provide the specificity for CCT to interact with particular substrates through multivalent interactions (Leroux and Hartl, 2000). Another unique property of Group II chaperonins is the presence of a flexible protrusion in the apical domain that serves, in the oligomer, to gate substrate entry and release. This opening and closing of the cavity relies on the ATPase cycle of the chaperonin, which is essential for activity (Meyer et al., 2003). Lastly, prefoldin, a jellyfish-shaped chaperone, cooperates with Group II chaperonins to assist protein folding (Siegers et al., 1999; Siegert et al., 2000; Vainberg et al., 1998).

Until recently, eukaryotes were assumed to harbor one cytosolic chaperonin, CCT. A novel gene mutated in a rare human developmental disease causing hydrometrocolpos, polydactyly and congenital heart disease, McKusick-Kaufman syndrome (MKKS), was identified by (Stone et al., 2000) and found to encode a protein similar to Group II chaperonins. Several mutations in MKKS were subsequently associated with Bardet-Biedl syndrome (BBS), a more severe and clinically heterogeneous disease characterized by obesity, retinal degeneration, kidney anomalies, cardiomyopathy, diabetes, polydactyly, and other ailments (Katsanis et al., 2000; Slavotinek et al., 2000). Eight genes (*BBS1~8*) are now known to cause BBS, yet only one encodes a chaperonin-like protein, MKKS/BBS6 (Ansley et al., 2003; Badano et al., 2003; Chiang et al., 2004; Katsanis et al., 2000; Li et al., 2004; Mykytyn et al., 2001; Mykytyn et al., 2002; Nishimura et al., 2001; Slavotinek et al., 2000). Of the BBS proteins, BBS6 is among the

least characterized, but there is compelling evidence that all BBS proteins participate in a common cellular process, given that mutations in any *BBS* gene result in clinically indistinguishable phenotypes (Katsanis, 2004).

The most plausible hypothesis regarding a shared function for BBS proteins is that they assist microtubule-related transport and cellular organization processes, in particular relating to ciliary/flagellar and centrosomal activities. This hypothesis is supported by several studies using different model organisms. *C. elegans* BBS-1, 2, 3, 5, 7 and 8 homologues localize at the base of cilia in structures analogous to basal bodies (modified centrioles), and two mutants (*bbs-7* and *bbs-8*) display abnormal ciliary structures and defects in intraflagellar transport, a microtubule- and molecular motor-dependent trafficking activity required for cilia biogenesis and function (Ansley et al., 2003; Blacque et al., 2004; Li et al., 2004). Similarly, RNA silencing of Chlamydomonas *BBS5* leads to an aflagellar phenotype (Li et al., 2004). Mammalian BBS4, 5 and 8 also localize to centriolar structures, including the centrosome and basal bodies (Ansley et al., 2003; Kim et al., 2004; Li et al., 2004). BBS 4 facilitates the transport/targetting of PCM 1 to centrosomes, likely via the p150glued dynein motor subunit, and its knockdown by RNA interference causes PCM-1 dispersion and microtubule de-anchoring from centrosomes (Kim et al., 2004). A recent study on BBS4-null mice suggested that BBS4 is required for sperm flagella production, but the underlying cellular defects remain unclear (Mykytyn et al., 2004). In addition, Kulaga et al. (2004) showed that BBS1 and BBS4-deficient mice possessed defects in the structure of olfactory cilia and were anosmic.

Here we provide the first insight into the molecular properties and cellular function of BBS6, and shed light on the molecular etiology of a disease characterized by clinical problems commonly encountered in the general population. We show that BBS6 recently evolved from a CCT subunit and diverged rapidly to acquire specialized functions within the pericentriolar material that surrounds centrioles. BBS6 association with the centrosome is independent of the dynein molecular motor, and is conferred by its apical domain. This putative substrate-binding domain is likely important for its in vivo function, as several patient-derived mutations within it cause BBS6 to mislocalize. We also show that BBS6 plays an important role in cytokinesis, and demonstrate that it is enriched in tissues that either border, or contain, ciliated cells—consistent with a possible basal body/ciliary function that is shared among all BBS proteins.

3.3 Materials and methods

3.3.1 Plasmid constructs

cDNAs encoding full-length, apical domain, or DelGG mutant (Stone et al, 2000) of BBS6 were generated by PCR using different sets of 5' and 3' primer containing *EcoR*I *and Sal*I restriction sites, respectively, and subcloned into the expression vector pCMV-Myc (Clontech) or pEGFP-C2 (Clontech). pEGFP-C2 empty vector was used to express GFP. The *myc*-tagged p50-dynamitin expression vector was a gift from Dr. Richard Vallee. *BBS6* point mutations were generated with the Quick-change site directed mutagenesis kit (Stratagene). All constructs were verified by double-strand sequencing.

3.3.2 Antibodies

We generated polyclonal antibodies to BBS6 by immunizing rabbits with a 15-mer human BBS6 peptide (GCRIPVDFSSTQILL) conjugated to keyhole limpet hemocyanin (Alberta Peptide Institute, Edmonton). Antibodies were purified using a Nitrocellulose membrane-bound human BBS6 protein fragment (amino acids 114-225) encompassing the peptide sequence. The membrane containing the antigen was blocked with 3% BSA in TBS-T (0.05% Tween-20, 100 mM Tris, 150 mM NaCl, pH 7.5) and incubated with crude serum overnight at 4 °C. After washing with TBS-T, antibodies were eluted with 0.2 M glycine (pH 2.8) and neutralized with 1 M Tris-HCl, pH 8.0. We also used antibodies to *myc* (ClonTech), GFP (Roche), α-tubulin (Sigma), acetylated tubulin (Sigma), γ-tubulin (Sigma) and CCTα (*StressGen*). The UM1 and PCM1 polyclonal antibodies were kind gifts from Drs. Keith Willison (Institute of cancer research, London) and Andreas Merdes (U. of Edinburgh), respectively. Secondary antibodies to rabbit and mouse IgG were conjugated with Alexa Fluor 488 and 594 (Molecular probes).

3.3.3 Mammalian cell culture

HeLa, NIH 3T3 and COS-7 cells were maintained in DMEM (Gibco, BRL) supplemented with 10% Fetal Bovine Serum (FBS) at 37°C in 5% CO_2. IMCD-3 cells were maintained in 1:1 mixture of DMEM and Ham's F12 medium (Gibco, BRL) with 10% FBS at 37°C in 5% CO_2. For cell synchronization, cells were grown in 2 mM thymidine (Sigma) for 18 h, washed with PBS, and grown in medium without thymidine for 8 h. Cells were then incubated with 2 mM thymidine for 18 h, transferred to fresh medium, and fixed at various time points to monitor cell cycle progression. For

microtubule depolymerization and regrowth, IMCD3 cells were incubated in 25 μM nocodazole at 37°C for 1 hour. Following drug removal, cells were incubated for the indicated time to allow microtubule regrowth. DNA transfections were performed using Polyfect (Qiagen).

3.3.4 Centrosome purification

Centrosomes were isolated using the method described by Ou and Rattner (2000).

3.3.5 Immunoprecipitations

COS-7 cells were transfected with pEGFP-BBS6 and/or pCMV*myc*-BBS6 and harvested 24 h after transfection in co-immunoprecipitation (co-IP) buffer (150 mM NaCl, 50 mM TRIS-HCl pH 7.5, 1% NP-40) supplemented with protease inhibitor (Roche). Cell lysates were incubated overnight with 5 μg of anti-CCTα antibody or 10 μg anti-*myc* monoclonal antibody immobilized on sepharose beads (Covance). Immunoprecipitates were washed with co-IP buffer, resuspended in 0.2 M glycine (pH 2.8), and subjected to Western blot analysis.

3.3.6 Sucrose gradient fractionation

IMCD3 cells were harvested into 10 ml cold PBS, pelleted and washed in PBS and cold TES buffer (20 mM Tris pH 7.4, 5 mM EDTA, 250 mM Sucrose, 1X protease inhibitor without EDTA). The final cell pellet was resuspended in 700 μl TES buffer with 1% Triton X-100. Cells in Triton-containing buffer were vortexed and incubated on ice for 30 minutes. 300 μl of each cell lysate was loaded on top of discontinuous sucrose gradients comprising 10 steps of 300 μl each, prepared in 20 mM Tris pH 7.4, 10% glycerol, and the appropriate sucrose concentration). Samples were centrifuged at

100,000 *g* for 16 hours at 4°C. Fractions (300 µl) collected from the top were subjected to Western blot analysis.

3.3.7 Fluorescence microscopy, immunohistochemistry and in situ hybridization

Cells grown on glass coverslips were rinsed in PBS, fixed in –20°C methanol for 10 minutes and blocked in PBS with 5.5% FBS for 60 minutes at room temp. Cells were then incubated for 60 minutes at room temp with the relevant primary antibody diluted in PBS. Antibody binding was visualized with Alexa-fluor 488 and 594 conjugated secondary antibodies. Nuclei were counterstained with DAPI. Slides were mounted in Prolong™ anti-fade reagent (Molecular Probes) and observed by fluorescence microscopy using standard epifluorescence, Leica TCS SP confocal, or Deltavision microscope systems. Immunofluorescent digital confocal microscopy and deconvolution were performed as described previously (Ou and Rattner, 2000). Immunohistochemistry of selected mouse tissues was performed as described previously (Ansley et al., 2003). Whole mount *in situ* hybridization on murine E10.5-E12 embryos was carried out according to standard protocols using a 1.2 Kb antisense RNA probe specific to the 3' end of *BBS6*, and it's complementary sense probe as a negative control.

3.3.8 Knockdown of *BBS6* expression by RNA interference

Knockdown of *BBS6* RNA levels was achieved using the vectors pSilencer™ and pSUPER. pSilencer™ 2.1-U6 neo siRNA expression vector (Ambion) was used to generate siRNA against *BBS6* by ligating annealed oligonucleotides into *Hin*dIII and *Bam*HI sites: sense: 5'-

GATCCCGCAGATTCTGCCTCTGTTGTTCAAGAGACAACAGAGGCAGAATCTG

CTTTTTTGGAAA-3', antisense: 5'-
AGCTTTTCCAAAAAAGCAGATTCTGCCTCTGTTGT-
CTCTTGAACAACAGAGGCAGAATCTGCGG-3' (underlined is the target sequence corresponding to human *BBS6*). Following transfection, COS-7 cells were subjected to neomycin selection (500 μg activity/ml) for 9 days and then analyzed by microscopy. For construction of the pSUPER vector, sense and antisense oligonucleotides corresponding to mouse *BBS6* were cloned into the pSUPER as described (Brummelkamp et al., 2002). Sense: 5'-
GATCCCCCAGTTATCTCAAGTCTGATTCAAGAGATCAGACTTGAGATAACTGT
-TTTTGGAAA-3', Antisense: 5'-AGCTTTTCCAAAAACAGTTATCTCAAGTC-
TGATCTCTTGAATCAGACTTGAGATAACTGGGG-3' (underlined is the target sequence corresponding to mouse *BBS6*). Transfection, selection, and analyses were as with the pSilencer™ vector.

3.3.9 Phylogenetic analyses

BBS6 sequences were added manually to an alignment of Group II chaperonins constructed previously (Archibald et al., 2000). The alignment used for phylogenetic analyses contained 217 unambiguously aligned positions, and corresponded to the regions of the alignment most conserved between BBS6 and Group II chaperonins. Phylogenetic trees were inferred using maximum likelihood (ML) and ML-distance methods. ML trees were constructed with PROML in PHYLIP 3.6 (http://evolution.genetics.washington.edu/phylip.html) using the Dayhoff amino acid substitution matrix, a single randomized sequence-input order, the global rearrangements option, and an among-site rate variation model using a six rate category discrete

approximation to the Γ distribution plus an additional invariable sites category. TREE-PUZZLE 5.0 (Strimmer and von Haeseler, 1996) was used to estimate relative rates for each category. ML-distance trees were inferred from Γ-corrected distance matrices (calculated using TREE-PUZZLE 5.0, as above) using Fitch-Margoliash (FITCH in PHYLIP 3.6) and BIONJ (Gascuel, 1997). For Fitch-Margoliash analyses, the global rearrangements option was used and the sequence input order was randomized once. Statistical support for ML and ML-distance trees was obtained by bootstrapping. For PROML trees, 100 bootstrap data sets were analyzed using a uniform-rates model, the global rearrangements option and a single randomization of the sequence input order. For the bootstrapping of ML-distance trees, Γ-corrected distance matrices were inferred from 100 re-sampled data sets using PUZZLEBOOT (A. Roger and M. Holder; http://www.tree-puzzle.de), using the parameters as described above.

3.4 Results

3.4.1 Phylogenetic analysis of BBS6 and Group II chaperonins

To elucidate the evolutionary origin of the single human *BBS6* gene, we constructed phylogenetic trees from an alignment of human and putative mouse, rat, zebrafish and tunicate BBS6 amino acid sequences, as well as Group II chaperonins (CCT subunits and archaeal chaperonins). Results from these analyses, shown in Figure 3-2A, indicated that BBS6 sequences are extremely divergent relative to Group II chaperonins. Furthermore, rather than observing an association between BBS6 and archaeal chaperonins, as suggested by the BLAST results of (Stone et al., 2000), our

studies suggest a more likely relationship between BBS6 and one of the eukaryotic CCT subunits, CCTα.

The putative BBS6 homologues from Ciona intestinalis (sea squirt) and Danio rerio cluster with the human, rat and mouse BBS6 proteins with high statistical support. This result is significant as it indicates that BBS6 originated prior to their divergence and is widespread in animals. The absence of *BBS6* genes from *Caenorhabditis elegans* or *Drosophila melanogaster* further suggests that BBS6 emerged prior to the appearance of vertebrates but after the protostome/deuterostome split. Interestingly, the degree of amino acid sequence identity shared between the BBS6 orthologues suggests that it is evolving much more rapidly than the different CCT orthologues (Figure 3-2B). For example, H. sapiens and C. intestinalis CCTα share 73.3% sequence identity, whereas the BBS6 sequences from the same organisms are only 21.4% identical. Likewise, all 8 human and mouse CCT orthologues share ~96 97% pairwise identity (Kubota et al., 1995), much greater than the corresponding mammalian BBS6 orthologues (77% identity).

Intriguingly, one of the most conserved Group I and II chaperonin sequence, GDGTT(S/T), which makes several contacts with ATP and is required for its hydrolysis (Ditzel et al., 1998), is significantly different in BBS6 proteins, whereas the corresponding sequences are well conserved between BBS6 from different species (Figure 3-2C; see also positions 119-124 in Figure 3-1). Other residues that are essentially invariant in Group II chaperonins and which are also anticipated to participate in ATP hydrolysis are not conserved in BBS6 proteins (e.g., residues ND in the conserved sequence NDGATIL are SQ, ST or TL in BBS6; positions 88-94 in Figure 3-1 alignment), potentially suggesting differences in ATP binding or hydrolysis. Altogether,

these observations indicate that BBS6 has diverged to a much greater degree than have CCT subunits in the same timeframe, and has likely evolved new function(s).

3.4.2 BBS6 is not associated with CCT and is enriched in centrosomal fractions

To provide insight on the cellular distribution and oligomeric nature of BBS6, and to compare its properties to those of other chaperonins, we generated polyclonal antibodies against a short peptide sequence of human BBS6. Following affinity purification, we confirmed the specificity of our antibody by probing a Western blot containing extracts from HeLa cells expressing wild-type or *myc*-tagged human BBS6. As shown in Figure 3-3A, the anti-BBS6 antibody recognized transiently expressed wild-type (~60 kDa; lane 2) and *myc*-tagged BBS6 (~62 kDa; lane 3). The antibody did not cross-react with additional proteins, demonstrating its specificity. Endogenous BBS6 was not detected by immunoblot analysis in HeLa cell lysates (Figure 3-3A, lane 1), or other mammalian cells (data not shown), due to the low levels of the protein. However, fractionation experiments revealed that a single species of the expected molecular weight (MW) for BBS6 was enriched for, and detected by immunoblotting, in purified centrosomal fractions (Figure 3-3A, lane 4).

We next investigated whether BBS6 can form a high-MW oligomer comparable to that of other chaperonins, and whether it might be a transient, minor substituent CCT subunit. Sucrose density gradients were used to compare the sedimentation behavior of transiently expressed wild-type BBS6 to that of endogenous CCT. Lysates from Triton X-disrupted IMCD3 cells were separated on 4-71% discontinuous gradients, and

fractions were analyzed by immunoblotting with antibodies recognizing CCT and BBS6. CCT was detected in the 24-28% sucrose fractions, consistent with an expected MW of ~800 kDa (Figure 3-3B, top panel). In contrast, the majority of BBS6 sedimented to the 71% sucrose and pellet fractions (Figure 3-3B, middle panel). The sedimentation behavior of the transiently expressed BBS6 is likely identical to that of endogenous BBS6, since both of their cellular localization patterns are indistinguishable (see Figure 3-4B below). The bulk of BBS6 co-sedimented with endogenous γ-tubulin, a known centrosomal marker (Figure 3-3B, bottom panel). Interestingly, this position on the gradient is comparable to that of BBS4, which was previously shown to associate with the centriolar satellites of centrosomes (Kim et al., 2004).

A small portion of wild-type BBS6 (and *myc*-tagged BBS6; data not shown) sedimented near the top of the gradient (4-8%), as either monomers or small oligomers (Figure 3-3B, middle panel). Supporting evidence for this conclusion was obtained by comparing estimated MWs of *in vitro* translated human BBS6, endogenous CCT, and several molecular weight markers by size exclusion chromatography (Figure 3-3C). CCT elutes at a position similar to thyroglobulin (669 kDa), whereas BBS6 elutes in fractions close to the 67 kDa protein marker, bovine serum albumin.

To determine if BBS6 forms small homo-oligomers (*e.g.*, dimers), we carried out immunoprecipitation experiments. Equivalent levels of GFP-BBS6 alone, or GFP-BBS6 and *myc*-BBS6 were expressed transiently in COS-7 cells, and supernatants from cell lysates containing the tagged proteins (Figure 3-3D, lanes 1 and 2, respectively) were immunoprecipitated. These tagged proteins behave identically to that of endogenous BBS6 with respect to their cellular localization pattern, suggesting that the tags do not

interfere with their folding (see Figure 3-4B below). An anti-*myc* monoclonal antibody immobilized on sepharose beads efficiently precipitated and enriched for *myc*-BBS6 in cells expressing *myc*-BBS6 but not in cells expressing GFP-BBS6 alone (Figure 3-3D, lanes 6 and 5, respectively). When GFP-BBS6 was co-expressed with *myc*-BBS6, the anti-*myc* antibody did not precipitate GFP-BBS6, showing that the two tagged BBS6 proteins do not interact (Figure 3-3D, lane 10). Importantly, our immunoprecipitation conditions were conducive for precipitating complexes, since an anti-CCTα antibody effectively precipitated the CCT complex, as detected with an antibody (UM1; (Hynes et al., 1995)) that recognizes multiple CCT subunits (Figure 3-3D, lane 12). Lastly, the lack of interaction between BBS6 monomers was further substantiated by yeast two-hybrid analyses (data not shown).

Together, our biochemical characterization of BBS6 provides strong evidence that it is not associated with the other known eukaryotic chaperonin, CCT, and that its oligomeric nature—likely that of a monomer—differs from that of chaperonins in general.

3.4.3 BBS6 is found at the centrosome and midbody during cell division

Our fractionation and sedimentation experiments suggested that the bulk of BBS6 is associated with the centrosome, and/or potentially other high-MW, Triton X-insoluble cell component(s). We investigated the cellular localization of BBS6 by fluorescence immunocytochemistry using our affinity-purified anti-BBS6 antibody. Different mammalian cell lines, including human HeLa, and murine IMCD3 and NIH 3T3 were fixed and probed with the anti-BBS6 antibody. Endogenous BBS6 was found at two perinuclear focal points in these cells (shown for IMCD3 cells; Figure 3-4A). Endogenous BBS6 protein co-localized with γ-tubulin, confirming its centrosomal

localization (Figure 3-4B, top panels). As further evidence that the BBS6 signal detected by our antibody was specific, we transiently expressed *myc*-BBS6 and GFP-BBS6 in IMCD3 cells and observed that both tagged proteins co-localize with γ-tubulin (Figure 3-4B, middle and bottom panels). We also noted that in IMCD3 and NIH 3T3 cells bearing primary cilia, BBS6 was associated with both the daughter and mother centrioles (basal bodies), but excluded from the ciliary axoneme (Figure 3-4C). BBS6 appears to be a core centrosomal protein, as it remained associated with centrosomes during the cell cycle (Figure 3-4D). Interestingly, we often observed BBS6 (GFP-tagged and endogenous) at the midbody during cytokinesis (47% of all telophase cells observed, n= 178, Figure 3-4E), consistent with the fact that several centrosomal proteins are known to localize to the midbody in telophase cells (*e.g.*, see (Tsvetkov et al., 2003)).

3.4.4 Cell cycle-dependent localization of BBS6 to different regions of the pericentriolar material

To define more precisely the position of BBS6 at the centrosome, we carried out immunolocalization studies of endogenous BBS6 in NIH 3T3 cells using digital confocal microscopy. As shown previously (Figure 3-4C), BBS6 was not detected along the axoneme of primary cilia (Figure 3-5A). Interestingly, we noted that the immunofluorescence signal of BBS6 may not overlap significantly with γ-tubulin. Instead, one view of BBS6 appeared as distinctive "O shaped" structures surrounding γ-tubulin (Figure 3-5A), suggesting that BBS6 is part of the PCM tube structure characterized by (Ou et al., 2003). To test this possibility, we co-stained cells in interphase or mitotic phase with our anti-BBS6 antibody and serum (M4491) that

specifically recognizes a subset of PCM proteins forming a tube-like structure around centrioles (Mack et al., 1998). BBS6 was consistently found to co-localize with the PCM tube in a side view, as seen in representative optical sections (Figure 3-5B, lower panels). Interestingly, BBS6 was confined to the lateral walls and excluded from the proximal and distal ends of the PCM tube in interphase cells (Figure 3-5B, upper panels). At the onset of mitosis, BBS6 levels increased and its signal was detected throughout the PCM tube (Figure 3-5B, lower panels). BBS6 is therefore a novel centrosomal protein that displays a variable, cell cycle-dependent localization at the PCM tube.

3.4.5 Centrosomal assembly of BBS6 is independent of microtubules or the dynein motor

We next queried how BBS6 assembles at centrosomes, which serve as nucleation and organizing sites for cytoplasmic microtubules. We first tested whether the association depends on polymerized microtubules. IMCD3 cells were treated with the drug nocodazole, which leads to microtubule depolymerization (Figure 3-6A; note the loss of microtubule structures at 0 minutes compared to the no drug control). In nocodazole-treated cells, BBS6 remained centrosomal, as did the core centrosomal protein, γ tubulin (Figure 3-6A; see arrowheads at 0 minutes). This suggested that the association of BBS6 with the centrosome does not depend on polymerized microtubules.

Many centrosomal proteins, including PCM1 and BBS4 are targeted to centrosomes via the microtubule-based dynein-dynactin molecular motor, whereas others (e.g., γ tubulin) are not (Kim et al., 2004). We therefore investigated if centrosomal assembly of BBS6 depends on dynein-dynactin by overexpressing p50-dynamitin, which antagonizes the function of the motor in vivo (Vaughan and Vallee, 1995). We confirmed

that overexpressing myc-tagged p50-dynamitin in IMCD3 cells causes PCM1 mislocalization (in 78% of the transfected cells, n=120, Figure 3-6B, left panel). In contrast, just as with γ-tubulin, the centrosomal localization of BBS6 was not affected in cells overexpressing p50-dynamitin (γ-tubulin: 6%, n=150, BBS6: 3%, n=100, Figure 3-6B, see arrows in the right and middle panels). From the above results, we concluded that BBS6 is assembled at the centrosome in a microtubule- and dynein-independent manner, as are other integral centrosomal components.

3.4.6 Several BBS6 protein variants found in patients are mislocalized

Since protein function depends on correct cell localization, we investigated whether BBS6 missense mutants found in patients fail to localize to centrosomes. Six GFP-tagged BBS6 constructs encompassing mutations in the equatorial, intermediate and apical domains (Figure 3-7A) were expressed at similar levels in COS-7 cells (Figure 3-7B). As reported above, GFP-tagged wild-type BBS6 is centrosomal in COS-7 cells, and two of the mutant fusion proteins, R156L and C499S also localized properly (Figure 3-7C, top panels). However, four mutant proteins, G52D, D285A, T325P and G345E consistently failed to associate with centrosomes (Figure 3-7C, bottom panels).

3.4.7 The isolated apical domain of BBS6 is sufficient for centrosomal localization

The mislocalization of three BBS6 variants with missense mutations in the apical domain (D285A, T325P and G345E) suggested that this putative substrate-binding domain may be needed to target BBS6 to the centrosome. We tested this possibility by expressing in COS-7 cells a GFP-fusion protein with the apical domain alone (amino acids 198-370; Figure 3-7A and B). Similar apical domain fragments have been shown to

be stable in isolation and have been crystallized (*e.g.*, the apical domain of CCT; (Pappenberger et al., 2002)). Remarkably, the GFP-tagged BBS6 apical domain associated with the centrosome (Figure 3-7D). In addition, we observed that a patient-derived truncated form of the protein that lacks most of the BBS6 C-terminal equatorial domain but retains an intact apical domain (denoted delGG in Stone et al, 2000; Figure 3-7A), also localizes normally (Figure 3-7D). Taken together, our localization studies on the isolated apical domain and missense/truncation variants show that the BBS6 apical domain region is important for centrosomal localization.

3.4.8 *BBS6* silencing by siRNA causes cytokinesis and other defects

To investigate the cellular function of BBS6, we sought to reduce *BBS6* expression levels in mammalian cells by using RNA interference (RNAi). We transfected COS-7 cells with an expression vector, pSilencer-BBS6, that contains a neomycin resistance gene and a U6 RNA polymerase III promoter and produces a short interfering RNA (siRNA) specific for the human BBS6 sequence. Untransfected cells were selected against by incubation in G418-containing media. Real-time quantitative RT-PCR demonstrated that *BBS6* expression was reduced 16-fold compared to control cells containing vector alone (pSilencer-empty).

Phase-contrast microscopic observation of cells transfected with pSilencer-empty vector and pSilencer-BBS6 revealed a conspicuous phenotype for the *BBS6*-silenced cells, namely that of a large proportion of cells attached by thin intercellular bridges (Figure 3-8A, top panels). This suggested that cells had undergone multiple rounds of divisions without completing cytokinesis. Consistent with this observation, a greater percentage of *BBS6*-silenced cells were bi- or multi-nucleated relative to empty vector-transfected

control cells (BBS6 knockdown, 11.9%, n=277 cells; control, 5.3%, n=300 cells). These results are in agreement with the known role of centrosomes in the resolution of the intercellular bridge (Piel et al., 2001), and the presence of BBS6 in the bridge (Figure 3-4E). We also investigated whether the *BBS6*-silenced cells displayed centrosomal anomalies. Staining with the anti-γ-tubulin antibody revealed an increase in the percent of *BBS6*-silenced cells containing abnormal numbers of centrosomes compared to control cells (greater than 4 centrosomes in interphase or dividing cells; *BBS6* knockdown, 19.1%, n=440; Control, 6%, n=350; Figure 3-8A, top panels). To ensure that these γ-tubulin foci were constituents of *bona fide* centrosomes, we confirmed by immunofluorescence microscopy that another centrosomal protein (pericentrin) co-localized with the γ-tubulin signals (Figure 3-9). Some *BBS6* knockdown cells lacked centrosomes altogether (data not shown). Importantly, similar results were obtained with two additional siRNA constructs targeted to different regions of the *BBS6* transcript and expressed in the COS-7 cells (data not shown).

To corroborate the results obtained with the COS-7 cells, we conducted similar experiments using a different cell line (NIH 3T3) and a different siRNA expression vector (pSUPER; (Brummelkamp et al., 2002)) targeting a different region of *BBS6*. After selection in G418, we isolated two different clonal lines (A and B) and measured the levels of *BBS6* expression by real-time quantitative RT-PCR. Both lines showed a significant reduction in *BBS6* expression (4 and 16-fold reduction, respectively). In addition, our quantitative immunocytochemistry analysis on both line A and B revealed that the fluorescent signal of BBS6 decreased by 2- and 3.5-fold respectively, and also that this decrease is tightly correlated with the cytokinesis and centrosome defects (Figure

3-10). As with the COS-7 cells, we found that *BBS6*-silenced cells displayed a high incidence of cytokinesis-arrested cells with unresolved intercellular bridges (Figure 3-8A, bottom panels). This cytokinesis defect in NIH 3T3 cells was reproducible and not observed in control cells transfected with empty pSUPER vector, although it was somewhat less pronounced than that observed in COS-7 cells. This difference, which allowed us to maintain (unhealthy) cell lines, potentially indicates cell type-specific effects of reducing BBS6 levels. The two *BBS6*-silenced NIH 3T3 cell lines also revealed a significant increase in bi- or multi-nucleated cells compared to control cells (line A: 8.3%, n=361; line B: 10.5%, n=388; control: 2.6%, n=386; Figure 3-8A). Finally, siRNA treatment resulted in a greater proportion of cells containing more than two pairs of centrosomes (line A: 13.3%, n=408; line B: 17.5%, n=450; control: 4%, n=719; Figure 3-8A).

Altogether, our results indicate that diminishing BBS6 levels in two cell types leads to cytokinesis failure, as well as an accumulation of cells containing abnormal numbers of nuclei and centrosomes. Interestingly, knockdown of BBS4 similarly leads to a cell division arrest and an accumulation of multi-nucleated and multi-centrosomal cells, likely as a result of microtubule release (de-anchoring) from the centrosome (Kim et al., 2004). We therefore tested if *BBS6*-silencing in COS-7 cells results in alterations in microtubule organization in interphase and dividing cells. Intriguingly, our results demonstrate that the microtubule architecture appears normal in *BBS6*-silenced cells (especially compared to *BBS4*-silenced cells), as no conspicuous abnormalities are observed throughout the cell cycle in cells that ultimately fail to undergo cytokinesis (Figure 3-8B). Given the presence of BBS6 at the midbody, the observed cytokinesis

defects could conceivably be ascribed to a specific role of the chaperonin-like protein in the abscission of the intercellular bridge.

3.4.9 BBS6 is expressed in organs pertinent to BBS and at high levels in ciliated tissues

To shed light on how the centrosomal and cytokinesis defects observed in cultured cells relates to the *in vivo* function of BBS6 and its link to a pleiotropic disorder that affects numerous tissues, we studied its expression pattern in mouse embryos and tissues. Whole-mount *in situ* analyses of developing (E10.5-E12) embryos with an RNA probe specific for the *BBS6* transcript revealed prominent staining in the heart, brain, retina and limb buds (Figure 3-11A), as well as in the developing neural tube (not shown). This expression pattern reflects the known organs and ailments that are affected in BBS patients (*i.e.*, limb buds, polydactyly; heart, congenital heart disease; retina, retinal degeneration; brain and neural tube, neurological phenotypes). In addition, we observed prominent staining in the first and second branchial arches, raising the possibility that mis-patterning of these structures might be responsible for the dysmorphic facial and tooth features of BBS (Beales et al., 1999). We also used our affinity-purified anti-BBS6 antibody to stain paraffin-embedded tissue sections of mice brain, kidney, retina, olfactory epithelium, and the ependymal layer of ventricles (Figure 3-11B-F). Interestingly, BBS6 was detected only in restricted regions of these tissue sections, including the ciliated border of renal tubules, the connecting cilium and the inner and outer nuclear layers of retina, the ciliated layer of olfactory epithelia. These results indicated that BBS6 is preferentially enriched in regions that contain or border ciliated cells, similar to that observed for BBS4 and BBS8 (Ansley et al., 2003; Kim et al., 2004).

BBS4 has been implicated in the assembly of sperm flagella (Mykytyn et al., 2004). Consistent with this observation, we detected BBS6 in cells undergoing spermatogenesis in mouse testis sections. Figure 3-11G shows that BBS6 is confined to the centrosomes/basal bodies in this tissue and is not present along the flagellar axoneme in cells undergoing spermiogenesis. This localization pattern suggests that BBS6 may play an important role in sperm flagellation.

3.5 Discussion

We have shown that MKKS/BBS6, a previously uncharacterized chaperonin-like protein linked to the McKusick-Kaufman and Bardet-Biedl syndromes, is a highly divergent member of the CCT chaperonin family that has evolved unique structural and functional properties.

3.5.1 Phylogenetic distribution of BBS6

BBS6 emerged relatively late during the evolution of animals. It is absent in *C. elegans* and *Drosophila* (protostomes), and in unicellular eukaryotes such as *Chlamydomonas reinhardtii* (green alga) and *Saccharomyces cerevisiae* (yeast), but may be broadly distributed in deuterostomes, as it is found in vertebrates as well as the urochordate *C. intestinalis*. This contrasts with other BBS proteins, which appear to exist in all ciliated organisms, from unicellular *Chlamydomonas* and *Tetrahymena*, to the multicellular organisms *C. elegans*, *Drosophila* and humans. This, combined with our findings, suggest that BBS6 co-evolved with, and potentially assists the function or localization of, other protein(s) that emerged in the deuterostome lineage.

3.5.2 BBS6 as a molecular chaperone

Is BBS6 a molecular chaperone? Although the primary structure of BBS6 is clearly similar to that of Group II chaperonins, including the presence of an apical domain protrusion used to encapsulate substrates by CCT and the archaeal chaperonin (Figure 3-1), several lines of evidence suggest that BBS6 may not function like a *bona fide* chaperonin that assists protein folding. First, the soluble form of the protein does not form oligomers like other chaperonins, an important distinction considering that oligomerization is widely believed to be a requisite for chaperonin activity (Weber et al., 1998). As the centrosomal localization of BBS6 necessitates only the apical domain (which is unlikely to oligomerize; (Carrascosa et al., 2001)), it is possible that BBS6 does not need to form oligomers in the PCM to interact with its binding partner(s)/substrate(s). Furthermore, several residues critical for ATP binding/hydrolysis in other chaperonins are different in BBS6, suggesting that BBS6 may have reduced/absent ATP-dependent conformational changes compared to other chaperonins and thus may not function as other chaperonins (Figure 3-1 and Figure 3-2; see also (Ditzel et al., 1998)). Despite our efforts, we have not been able to produce soluble or refolded recombinant BBS6 from bacterial or insect expression systems, making it difficult to directly test any potential chaperone or ATP binding/hydrolysis activities.

3.5.3 Effect of patient-associated mutations in BBS6

To investigate the effects of BBS6 mutations found in patients, we expressed in mammalian cells seven different mutant forms of the protein. Four of the BBS6 missense mutants failed to localize to the centrosome, three of which were affected in their apical domain. Combined with our observation that the isolated BBS6 apical domain associates

with the centrosome, as does a truncated form of the protein retaining the apical domain, our data suggests that in some BBS patients, the failure of BBS6 to localize to the centrosome may result in disease. This is an important finding, because it provides evidence that the *in vivo* function of BBS6 is dependent on its association with the centrosome/basal body.

3.5.4 BBS6 in cytokinesis and cilia function

The ubiquitous presence of BBS6 in the PCM of centrosomes and basal bodies suggests that it likely plays a constitutive role in association with centrioles. We demonstrated that this role impacts cytokinesis and produces multi-nucleate, multi-centrosomal cells, but it may also have more subtle effects on other centrosome/basal body-based functions, including ciliogenesis and cytoskeletal organization. The exact role of BBS6 in cytokinesis and the midbody merits further investigation. Although cleavage furrow formation appears normal in cells treated with *BBS6* siRNAs (Figure 3-8B), it is possible that subtle defects have occurred in the organization of microtubules that underlie the intercellular bridge, or in the localization of specific proteins, such as myosin II, which is required for furrow formation and abscission. It is known that membrane trafficking to the furrow is important for assembling the cytokinesis machinery; for example, disruption of clathrin function results in failed cytokinesis (O'Halloran, 2000). Thus, similar to the recruitment of PCM1 by BBS4 to the centrosome, BBS6 at the midbody may recruit proteins required for cytokinesis *via* microtubule-dependent membrane trafficking. In this respect, it is intriguing that the newly-identified BBS3 protein belongs to the ARF/ARL family of small GTP-binding proteins, which are collectively involved in trafficking vesicle-associated proteins (Chiang et al., 2004).

Given the roles of *C. elegans*, *Chlamydomonas* and murine BBS proteins in the structural integrity of cilia/flagella (Blacque et al., 2004; Li et al., 2004; Mykytyn et al., 2004), we tested the effect of reducing *BBS6* expression by siRNA in ciliated NIH 3T3 cells. We found, however, that compared to empty vector-transfected control cells, *BBS6* silencing did not significantly affect the frequency (*BBS6* knockdown: 10.5%, n=439; control: 10.3%, n=321) nor the gross morphology (average length) of cilia (*BBS6* knockdown: 3.09 μm, n=77; control: 3.18 μm, n=138). This observation raises several possibilities: (a) siRNA treatment of the cells is ineffective in producing a ciliary phenotype, or (b) the cilia are affected in function but not structure, or (c) a putative ciliary dysfunction in BBS6 patients results from an indirect effect of the cytokinesis defect on the function of ciliated epithelial cells/tissues. These possible scenarios will likely need to be investigated using a *BBS6* knockout mouse model system.

In conclusion, our study demonstrates that BBS6, a chaperonin-like protein related to CCT, plays specialized role(s) at the pericentriolar material of the centrosome, and suggests that centrosomal/basal body and cytokinesis defects in ciliated tissues may be responsible for the pathogenicity of Bardet-Biedl syndrome.

3.6 Figures

Figure 3-1 Amino acid sequence alignment of BBS6, CCT and archaeal chaperonin sequences.

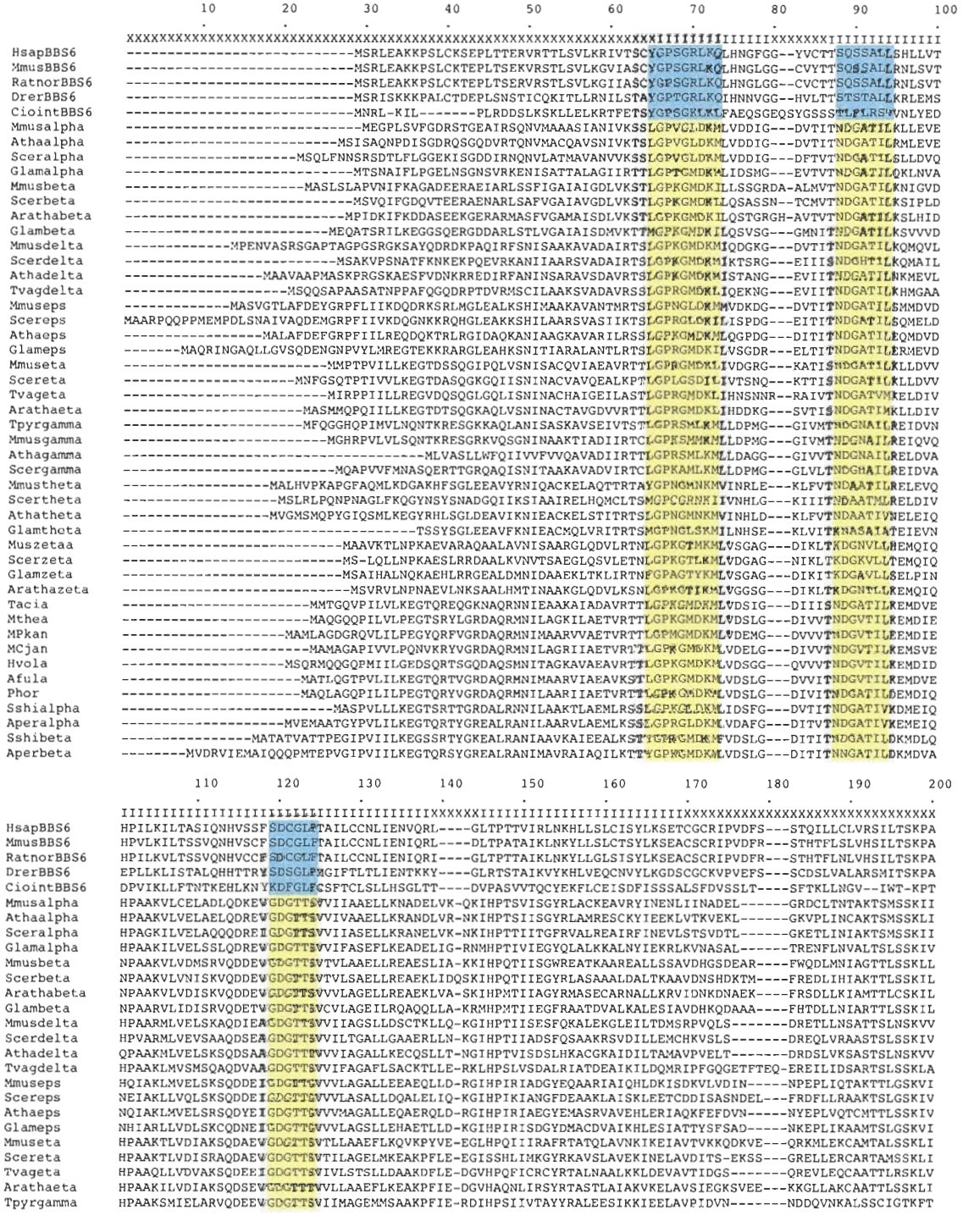

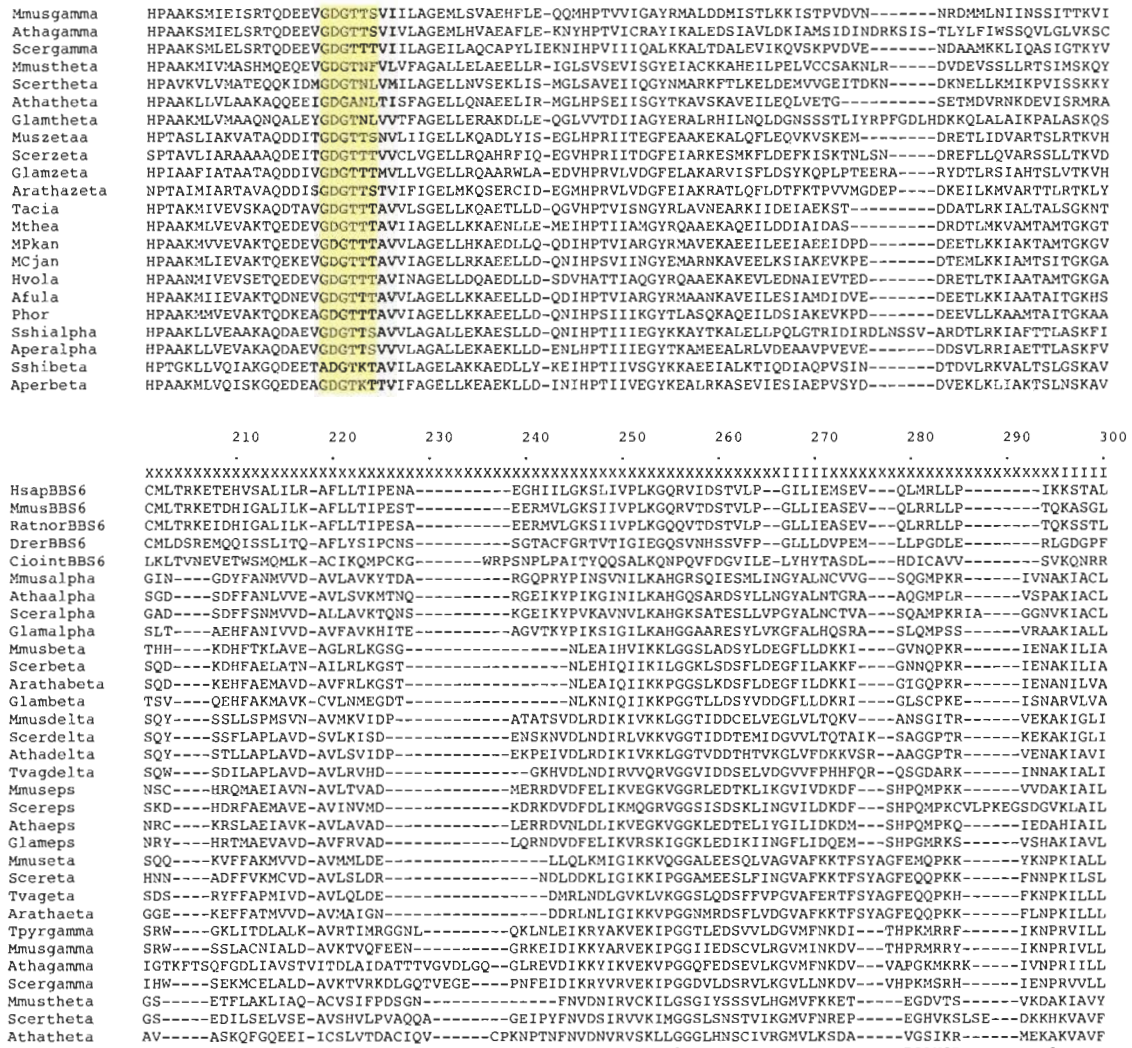
Mmusgamma HPAAKSMIEISRTQDEEVGDGTTSVIILAGEMLSVAEHFLE-QQMHPTVVIGAYRMALDDMISTLKKISTPVDVN-------NRDMMLNIINSSITTKVI
Athagamma HPAAKSMIELSRTQDEEVGDGTTSVIVLAGEMLHVAEAFLE-KNYHPTVICRAYIKALEDSIAVLDKIAMSIDINDRKSIS-TLYLFIWSSQVLGLVKSC
Scergamma HPAAKSMLELSRTQDEEVGDGTTTVIILAGEILAQCAPYLIEKNIHPVIIIQALKKALTDALEVIKQVSKPVDVE-------NDAAMKKLIQASIGTKYV
Mmustheta HPAAKMIVMASHMQEQEVGDGTNFVLVFAGALLELAEELLR-IGLSVSEVISGYEIACKKAHEILPELVCCSAKNLR-----DVDEVSSLLRTSIMSKQY
Scertheta HPAVKVLVMATEQQKIDMGDGTNLVMILAGELLNVSEKLIS-MGLSAVEIIQGYNMARKFTLKELDEMVVGEITDKN-----DKNELLKMIKPVISSKKY
Athatheta HPAAKLLVLAAKAQQEEIGDGANLTISFAGELLQNAEELIR-MGLHPSEIISGYTKAVSKAVEILEQLVETG----------SETMDVRNKDEVISRMRA
Glamtheta HPAAKMLVMAAQNQALEYGDGTNLVVTFAGELLERAKDLLE-QGLVVTDIIAGYERALRHILNQLDGNSSSTLIYRPFGDLHDKKQLALAIKPALASKQS
Muszetaa HPTASLIAKVATAQDDITGDGTTSNVLIIGELLKQADLYIS-EGLHPRIITEGFEAAAKEKALQFLEQVKVSKEM--------DRETLIDVARTSLRTKVH
Scerzeta SPTAVLIARAAAAQDEITGDGTTTVVCLVGELLRQAHRFIQ-EGVHPRIITDGFEIARKESMKFLDEFKISKTNLSN-----DREFLLQVARSSLLTKVD
Glamzeta HPIAAFIATAATAQDDIVGDGTTMVLLVGELLRQAARWLA-EDVHPRVLVDGFELAKARVISFLDSYKQPLPTEERA----RYDTLRSIAHTSLVTKVH
Arathazeta NPTAIMIARTAVAQDDISGDGTTSTVIFIGELMKQSERCID-EGMHPRVLVDGFEIAKRATLQFLDTFKTPVVMGDEP----DKEILKMVARTTLRTKLY
Tacia HPTAKMIVEVSKAQDTAVGDGTTTAVVLSGELLKQAETLLD-QGVHPTVISNGYRLAVNEARKIIDEIAEKST---------DDATLRKIALTALSGKNT
Mthea HPAAKMLVEVAKTQEDEVGDGTTTAVIIAGELLKKAENLLE-MEIHPTIIAMGYRQAAEKAQEILDDIAIDAS---------DRDTLMKVAMTAMTGKGT
MPkan HPAAKMVVEVAKTQEDEVGDGTTTAVVLAGELLHKAEDLLQ-QDIHPTVIARGYRMAVEKAEEILEEIAEEIDPD-------DEETLKKIAKTAMTGKGV
MCjan HPAAKMLIEVAKTQEKEVGDGTTTAVVIAGELLRKAEELLD-QNIHPSVIINGYEMARNKAVEELKSIAKEVKPE-------DTEMLKKIAMTSITGKGA
Hvola HPAANMIVEVSETQEDEVGDGTTTAVINAGELLDQAEDLLD-SDVHATTIAQGYRQAAEKAKEVLEDNAIEVTED-------DRETLTKIAATAMTGKGA
Afula HPAAKMIIEVAKTQDNEVGDGTTTAVVLAGELLKKAEELLD-QDIHPTVIARGYRMAANKAVEILESIAMDIDVE-------DEETLKKIAATAITGKHS
Phor HPAAKMMVEVAKTQDKEAGDGTTTAVVIAGELLKKAEELLD-QNIHPSIIIKGYTLASQKAQEILDSIAKEVKPD-------DEEVLLKAAMTAITGKAA
Sshialpha HPAAKLLVEAAKAQDAEVGDGTTSAVVLAGALLEKAESLLD-QNIHPTIIIEGYKKAYTKALELLPQLGTRIDIRDLNSSV-ARDTLRKIAFTTLASKFI
Aperalpha HPAAKLLVEVAKAQDAEVGDGTTSVVVLAGALLEKAEKLLD-ENLHPTIIIEGYTKAMEEALRLVDEAAVPVEVE-------DDSVLRRIAETTLASKFV
Sshibeta HPTGKLLVQIAKGQDEETADGTKTAVILAGELAKKAEDLLY-KEIHPTIIVSGYKKAEEIALKTIQDIAQPVSIN-------DTDVLRKVALTSLGSKAV
Aperbeta HPAAKMLVQISKGQEDEACDGTKTTVIFAGELLKEAEKLLD-INIHPTIIVEGYKEALRKASEVIESIAEPVSYD-------DVEKLKLIAKTSLNSKAV
210 220 230 240 250 260 270 280 290 300
HsapBBS6 CMLTRKETEHVSALILR-AFLLTIPENA----------EGHIILGKSLIVPLKGQRVIDSTVLP--GILIEMSEV---QLMRLLP--------IKKSTAL
MmusBBS6 CMLTRKETDHIGALILK-AFLLTIPEST----------EERMVLGKSIIVPLKGQRVTDSTVLP--GLLIEASEV---QLRRLLP--------TQKASGL
RatnorBBS6 CMLTRKEIDHIGALILK-AFLLTIPESA----------EERMVLGKSIIVPLKGQQVTDSTVLP--GLLIEASEV---QLRRLLP--------TQKSSTL
DrerBBS6 CMLDSREMQQISSLITQ-AFLYSIPCNS----------SGTACFGRTVTIGIEGQSVNHSSVFP--GLLLDVPEM---LLPGDLE--------RLGDGPF
CiointBBS6 LKLTVNEVETWSMQMLK-ACIKQMPCKG-------WRPSNPLPAITYQQSALKQNPQVFDGVILE-LYHYTASDL---HDICAVV--------SVKQNRR
Mmusalpha GIN----GDYFANMVVD-AVLAVKYTDA----------RGQPRYPINSVNILKAHGRSQIESMLINGYALNCVVG---SQGMPKR------IVNAKIACL
Athaalpha SGD----SDFFANLVVE-AVLSVKMTNQ----------RGEIKYPIKGINILKAHGQSARDSYLLNGYALNTGRA---AQGMPLR------VSPAKIACL
Sceralpha GAD----SDFFSNMVVD-ALLAVKTQNS----------KGEIKYPVKAVNVLKAHGKSATESLLVPGYALNCTVA---SQAMPKRIA----GGNVKIACL
Glamalpha SLT----AEHFANIVVD-AVFAVKHITE----------AGVTKYPIKSIGILKAHGGAARESYLVKGFALHQSRA---SLQMPSS------VRAAKIALL
Mmusbeta THH----KDHFTKLAVE-AGLRLKGSG----------NLEAIHVIKKLGGSLADSYLDEGFLLDKKI----GVNQPKR------IENAKILIA
Scerbeta SQD----KDHFAELATN-AILRLKGST----------NLEHIQIIKILGGKLSDSFLDEGFILAKKF----GNNQPKR------IENAKILIA
Arathabeta SQD----KEHFAEMAVD-AVFRLKGST----------NLEAIQIIKKPGGSLKDSFLDEGFILDKKI----GIGQPKR------IENANILVA
Glambeta TSV----QEHFAKMAVK-CVLNMEGDT----------NLKNIQIIKKPGGTLLDSYVDDGFLLDKRI----GLSCPKE------ISNARVLVA
Mmusdelta SQY----SSLLSPMSVN-AVMKVIDP----------ATATSVDLRDIKIVKKLGGTIDDCELVEGLVLTQKV----ANSGITR------VEKAKIGLI
Scerdelta SQY----SSFLAPLAVD-SVLKISD----------ENSKNVDLNDIRLVKKVGGTIDDTEMIDGVVLTQTAIK--SAGGPTR------KEKAKIGLI
Athadelta SQY----STLLAPLAVD-AVLSVIDP----------EKPEIVDLRDIKIVKKLGGTVDDTHTVKGLVFDKKVSR--AAGGPTR------VENAKIAVI
Tvagdelta SQW----SDILAPLAVD-AVLRVHD----------GKHVDLNDIRVVQRVGGVIDDSELVDGVVFPHHFQR--QSGDARK------INNAKIALI
Mmuseps NSC----HRQMAEIAVN-AVLTVAD----------MERRDVDFELIKVEGKVGGRLEDTKLIKGVIVDKDF---SHPQMPKK------VVDAKIAIL
Scereps SKD----HDRFAEMAVE-AVINVMD----------KDRKDVDFDLIKMQGRVGGSISDSKLINGVILDKDF---SHPQMPKCVLPKEGSDGVKLAIL
Athaeps NRC----KRSLAEIAVK-AVLAVAD----------LERRDVNLDLIKVEGKVGGKLEDTELIYGILIDKDM---SHPQMPKQ------IEDAHIAIL
Glameps NRY----HRTMAEVAVD-AVFRVAD----------LQRNDVDFELIKVRSKIGGKLEDIKIINGFLIDQEM---SHPGMRKS------VSHAKIAVL
Mmuseta SQQ----KVFFAKMVVD-AVMMLDE----------LLQLKMIGIKKVQGGALEESQLVAGVAFKKTFSYAGFEMQPKK------YKNPKIALL
Scereta HNN----ADFFVKMCVD-AVLSLDR----------NDLDDKLIGIKKIPGGAMEESLFINGVAFKKTFSYAGFEQQPKK------FNNPKILSL
Tvageta SDS----RYFFAPMIVD-AVLQLDE----------DMRLNDLGVKLVKGGSLQDSFFVPGVAFERTFSYAGFEQQPKH------FKNPKILLL
Arathaeta GGE----KEFFATMVVD-AVMAIGN----------DDRLNLIGIKKVPGGNMRDSFLVDGVAFKKTFSYAGFEQQPKK------FLNPKILLL
Tpyrgamma SRW----GKLITDLALK-AVRTIMRGGNL---------QKLNLEIKRYAKVEKIPGGTLEDSVVLDGVMFNKDI---THPKMRRF------IKNPRVILL
Mmusgamma SRW----SSLACNIALD-AVKTVQFEEN----------GRKEIDIKKYARVEKIPGGIIEDSCVLRGVMINKDV---THPRMRRY------IKNPRIVLL
Athagamma IGTKFTSQFGDLIAVSTVITDLAIDATTTVGVDLGQ--GLREVDIKKYIKVEKVPGGQFEDSEVLKGVMFNKDV---VAPGKMKRK------IVNPRIILL
Scergamma IHW----SEKMCELALD-AVKTVRKDLGQTVEGE----PNFEIDIKRYVRVEKIPGGDVLDSRVLKGVLLNKDV---VHPKMSRH------IENPRVVLL
Mmustheta GS-----ETFLAKLIAQ-ACVSIFPDSGN----------FNVDNIRVCKILGSGIYSSSVLHGMVFKKET-----EGDVTS------VKDAKIAVY
Scertheta GS-----EDILSELVSE-AVSHVLPVAQQA--------GEIPYFNVDSIRVVKIMGGSLSNSTVIKGMVFNREP-----EGHVKSLSE---DKKHKVAVF
Athatheta AV-----ASKQFGQEEI-ICSLVTDACIQV------CPKNPTNFNVDNVRVSKLLGGGLHNSCIVRGMVLKSDA-----VGSIKR------MEKAKVAVF
Glamtheta GY-----EDFLSGLVAE-ACVQVIPEDSRL----------FNPESIRIAKVPGRSITDSFVVRGFVIPTLP-----RGAVQR------MQNCRIAVY
Muszetaa AEL----ADVLTEAVVD-SILAIRKKDEP----------IDLFMVEIMEMKHKSETDTSLIRGLVLDHGAR---HPDMKKR------VENAYILTC
Scerzeta ADL----TEVLTPIVTD-AVLSVYDAQADN----------LDLHMVEIMQMQHLSPKDTTFIKGLVLDHGGR---HPDMPTR------VKNAYVLIL
Glamzeta ADL----ANLLSDIVTE-AVLIVEKAAES---------KEQSFIDLHMVELMLMPSRLDVDTTLIKGLVMDHGSR---QSELTCAT-----MRSCFILTL
Arathazeta EGL----ADQLTDIVVN-SVLCIRKPQEP----------IDLFMVEIMHMRHKFDVDTRLVEGLVLDHGSR---HPDMKRR------AENCHILTC
Tacia GLS----NDFLADLVVK-AVNAVAEVR----------DGKTIVDTANIKVDKKNGGSVNDTQFISGIVIDKEKV---HSKMPDV------VKNAKIALI
Mthea EKA----REPLAELIVD-AVKQV----------EEDGEVEKDHIKIEKKEGAAVDDSTLVQGVIIDKERV---HPGMPKK------VENAKIALL
MPkan EKA----RDYLAELVVK-AVKQVAEEE----------DGEIVIDTDHIKLEKKEGGGLEDTELVKGMVIDKERV---HPGMPRR------VENAKIALL
MCjan EKA----REQLAEIVVE-AVRAVVD----------EETGKVDKDLIKVEKKEGAPIEETKLIRGVVIDKERV---NPQMPKK------VENAKIALL
Hvola ESA----KDLLSELVVD-AVLAV----------KDDDGIDTNNVSIEKVVGGTIDNSELVEGVIVDKERV---DENMPYA------VEDANIAIL
Afula EYA----LDHLSSLVVE-AVKRVAEKV----------DDRYKVDEDNIKLEKRQGGSVADTKLVNGIVIDKEVV---HPGMPKR------VKNAKIAVL
Phor EEE----REYLAKLAVE-AVKLVAEEK----------DGKLKVDIDNIKLEKKEGGAVRDTRLIRGVVIDKEVV---HPGMPKR------IENAKIALI
Sshialpha AEGAE--LNKIIDMVID-AIVNVAEPLP----------NGGYNVSLDLIKIDKKKGGSIEDSVLVKGLVLDKEVV---HPGMPRR------VTKAKIAVL
Aperalpha GTGPE--RDKIISMVID-AIRTVAEKRP----------DGGYEVDLDYVKIEKKKGGSLLDSKLVRGIVLDKEVV---HPAMPKR------VENAKILVL
Sshibeta AGA----REYLADLVVK-AVAQVAELR----------GDKWYVDLDNVQIVKKHGGSINDTQLVYGIVVDKEVV---HPGMPKR------IENAKIALL
Aperbeta AEA----RDYFAELAVE-AVRTVAERR----------GDRWYVDLNNIQIVKKHGGSLRDTRLVRGIVLDKEVV---HPDMPRR------VENARIALL

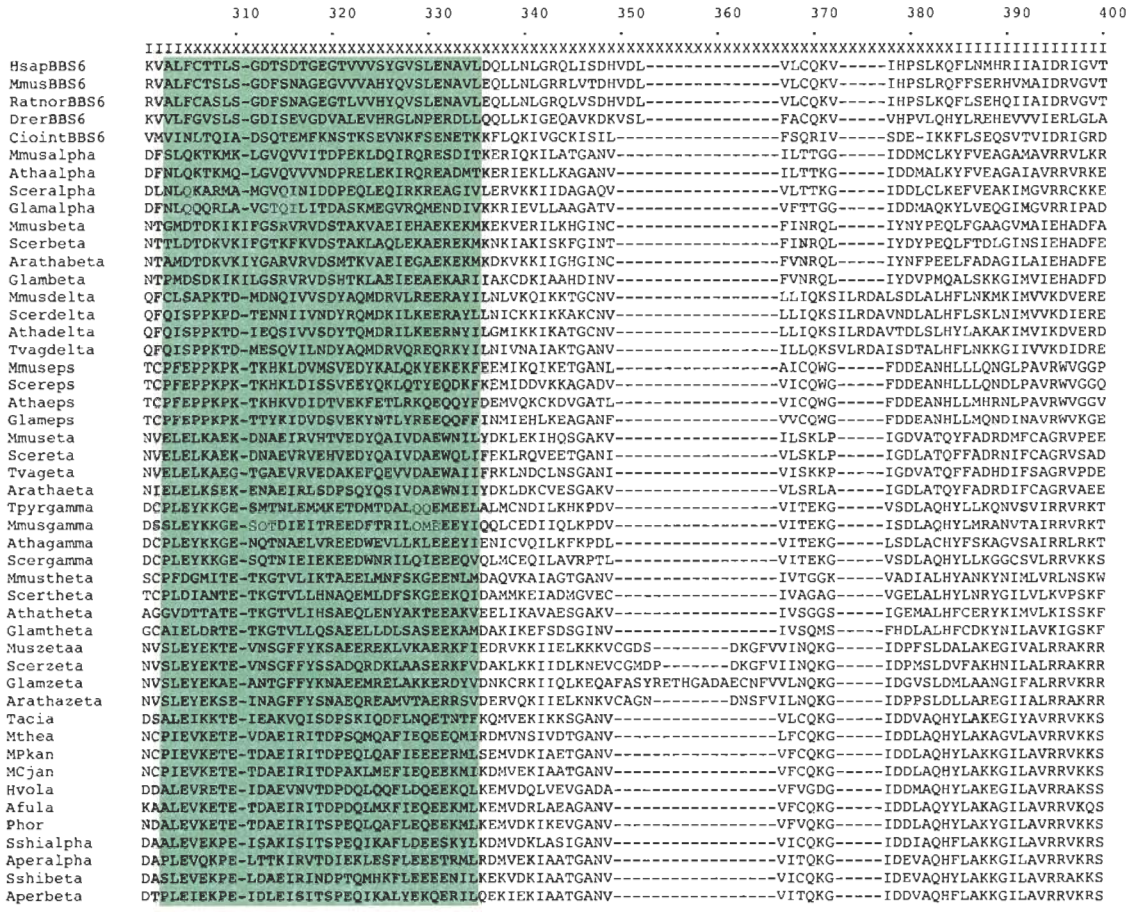
310 320 330 340 350 360 370 380 390 400
HsapBBS6
MmusBBS6
RatnorBBS6
DrerBBS6
CiointBBS6
Mmusalpha
Athaalpha
Sceralpha
Glamalpha
Mmusbeta
Scerbeta
Arathabeta
Glambeta
Mmusdelta
Scerdelta
Athadelta
Tvagdelta
Mmuseps
Scereps
Athaeps
Glameps
Mmuseta
Scereta
Tvageta
Arathaeta
Tpyrgamma
Mmusgamma
Athagamma
Scergamma
Mmustheta
Scertheta
Athatheta
Glamtheta
Muszetaa
Scerzeta
Glamzeta
Arathazeta
Tacia
Mthea
MPkan
MCjan
Hvola
Afula
Phor
Sshialpha
Aperalpha
Sshibeta
Aperbeta

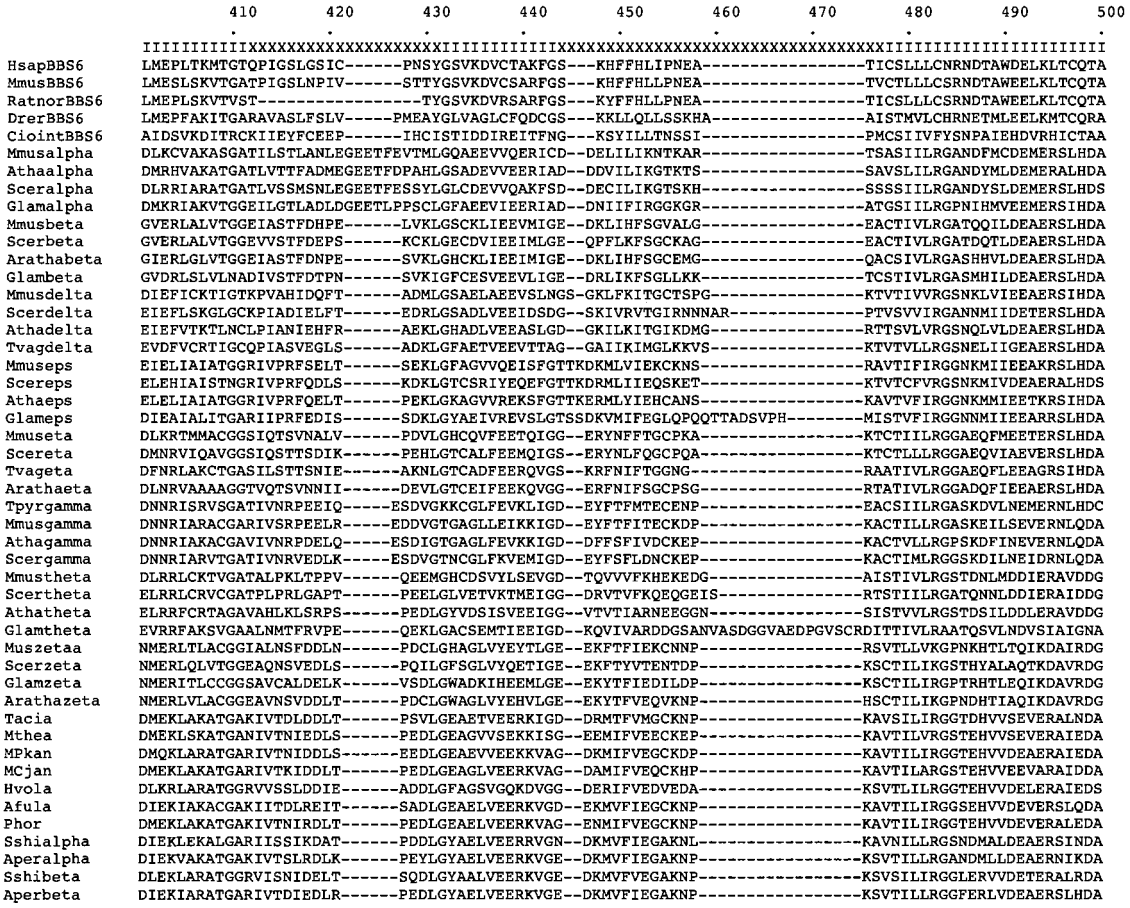
410 420 430 440 450 460 470 480 490 500
HsapBBS6 LMEPLTKMTGTQPIGSLGSIC------PNSYGSVKDVCTAKFGS---KHFFHLIPNEA----------TICSLLLCNRNDTAWDELKLTCQTA
MmusBBS6 LMESLSKVTGATPIGSLNPIV------STTYGSVKDVCSARFGS---KHFFHLLPNEA----------TVCTLLLCSRNDTAWEELKLTCQTA
RatnorBBS6 LMEPLSKVTVST----------TYGSVKDVRSARFGS---KYFFHLLPNEA----------TICSLLLCSRNDTAWEELKLTCQTA
DrerBBS6 LMEPFAKITGARAVASLFSLV-----PMEAYGLVAGLCFQDCGS---KKLLQLLSSKHA----------AISTMVLCHRNETMLEELKMTCQRA
CiointBBS6 AIDSVKDITRCKIIEYFCEEP------IHCISTIDDIREITFNG---KSYILLTNSSI----------PMCSIIVFYSNPAIEHDVRHICTAA
Mmusalpha DLKCVAKASGATILSTLANLEGEETFEVTMLGQAEEVVQERICD--DELILIKNTKAR----------TSASIILRGANDFMCDEMERSLHDA
Athaalpha DMRHVAKATGATLVTTFADMEGEETFDPAHLGSADEVVEERIAD--DDVILIKGTKTS----------SAVSLILRGANDYMLDEMERALHDA
Sceralpha DLRRIARATGATLVSSMSNLEGEETFESSYLGLCDEVVQAKFSD--DECILIKGTSKH----------SSSSIILRGANDYSLDEMERSLHDS
Glamalpha DMKRIAKVTGGEILGTLADLDGEETLPPSCLGFAEEVIEERIAD--DNIIFIRGGKGR----------ATGSIILRGPNIHMVEEMERSIHDA
Mmusbeta GVERLALVTGGEIASTFDHPE------LVKLGSCKLIEEVMIGE--DKLIHFSGVALG----------EACTIVLRGATQQILDEAERSLHDA
Scerbeta GVERLALVTGGEVVSTFDEPS------KCKLGECDVIEEIMLGE--QPFLKFSGCKAG----------EACTIVLRGATDQTLDEAERSLHDA
Arathabeta GIERLGLVTGGEIASTFDNPE------SVKLGHCKLIEEIMIGE--DKLIHFSGCEMG----------QACSIVLRGASHHVLDEAERSLHDA
Glambeta GVDRLSLVLNADIVSTFDTPN------SVKIGFCESVEEVLIGE--DRLIKFSGLLKK----------TCSTIVLRGASMHILDEAERSLHDA
Mmusdelta DIEFICKTIGTKPVAHIDQFT------ADMLGSAELAEEVSLNGS-GKLFKITGCTSPG----------KTVTIVVRGSNKLVIEEAERSIHDA
Scerdelta EIEFLSKGLGCKPIADIELFT------EDRLGSADLVEEIDSDG--SKIVRVTGIRNNNAR----------PTVSVVIRGANNMIIDETERSLHDA
Athadelta EIEFVTKTLNCLPIANIEHFR------AEKLGHADLVEEASLGD--GKILKITGIKDMG----------RTTSVLVRGSNQLVLDEAERSLHDA
Tvagdelta EVDFVCRTIGCQPIASVEGLS------ADKLGFAETVEEVTTAG--GAIIKIMGLKKVS----------KTVTVLLRGSNELIIGEAERSLHDA
Mmuseps EIELIAIATGGRIVPRFSELT------SEKLGFAGVVQEISFGTTKDKMLVIEKCKNS----------RAVTIFIRGGNKMIIEEAKRSLHDA
Scereps ELEHIAISTNGRIVPRFQDLS------KDKLGTCSRIYEQEFGTTKDRMLIIEQSKET----------KTVTCFVRGSNKMIVDEAERALHDS
Athaeps ELELIAIATGGRIVPRFQELT------PEKLGKAGVVREKSFGTTKERMLYIEHCANS----------KAVTVFIRGGNKMMIEETKRSIHDA
Glameps DIEAIALITGARIIPRFEDIS------SDKLGYAEIVREVSLGTSSDKVMIFEGLQPQQTTADSVPH---------MISTVFIRGGNNMIIEEARRSLHDA
Mmuseta DLKRTMMACGGSIQTSVNALV------PDVLGHCQVFEETQIGG--ERYNFFTGCPKA----------KTCTIILRGGAEQFMEETERSLHDA
Scereta DMNRVIQAVGGSIQSTTSDIK------PEHLGTCALFEEMQIGS--ERYNLFQGCPQA----------KTCTLLLRGGAEQVIAEVERSLHDA
Tvageta DFNRLAKCTGASILSTTSNIE------AKNLGTCADFEERQVGS--KRFNIFTGGNG----------RAATIVLRGGAEQFLEEAGRSIHDA
Arathaeta DLNRVAAAAGGTVQTSVNNII------DEVLGTCEIFEEKQVGG--ERFNIFSGCPSG----------RTATIVLRGGADQFIEEAERSLHDA
Tpyrgamma DNNRISRVSGATIVNRPEEIQ-----ESDVGKKCGLFEVKLIGD--EYFTFMTECENP----------EACSIILRGASKDVLNEMERNLHDC
Mmusgamma DNNRIARACGARIVSRPEELR-----EDDVGTGAGLLEIKKIGD--EYFTFITECKDP----------KACTILLRGASKEILSEVERNLQDA
Athagamma DNNRIAKACGAVIVNRPDELQ-----ESDIGTGAGLFEVKKIGD--DFFSFIVDCKEP----------KACTVLLRGPSKDFINEVERNLQDA
Scergamma DNNRIARVTGATIVNRVEDLK-----ESDVGTNCGLFKVEMIGD--EYFSFLDNCKEP----------KACTIMLRGGSKDILNEIDRNLQDA
Mmustheta DLRRLCKTVGATALPKLTPPV------QEEMGHCDSVYLSEVGD--TQVVVFKHEKEDG----------AISTIVLRGSTDNLMDDIERAVDDG
Scertheta ELRRLCRVCGATPLPRLGAPT------PEELGLVETVKTMEIGG--DRVTVFKQEQGEIS----------RTSTIILRGATQNNLDDIERAIDDG
Athatheta ELRRFCRTAGAVAHLKLSRPS------PEDLGYVDSISVEEIGG--VTVTIARNEEGGN----------SISTVVLRGSTDSILDDLERAVDDG
Glamtheta EVRRFAKSVGAALNMTFRVPE------QEKLGACSEMTIEEIGD--KQVIVARDDGSANVASDGGVAEDPGVSCRDITTIVLRAATQSVLNDVSIAIGNA
Muszetaa NMERLTLACGGIALNSFDDLN------PDCLGHAGLVYEYTLGE--EKFTFIEKCNNP----------RSVTLLVKGPNKHTLTQIKDAIRDG
Scerzeta NMERLQLVTGGEAQNSVEDLS------PQILGFSGLVYQETIGE--EKFTYVTENTDP----------KSCTILIKGSTHYALAQTKDAVRDG
Glamzeta NMERITLCCGGSAVCALDELK------VSDLGWADKIHEEMLGE--EKYTFIEDILDP----------KSCTILIRGPTRHTLEQIKDAVRDG
Arathazeta NMERLVLACGGEAVNSVDDLT------PDCLGWAGLVYEHVLGE--EKYTFVEQVKNP----------HSCTILIKGPNDHTIAQIKDAVRDG
Tacia DMEKLAKATGAKIVTDLDDLT------PSVLGEAETVEERKIGD--DRMTFVMGCKNP----------KAVSILIRGGTDHVVSEVERALNDA
Mthea DMEKLSKATGANIVTNIEDLS------PEDLGEAGVVSEKKISG--EEMIFVEECKEP----------KAVTILVRGSTEHVVSEVERAIEDA
MPkan DMQKLARATGARIVTNIDDLS------EEDLGEAEVVEEKKVAG--DKMIFVEGCKDP----------KAVTILIRGGTEHVVDEAERAIEDA
MCjan DMEKLAKATGARIVTKIDDLT------PEDLGEAGLVEERKVAG--DAMIFVEQCKHP----------KAVTILARGSTEHVVEEVARAIDDA
Hvola DLKRLARATGGRVVSSLDDIE------ADDLGFAGSVGQKDVGG--DERIFVEDVEDA----------KSVTLILRGGTEHVVDELERAIEDS
Afula DIEKIAKACGAKIITDLREIT------SADLGEAELVEERKVGD--EKMVFIEGCKNP----------KAVTILIRGGSEHVVDEVERSLQDA
Phor DMEKLAKATGAKIVTNIRDLT------PEDLGEAELVEERKVAG--ENMIFVEGCKNP----------KAVTILIRGGTEHVVDEVERALEDA
Sshialpha DIEKLEKALGARIISSIKDAT------PDDLGYAELVEERRVGN--DKMVFIEGAKNL----------KAVNILLRGSNDMALDEAERSINDA
Aperalpha DIEKVAKATGAKIVTSLRDLK------PEYLGYAELVEERKVGE--DKMVFIEGAKNP----------KSVTILLRGANDMLLDEAERNIKDA
Sshibeta DLEKLARATGGRVISNIDELT------SQDLGYAALVEERKVGE--DKMVFVEGAKNP----------KSVSILIRGGLERVVDETERALRDA
Aperbeta DIEKIARATGARIVTDIEDLR------PEDLGYAELVEERKVGE--DKMVFIEGAKNP----------KSVTILLRGGFERLVDEAERSLHDA

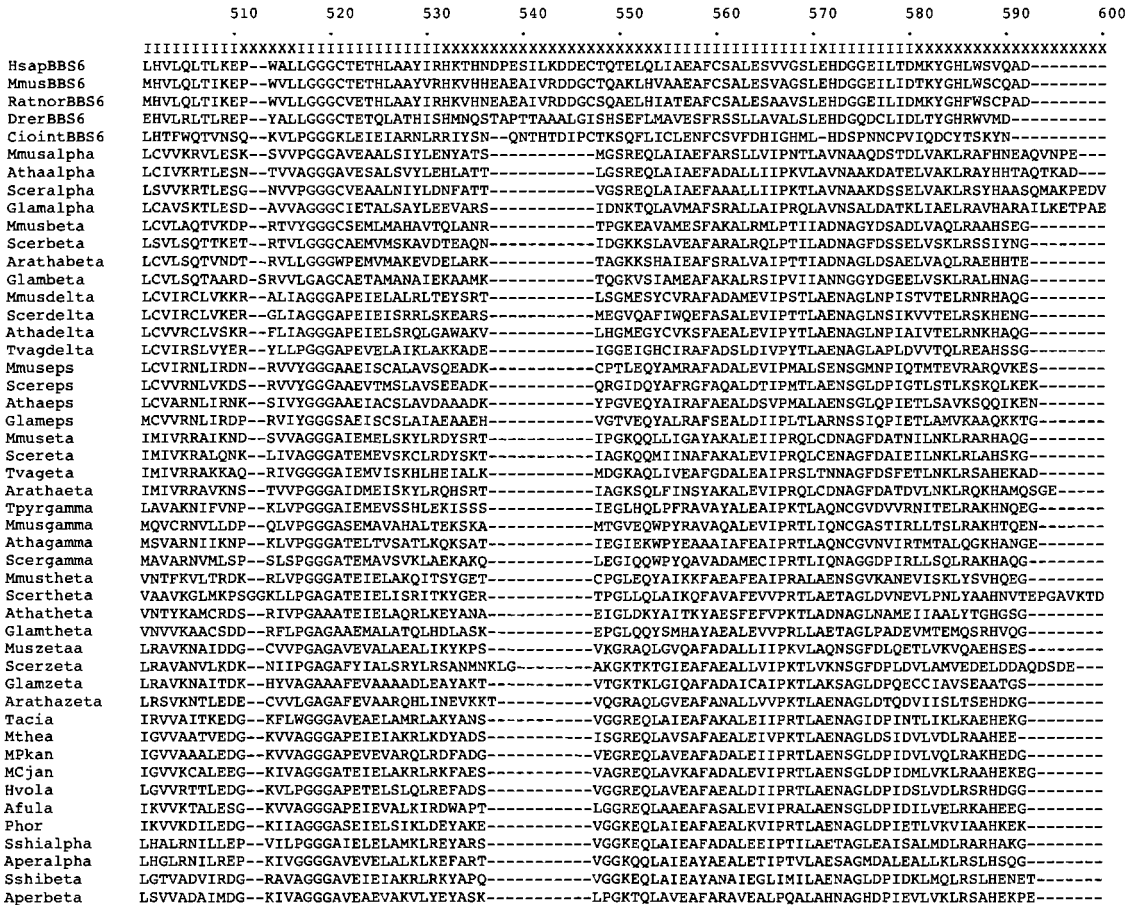
510 520 530 540 550 560 570 580 590 600
HsapBBS6 LHVLQLTLKEP--WALLGGGCTETHLAAYIRHKTHNDPESILKDDECTQTELQLIAEAFCSALESVVGSLEHDGGEILTDMKYGHLWSVQAD--------
MmusBBS6 MHVLQLTIKEP--WVLLGGGCTETHLAAYVRHKVHHEAEAIVRDDGCTQAKLHVAAEAFCSALESVAGSLEHDGGEILIDTKYGHLWSCQAD--------
RatnorBBS6 MHVLQLTIKEP--WVLLGGGCVETHLAAYIRHKVHNEAEAIVRDDGCSQAELHIATEAFCSALESAAVSLEHDGGEILIDMKYGHFWSCPAD--------
DrerBBS6 EHVLRLTLREP--YALLGGGCTETQLATHISHMNQSTAPTTAAALGISHSEFLMAVESFRSSLLAVALSLEHDGQDCLIDLTYGHRWVMD----------
CiointBBS6 LHTFWQTVNSQ--KVLPGGGKLEIEIARNLRRIYSN--QNTHTDIPCTKSQFLICLENFCSVFDHIGHML-HDSPNNCPVIQDCYTSKYN----------
Mmusalpha LCVVKRVLESK--SVVPGGGAVEAALSIYLENYATS----------MGSREQLAIAEFARSLLVIPNTLAVNAAQDSTDLVAKLRAFHNEAQVNPE---
Athaalpha LCIVKRTLESN--TVVAGGGAVESALSVYLEHLATT----------LGSREQLAIAEFADALLIIPKVLAVNAAKDATELVAKLRAYHHTAQTKAD---
Sceralpha LSVVKRTLESG--NVVPGGGCVEAALNIYLDNFATT----------VGSREQLAIAEFAAALLIIPKTLAVNAAKDSSELVAKLRSYHAASQMAKPEDV
Glamalpha LCAVSKTLESD--AVVAGGGCIETALSAYLEEVARS----------IDNKTQLAVMAFSRALLAIPRQLAVNSALDATKLIAELRAVHARAILKETPAE
Mmusbeta LCVLAQTVKDP--RTVYGGGCSEMLMAHAVTQLANR----------TPGKEAVAMESFAKALRMLPTIIADNAGYDSADLVAQLRAAHSEG--------
Scerbeta LSVLSQTTKET--RTVLGGGCAEMVMSKAVDTEAQN----------IDGKKSLAVEAFARALRQLPTILADNAGFDSSELVSKLRSSIYNG--------
Arathabeta LCVLSQTVNDT--RVLLGGGWPEMVMAKEVDELARK----------TAGKKSHAIEAFSRALVAIPTTIADNAGLDSAELVAQLRAEHHTE--------
Glambeta LCVLSQTAARD-SRVVLGAGCAETAMANAIEKAAMK----------TQGKVSIAMEAFAKALRSIPVIIANNGGYDGEELVSKLRALHNAG--------
Mmusdelta LCVIRCLVKKR--ALIAGGGAPEIELALRLTEYSRT----------LSGMESYCVRAFADAMEVIPSTLAENAGLNPISTVTELRNRHAQG--------
Scerdelta LCVIRCLVKER--GLIAGGGAPEIEISRRLSKEARS----------MEGVQAFIWQEFASALEVIPTTLAENAGLNSIKVVTELRSKHENG--------
Athadelta LCVVRCLVSKR--FLIAGGGAPEIELSRQLGAWAKV----------LHGMEGYCVKSFAEALEVIPYTLAENAGLNPIAIVTELRNKHAQG--------
Tvagdelta LCVIRSLVYER--YLLPGGGAPEVELAIKLAKKADE----------IGGEIGHCIRAFADSLDIVPYTLAENAGLAPLDVVTQLREAHSSG--------
Mmuseps LCVIRNLIRDN--RVVYGGGAAEISCALAVSQEADK----------CPTLEQYAMRAFADALEVIPMALSENSGMNPIQTMTEVRARQVKES-------
Scereps LCVVRNLVKDS--RVVYGGGAAEVTMSLAVSEEADK----------QRGIDQYAFRGFAQALDTIPMTLAENSGLDPIGTLSTLKSKQLKEK-------
Athaeps LCVARNLIRNK--SIVYGGGAAEIACSLAVDAAADK----------YPGVEQYAIRAFAEALDSVPMALAENSGLQPIETLSAVKSQQIKEN-------
Glameps MCVVRNLIRDP--RVIYGGGSAEISCSLAIAEAAEH----------VGTVEQYALRAFSEALDIIPLTLARNSSIQPIETLAMVKAAQKKTG-------
Mmuseta IMIVRRAIKND--SVVAGGGAIEMELSKYLRDYSRT----------IPGKQQLLIGAYAKALEIIPRQLCDNAGFDATNILNKLRARHAQG--------
Scereta IMIVKRALQNK--LIVAGGGATEMEVSKCLRDYSKT----------IAGKQQMIINAFAKALEVIPRQLCENAGFDAIEILNKLRLAHSKG--------
Tvageta IMIVRRAKKAQ--RIVGGGGAIEMVISKHLHEIALK----------MDGKAQLIVEAFGDALEAIPRSLTNNAGFDSFETLNKLRSAHEKAD-------
Arathaeta IMIVRRAVKNS--TVVPGGGAIDMEISKYLRQHSRT----------IAGKSQLFINSYAKALEVIPRQLCDNAGFDATDVLNKLRQKHAMQSGE-----
Tpyrgamma LAVAKNIFVNP--KLVPGGGAIEMEVSSHLEKISSS----------IEGLHQLPFRAVAYALEAIPKTLAQNCGVDVVRNITELRAKHNQEG-------
Mmusgamma MQVCRNVLLDP--QLVPGGGASEMAVAHALTEKSKA----------MTGVEQWPYRAVAQALEVIPRTLIQNCGASTIRLLTSLRAKHTQEN-------
Athagamma MSVARNIIKNP--KLVPGGGATELTVSATLKQKSAT----------IEGIEKWPYEAAAIAFEAIPRTLAQNCGVNVIRTMTALQGKHANGE-------
Scergamma MAVARNVMLSP--SLSPGGGATEMAVSVKLAEKAKQ----------LEGIQQWPYQAVADAMECIPRTLIQNAGGDPIRLLSQLRAKHAQG--------
Mmustheta VNTFKVLTRDK--RLVPGGGATEIELAKQITSYGET----------CPGLEQYAIKKFAEAFEAIPRALAENSGVKANEVISKLYSVHQEG--------
Scertheta VAAVKGLMKPSGGKLLPGAGATEIELISRITKYGER----------TPGLLQLAIKQFAVAFEVVPRTLAETAGLDVNEVLPNLYAAHNVTEPGAVKTD
Athatheta VNTYKAMCRDS--RIVPGAAATEIELAQRLKEYANA----------EIGLDKYAITKYAESFEFVPKTLADNAGLNAMEIIAALYTGHGSG--------
Glamtheta VNVVKAACSDD--RFLPGAGAAEMALATQLHDLASK----------EPGLQQYSMHAYAEALEVVPRLLAETAGLPADEVMTEMQSRHVQG--------
Muszetaa LRAVKNAIDDG--CVVPGAGAVEVALAEALIKYKPS----------VKGRAQLGVQAFADALLIIPKVLAQNSGFDLQETLVKVQAEHSES--------
Scerzeta LRAVANVLKDK--NIIPGAGAFYIALSRYLRSANMNKLG---------AKGKTKTGIEAFAEALLVIPKTLVKNSGFDPLDVLAMVEDELDDAQDSDE---
Glamzeta LRAVKNAITDK--HYVAGAAAFEVAAAADLEAYAKT----------VTGKTKLGIQAFADAICAIPKTLAKSAGLDPQECCIAVSEAATGS--------
Arathazeta LRSVKNTLEDE--CVVLGAGAFEVAARQHLINEVKKT----------VQGRAQLGVEAFANALLVVPKTLAENAGLDTQDVIISLTSEHDKG--------
Tacia IRVVAITKEDG--KFLWGGGAVEAELAMRLAKYANS----------VGGREQLAIEAFAKALEIIPRTLAENAGIDPINTLIKLKAEHEKG--------
Mthea IGVVAATVEDG--KVVAGGGAPEIEIAKRLKDYADS----------ISGREQLAVSAFAEALEIVPKTLAENAGLDSIDVLVDLRAAHEE---------
MPkan IGVVAAALEDG--KVVAGGGAPEVEVARQLRDFADG----------VEGREQLAVEAFADALEIIPRTLAENSGLDPIDVLVQLRAKHEDG--------
MCjan IGVVKCALEEG--KIVAGGGATEIELAKRLRKFAES----------VAGREQLAVKAFADALEVIPRTLAENSGLDPIDMLVKLRAAHEKEG-------
Hvola LGVVRTTLEDG--KVLPGGGAPETELSLQLREFADS----------VGGREQLAVEAFAEALDIIPRTLAENAGLDPIDSLVDLRSRHDGG--------
Afula IKVVKTALESG--KVVAGGGAPEIEVALKIRDWAPT----------LGGREQLAAEAFASALEVIPRALAENSGLDPIDILVELRKAHEEG--------
Phor IKVVKDILEDG--KIIAGGGASEIELSIKLDEYAKE----------VGGKEQLAIEAFAEALKVIPRTLAENAGLDPIETLVKVIAAHKEK--------
Sshialpha LHALRNILLEP--VILPGGGAIELELAMKLREYARS----------VGGKEQLAIEAFADALEEIPTILAETAGLEAISALMDLRARHAKG--------
Aperalpha LHGLRNILREP--KIVGGGGAVEVELALKLKEFART----------VGGKQQLAIEAYAEALETIPTVLAESAGMDALEALLKLRSLHSQG--------
Sshibeta LGTVADVIRDG--RAVAGGGAVEIEIAKRLRKYAPQ----------VGGKEQLAIEAYANAIEGLIMILAENAGLDPIDKLMQLRSLHENET-------
Aperbeta LSVVADAIMDG--KIVAGGGAVEAEVAKVLYEYASK----------LPGKTQLAVEAFARAVEALPQALAHNAGHDPIEVLVKLRSAHEKPE-------

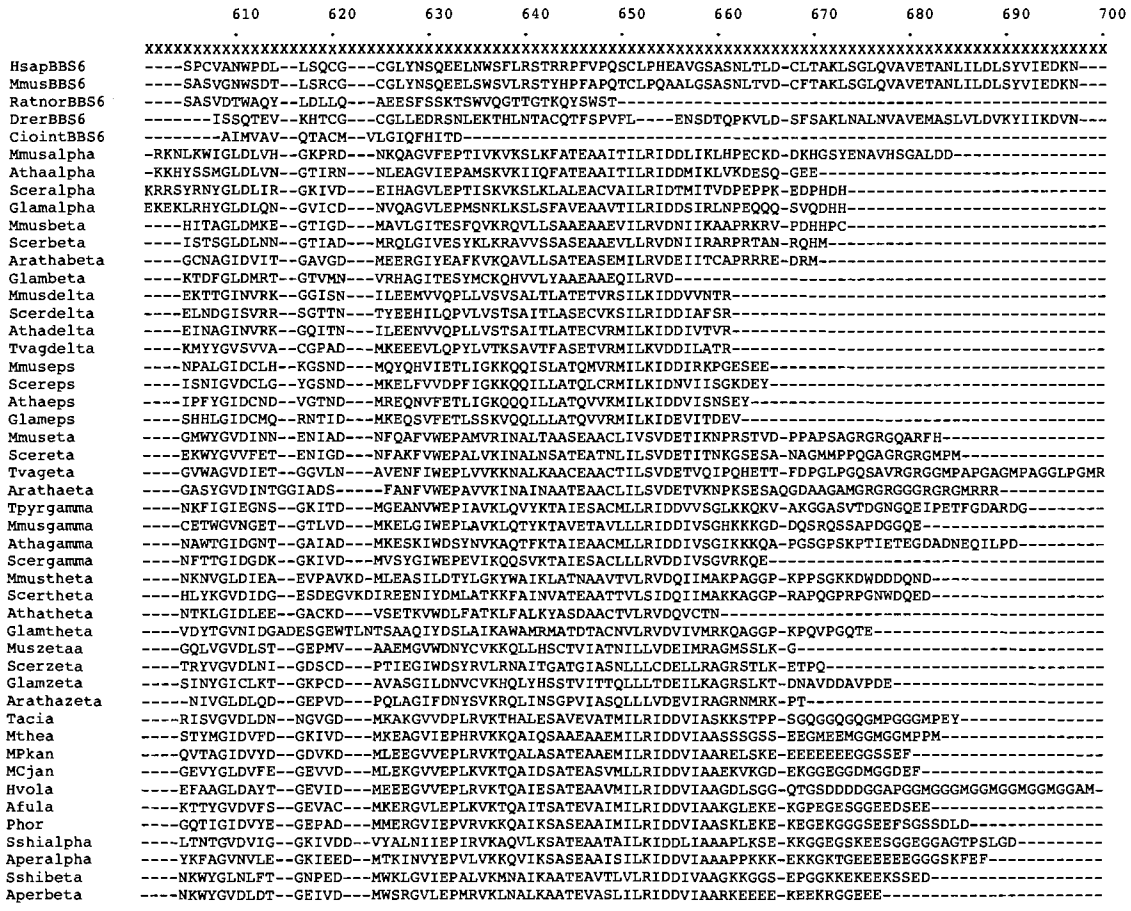

Amino acid positions (numbers on top of the sequences) are relative to the start of the alignment, not any particular chaperonin sequence. I and X respectively indicate positions which were included, or not included, in the phylogenetic analyses. Regions highlighted in light blue represent conserved sequences in BBS6 which differ substantially in other chaperonins (whose corresponding regions are highlighted in yellow). The region highlighted in green is the apical domain region of CCT and archaeal chaperonins, and putative apical domain of BBS6.

Figure 3-2 BBS6 is a highly divergent eukaryotic Group II chaperonin related to CCT.

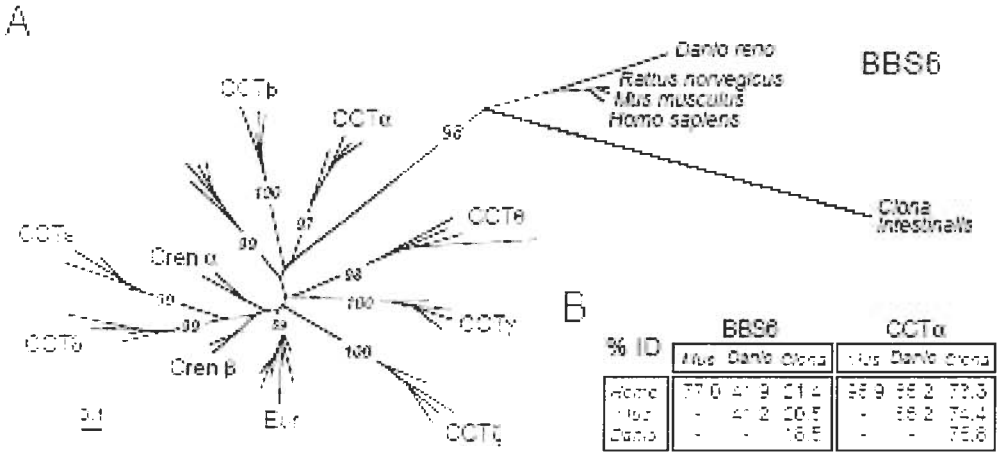

(A) BBS6 has diverged to a much greater degree than have CCT subunits in the same timeframe. Maximum likelihood phylogenetic tree constructed from an alignment containing 5 BBS6 sequences, 11 archaeal chaperonins, and 32 eukaryotic CCTs (4 from each of the 8 CCT subunits). The BBS6 sequences are highlighted, and PROML bootstrap support values are provided for significant nodes on the tree where >50%. The BBS6 proteins show a weakly supported but consistently observed relationship with the α subunit of CCT, suggesting that the gene encoding BBS6 is a divergent, duplicated CCTα subunit. The scale bar indicates the estimated number of amino acid substitutions per site. Abbreviations: Cren; Crenarchaeotes, Eur; Euryarchaeotes. **(B)** Amino acid identities shared between *Homo*, *Mus*, *Danio* and *Ciona* BBS6 and CCTα protein sequences.

C

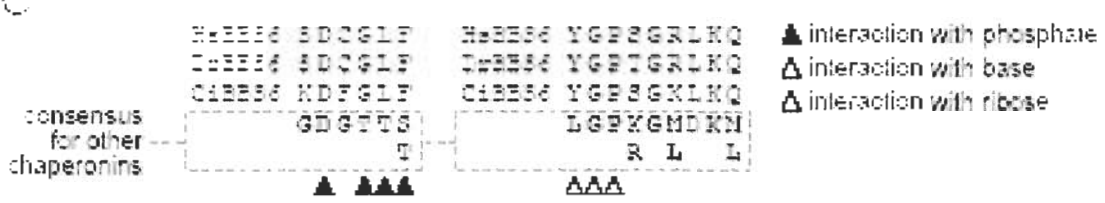

(C) BBS6 proteins share signature sequences that differ from other chaperonins. Alignments of two sequences from human BBS6 (HsBBS6 a.a 36~45 and 88~93), *Danio* BBS6 (DrBBS6) and *Ciona* BBS6 (CiBBS6) are compared to a consensus sequence derived from CCT and archaeal chaperonins (see Figure 3-1). Positions known to interact with the different regions of the ATP moiety (Ditzel et al., 1998) are indicated with inverted triangles under the alignments.

Figure 3-3 BBS6 is enriched in centrosomal fractions and its minor soluble form does not associate with CCT or oligomerize.

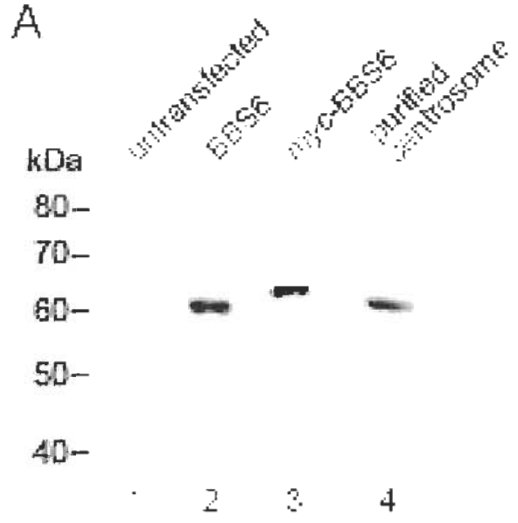

(A) BBS6 is highly enriched in centrosomes purified from NIH 3T3 cells. HeLa cells were either untransfected or transfected with pCMV*myc*-BBS6 or pCMV-BBS6, and total cell lysates were probed by Western blot analysis with an affinity-purified polyclonal BBS6 antibody. Wild-type (~60 kDa) and *myc*-tagged BBS6 (~62 kDa) can be observed in the transfected cells.

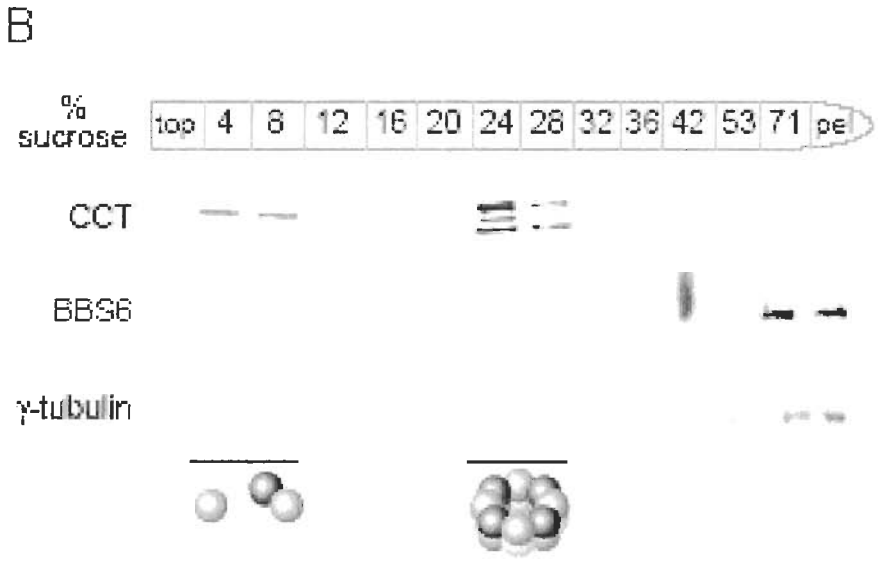

(B) Most of BBS6 exists as high-MW Triton X-insoluble forms distinct from that of cytosolic CCT. Total lysates of IMCD3 cell expressing pCMV-BBS6 were loaded on discontinuous 4-71% sucrose gradient (the top, bottom and sucrose steps in the gradient are indicated). After centrifugation, each fraction was analyzed on a 10 % SDS polyacrylamide gel and subjected to Western blot analyses with antibodies to BBS6, CCT, or γ-tubulin, as indicated. Most of the BBS6 and γ-tubulin is found in 71 % and pellet fractions, while the majority of CCT forms a peak at ~24 % sucrose.

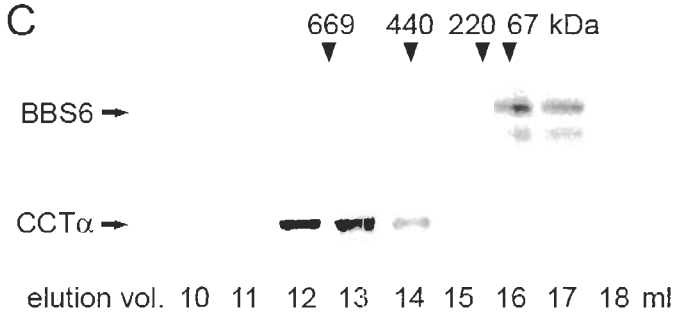

(C) Size exclusion chromatography analyses of ^{35}S-labeled, *in vitro* translated BBS6 (top panel) and endogenous CCT from HeLa cells. Fractions were analyzed by autoradiography (for BBS6) and Western blotting with a UM1 antibody (for CCT). The positions of the MW markers are indicated.

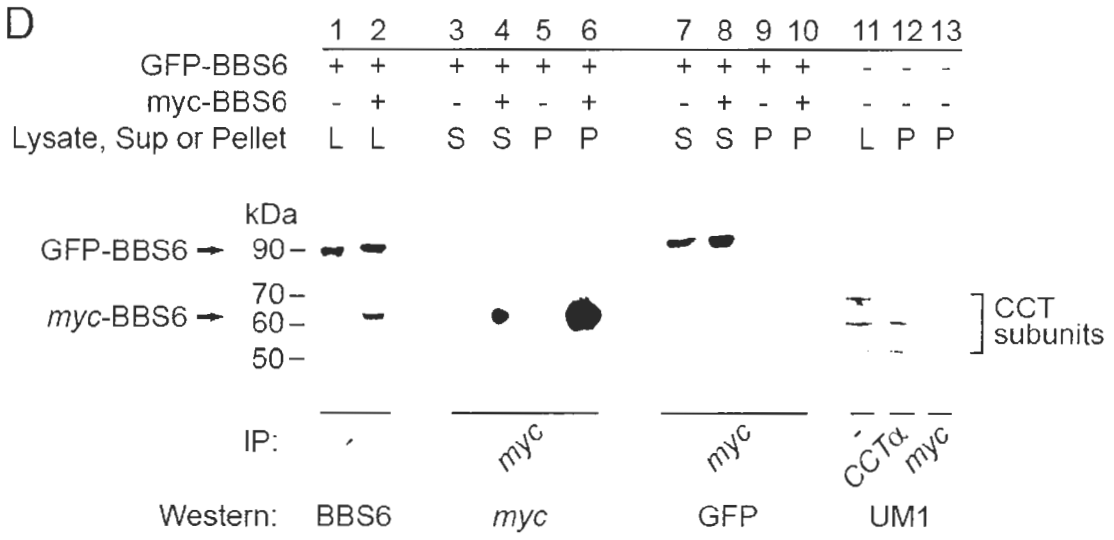

(D) BBS6 does not form homo-oligomers. Extracts of COS-7 cells transiently expressing different constructs (*i.e.*, pEGFP-BBS6 or pCMV*myc*-BBS6, as indicated), or untransfected, were immunoprecitated (IP) with antibodies to *myc*, GFP or CCTα. Lysates (L), immune supernatants (S) or immune pellets (P) were subjected to Western blot analyses using antibodies against BBS6, *myc*, GFP or CCT (UM1 antibody), as indicated. The respective positions of *myc*-BBS6, GFP-BBS6 and CCT subunits are noted.

Figure 3-4 BBS6 is a centrosomal protein that is also found at the midbody during cytokinesis.

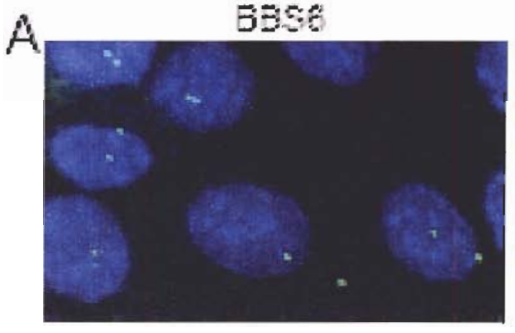

(A) BBS6 localizes at two perinuclear foci. Two discrete perinuclear signals are observed in IMCD3 cells by immunocytochemistry using an affinity-purified anti-BBS6 polyclonal antibody (green).

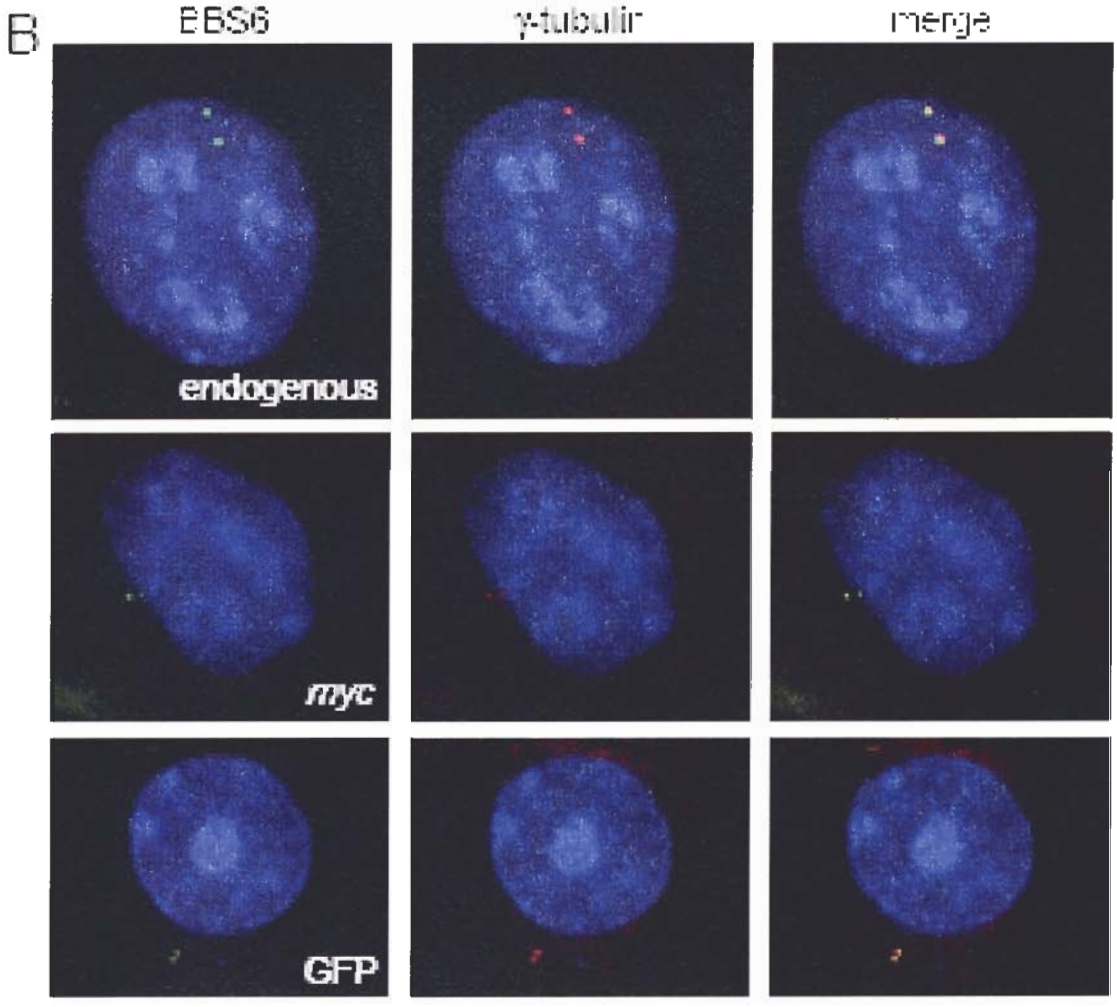

(B) BBS6 and γ-tubulin are co-localized in the cell. Immunolocalization studies of endogenous BBS6 (top panels) and transiently expressed *myc*-tagged, and GFP-tagged BBS6 (middle and bottom panels, respectively) show that BBS6 co-localizes with the centrosomal marker, γ-tubulin. The transfected cells were fixed and costained with antibodies to *myc* and γ-tubulin, and GFP-BBS6 signal was detected by direct GFP fluorescence (middle and bottom panels). Left, middle and right panels respectively show BBS6 (green), γ-tubulin (red) and a merge of the two signals (yellow indicates overlap).

C

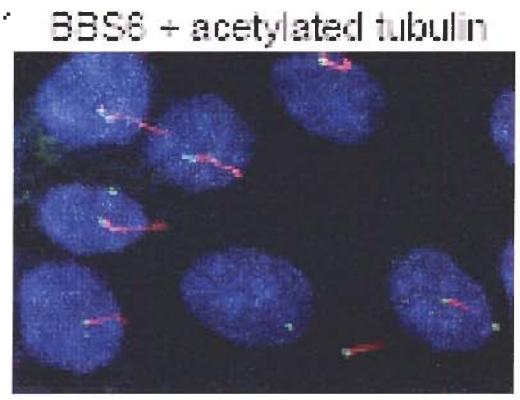

(C) Endogenous BBS6 is found at both basal bodies (mother centrosomes, displaying a primary cilium) and daughter centrosomes. BBS6 is stained green; cilia are stained red with anti-acetylated-tubulin antibodies, respectively.

D

(D) BBS6 remains associated with centrosomes throughout the cell cycle. Synchronized IMCD3 cells were co-stained with antibodies to BBS6 (green) and γ-tubulin (red); yellow indicates overlapping signals.

(E) BBS6 is localized at the midbody during the mitosis. BBS6 is found at the centrosomes (indicated by arrowheads) and midbody region (indicated by an arrow) during telophase, as judged by its co-localization with γ-tubulin.

Figure 3-5 BBS6 is localized within the pericentriolar material (PCM) tube and shows a dynamic distribution during the cell cycle.

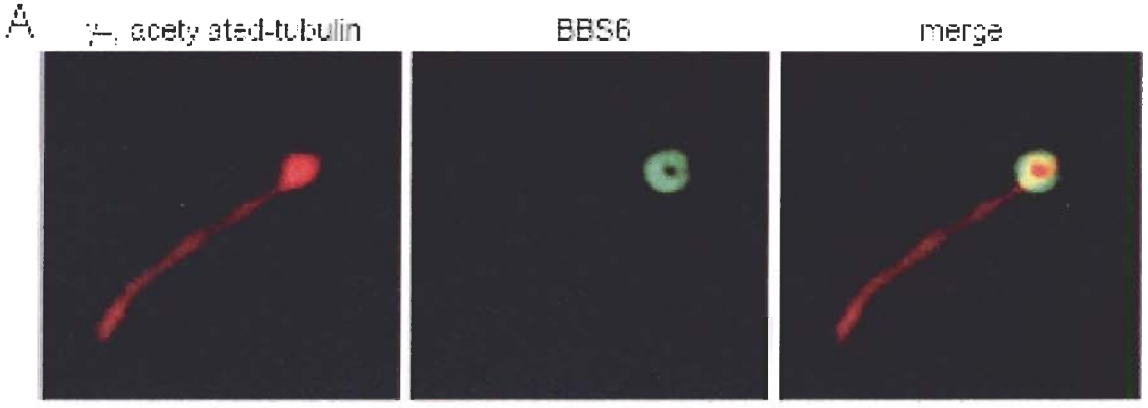

(A) BBS6 localizes at the O-shaped structure surrounding the γ-tubulin. High resolution digital microscopy optical sections of NIH 3T3 cells co-stained with antibodies against BBS6 (green) and γ- and acetylated-tubulin (red).

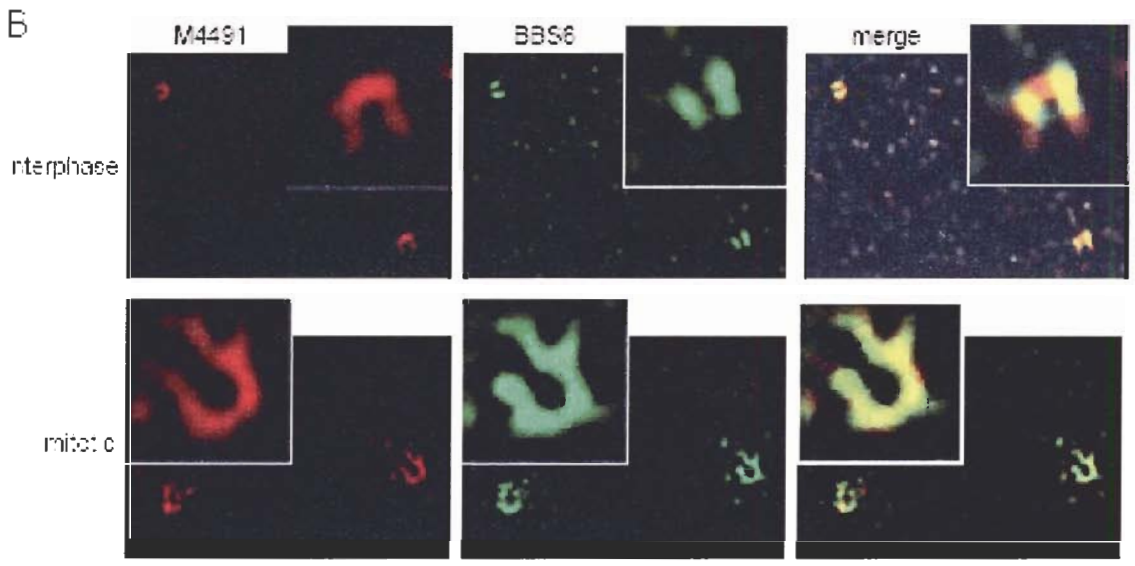

(B) BBS6 localizes at the PCM tube structure. Optical sections of BBS6 (green) and PCM tube (red) signals in the same focal plane from interphase or mitotic NIH 3T3 cells. The PCM tube was detected using an antibody, M4491, that recognizes multiple PCM components. Closeups of the PCM (insets), BBS6 and merged signals are also shown.

Figure 3-6 Centrosomal assembly of BBS6 is not dependent on polymerized microtubules or the dynein-dynactin molecular motor.

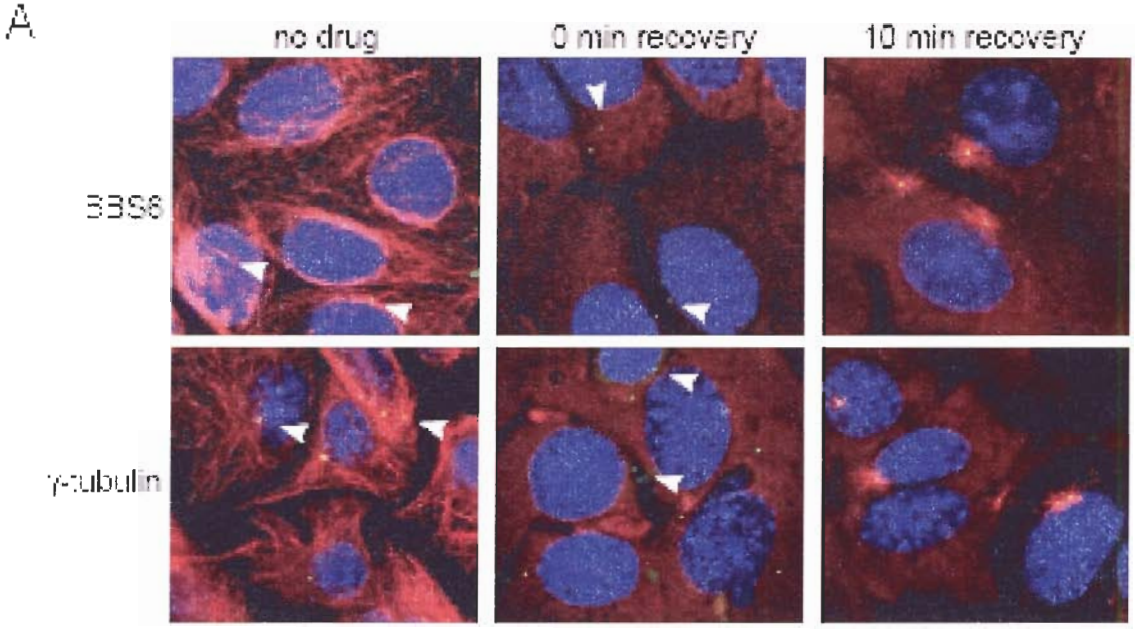

(A) Centrosomal localization of BBS6 is not affected by the disassembly of microbule. IMCD3 cells were either mock-treated (no drug) or treated with nocodazole for 1 hour and allowed to recover for 0 or 10 minutes. Cells were then co-stained with antibodies to BBS6 or γ-tubulin (green) and α-tubulin (red).

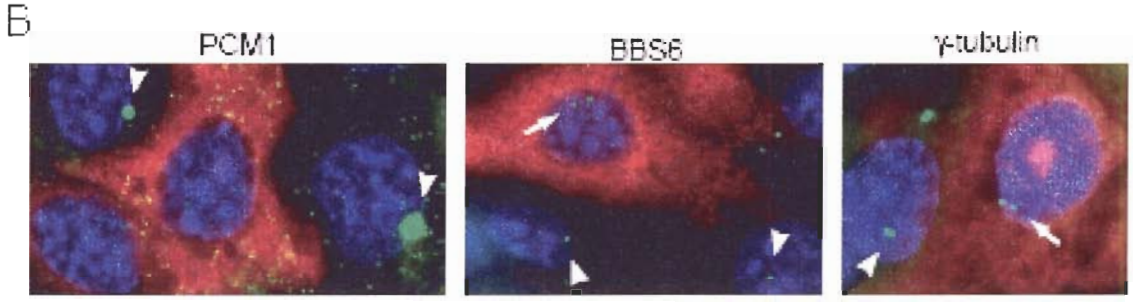

(B) BBS6 is delivered to the centrosome in the dynein-independent manner. IMCD3 cells were transiently transfected with *myc*-tagged p50-dynamitin, which inhibits dynein-dynactin motor function. Cells were then stained with an anti-*myc* antibody (red) and co-strained with antibodies to BBS6, PCM1 or γ-tubulin (green). Arrows denote centrosomal BBS6 and γ-tubulin signals from p50-dynamitin-transfected cells, and arrowheads denote centrosomal BBS6, PCM1 and γ-tubulin in untransfected cells. Note the dispersed PCM1 signal in transfected cells.

Figure 3-7 The centrosomal localization of BBS6 is abrogated by several mutations found in patients, and is conferred by the apical domain region.

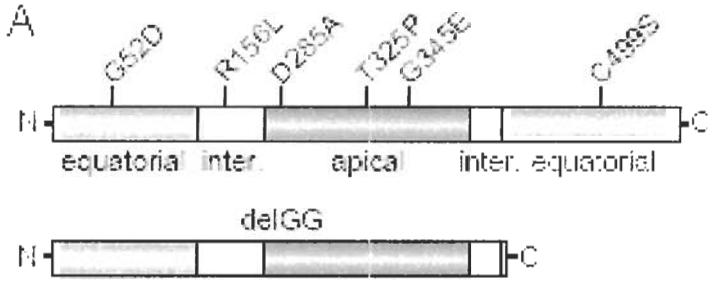

(A) Schematic diagram of the BBS6 variants tested. The equatorial, intermediate and apical domain regions are indicated, along with the positions of the 6 missense variants, and the extent of the truncation in the delGG mutant.

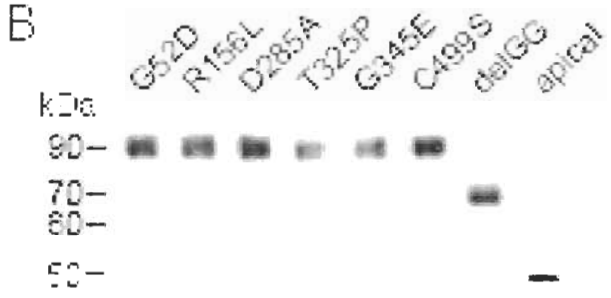

(B) Western blot analysis of all GFP-tagged BBS6 variants expressed in COS-7 cells, detected using an anti-GFP antibody.

C

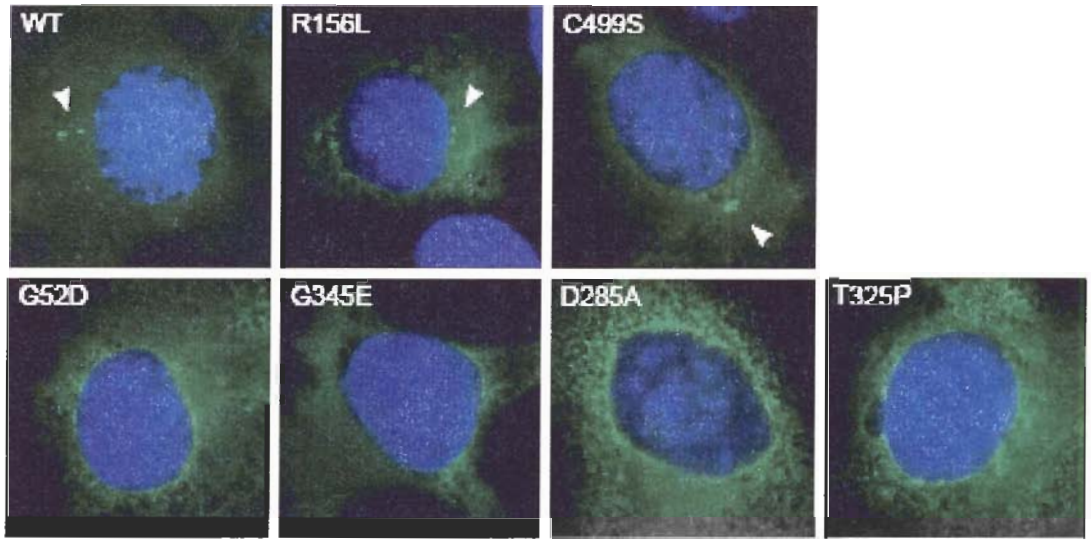

(C) Several BBS4 mutants found in BBS patients are mislocalized. Localization of GFP-tagged BBS6 variants were detected *via* GFP fluorescence. Two mutants (R156L and C499S) localize to the centrosome, as with GFP-tagged wild-type (WT) BBS6 (WT: 69% of the cells show centrosomal localization, n=190, R156: 53%, n=130, C499S: 72%, n=130, top panels); four variants fail to localize to the centrosome (G52D: 2% of the cells show centrosomal localization, n=155, G345E: 1%, n=100, D285A: 7%, n=150 and T325P: 0%, n=128; bottom panels).

D

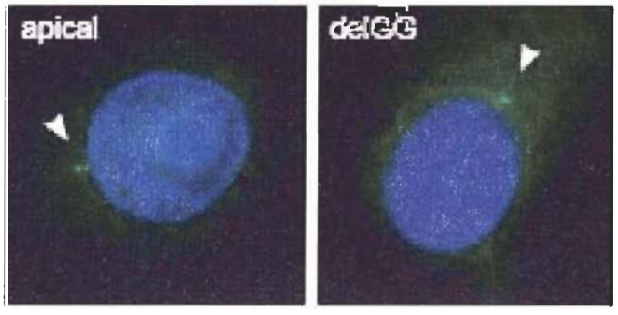

(D) The GFP-tagged apical domain of BBS6 localizes to the centrosome, as does the delGG truncation mutant (apical: 46% of the cells show centrosomal localization, n=144, delGG: 34%, n=200).

Figure 3-8 **Silencing of *BBS6* by RNA interference in COS-7 and NIH 3T3 cells produces multi-nucleated and multi-centrosomal cells, and cytokinesis defects.**

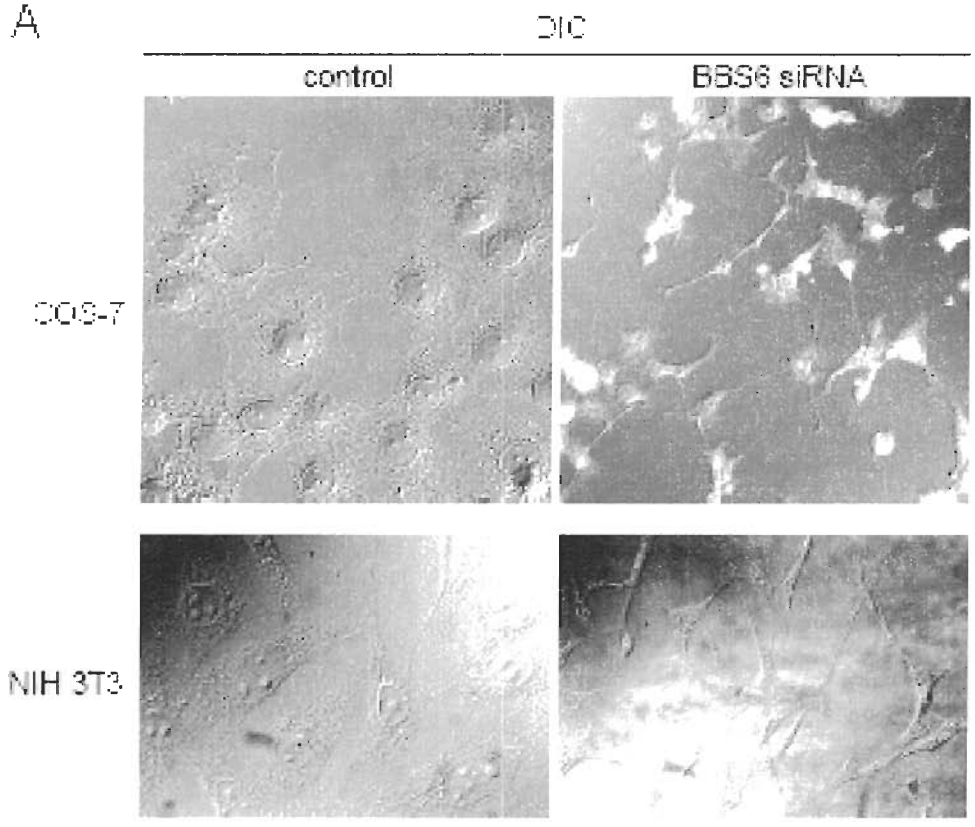

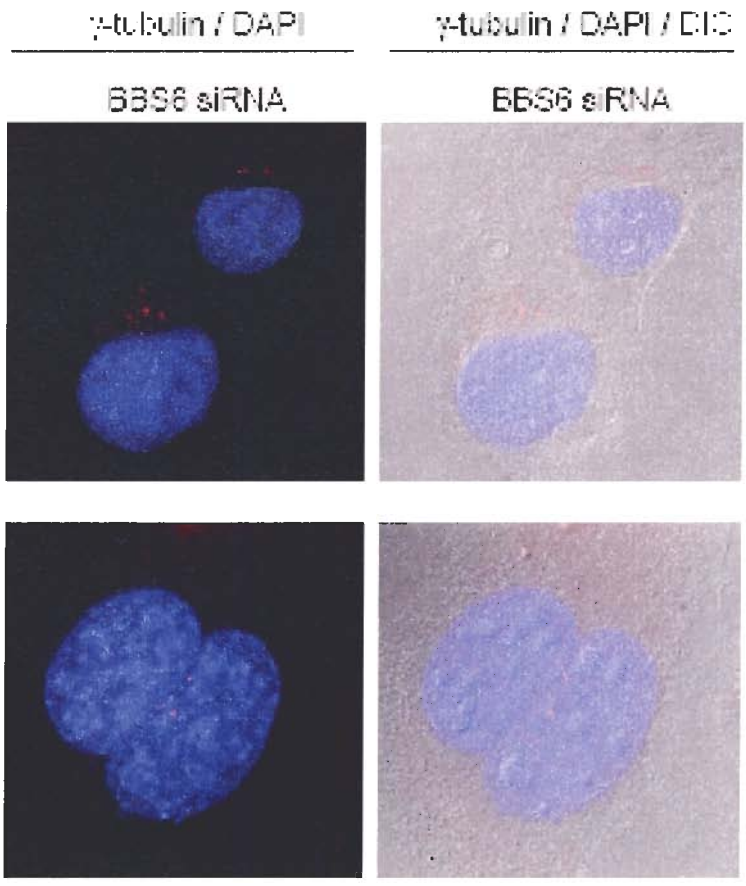

(A) BBS6 knock-down induces the cytokinesis defects in mammalian cultured cells. DIC images of COS-7 and NIH 3T3 cells 9 days after transfection with *BBS6* siRNA expression vector (pSilencer-BBS6 or pSuper-BBS6, respectively) show cells connected with long intercellular bridges as a result of defective cytokinesis. Immunocytochemistry experiments with γ-tubulin (red) and DAPI (blue) show that *BBS6* silencing causes bi-nucleated and multi-centrosomal phenotypes in both COS-7 and NIH 3T3 cells. The merged images (right panels) show 2 nuclei in single cells

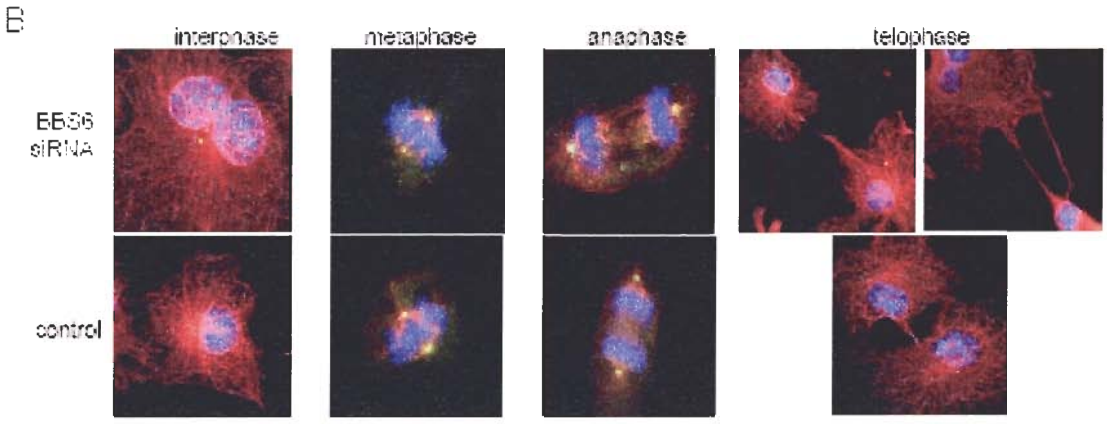

(B) BBS6 knock-down cells do not show microtubule disorganization. Microtubule organization is not significantly altered during cell cycle progression in COS-7 cells transfected with pSilencer-BBS6 (upper panels) compared with cells transfected with pSilencer empty vector (lower panels). Cells were stained with antibodies to α-tubulin (red), γ-tubulin (green), and DAPI (blue). Only merged images are shown; yellow indicates overlapping α-tubulin and γ-tubulin signals.

Figure 3-9 *BBS6* silenced NIH3T3 cells display centrosomal anomalies

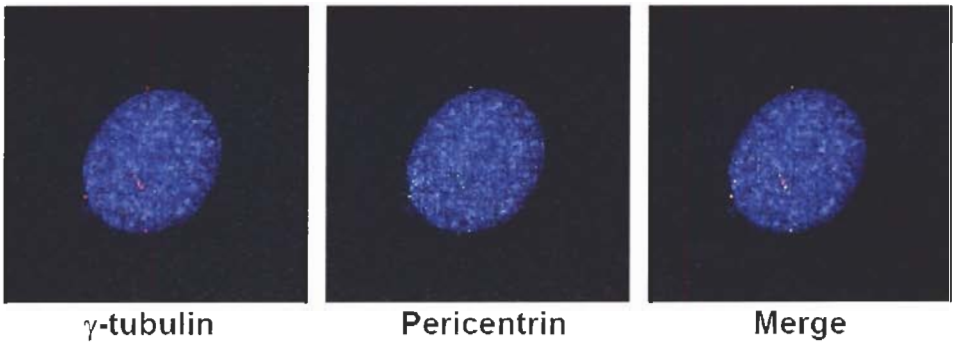

Immunocytochemistry experiment with γ-tubulin and pericentrin antibody shows that *BBS6* silencing causes multi-centrosomal phenotypes in NIH3T3. Note that multiple γ-tubulin spots overlap with pericentrin suggesting the γ-tubulin spots are constituents of bona fide centrosomes.

Figure 3-10 Reduction of *BBS6* expression level correlates with the observed cytokinesis and centrosome defects

	Control	Line A	Line B
BBS6 immunocytochemistry signal	64507 (N=120)	31859 (N=150)	18629 (N=107)
Binuclear cells	2.6% (N=386)	8.3% (N=361)	10.5% (N=388)
Multicentrosomal cells	4% (N=719)	13.3% (N=408)	17.5% (N=450)

Quantitative immunocytochemistry analysis on both line A and B shows that the fluorescent signal of BBS6 decreased by 2 and 3.5 fold respectively and also that this decrease is tightly correlated to the cytokinesis and centrosome defects. Note that the discrepancy in the degree of the observed reduction level between the quantitative RT-PCR and indirect immunocytochemistry can simply be explained by the possible saturation of the fluorescent signal during the fluorescent microscopy.

Figure 3-11 BBS6 is enriched in organs affected in BBS and in ciliated cells.

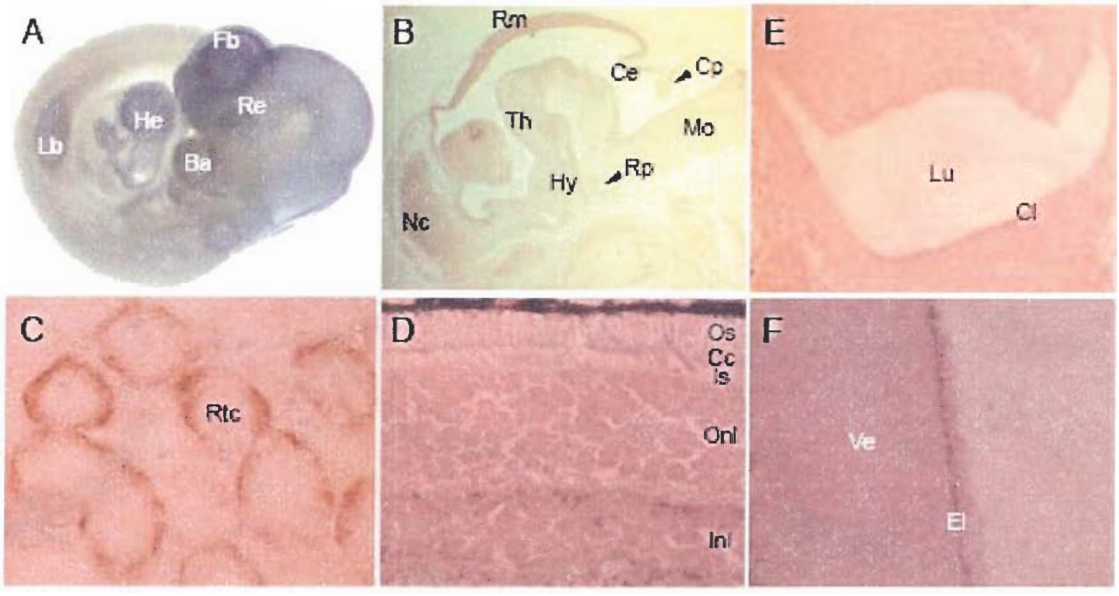

(**A**) Wholemount RNA *in* situ hybridization of an E10 mouse embryo showing strong *BBS6* expression in the forebrain (Fb), retina (Re), branchial arches (Ba), developing heart (He) and limb bud (Lb). (**B**) Immunohistochemistry using BBS6 antibody; saggital section of a mouse E13.5 brain showing protein staining in the developing nervous system, including the neopallial cortex (Nc), the roof of the midbrain (Rm), the cerebellar primordium (Ce), the choroid plexus (Cp), the hypothalamus (Hy) and Rathke's pouch (Rp). Modest BBS6 protein staining is also detectable in the thalamus (Th) and the medulla oblongata (Mo). (**C**) In the adult kidney, BBS6 localizes to the ciliated border of renal tubular cells (Rtc). (**D**) In the adult photoreceptor, BBS6 is detected in the connecting cilium (Cc) and the inner and outer nuclear layers (Inl, Onl) but not the outer or inner segment (Os, Is). (**E, F**) BBS6 localizes to the ciliated layer of the olfactory epithelium (cl) as well as the ependymal layer (El) of ventricles (Ve); Lu, lumen.

G

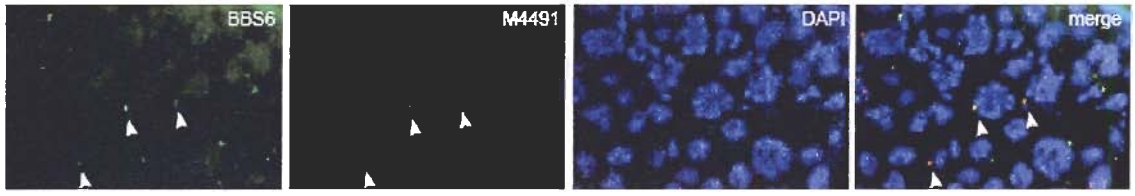

(**G**) **BBS6 localizes at the centrosome in both mitotic and meiotic cells.** A section of mouse testis is stained for BBS6 (green) and the PCM tube (antibody M4491; red). The area shown is taken from the periphery of a semineferous tubule containing both meiotic and spermatogenic cells. BBS6 co-localizes to centrosomes/basal bodies, but not the flagellar axoneme, in spermatogenic cells. Also shown are nuclei (DAPI stained, blue) and a merged image. (This experiment was conducted through collaboration with Dr. Jerome Rattner).

3.7 Reference list

Ansley, S. J., Badano, J. L., Blacque, O. E., Hill, J., Hoskins, B. E., Leitch, C. C., Kim, J. C., Ross, A. J., Eichers, E. R., Teslovich, T. M., et al. (2003). Basal body dysfunction is a likely cause of pleiotropic Bardet-Biedl syndrome. Nature 425, 628-633.

Archibald, J. M., Logsdon, J. M., and Doolittle, W. F. (1999). Recurrent paralogy in the evolution of archaeal chaperonins. Curr Biol 9, 1053-1056.

Archibald, J. M., Logsdon, J. M., Jr., and Doolittle, W. F. (2000). Origin and evolution of eukaryotic chaperonins: phylogenetic evidence for ancient duplications in CCT genes. Mol Biol Evol 17, 1456-1466.

Badano, J. L., Ansley, S. J., Leitch, C. C., Lewis, R. A., Lupski, J. R., and Katsanis, N. (2003). Identification of a novel Bardet-Biedl syndrome protein, BBS7, that shares structural features with BBS1 and BBS2. Am J Hum Genet 72, 650-658.

Beales, P. L., Elcioglu, N., Woolf, A. S., Parker, D., and Flinter, F. A. (1999). New criteria for improved diagnosis of Bardet-Biedl syndrome: results of a population survey. J Med Genet 36, 437-446.

Blacque, O. E., Reardon, M. J., Li, C., McCarthy, J., Mahjoub, M. R., Ansley, S. J., Badano, J. L., Mah, A. K., Beales, P. L., Davidson, W. S., et al. (2004). Loss of *C. elegans* BBS-7 and BBS-8 protein function results in cilia defects and compromised intraflagellar transport. Genes Dev 18, 1630-1642.

Brummelkamp, T. R., Bernards, R., and Agami, R. (2002). A system for stable expression of short interfering RNAs in mammalian cells. Science 296, 550-553.

Carrascosa, J. L., Llorca, O., and Valpuesta, J. M. (2001). Structural comparison of prokaryotic and eukaryotic chaperonins. Micron 32, 43-50.

Chiang, A. P., Nishimura, D., Searby, C., Elbedour, K., Carmi, R., Ferguson, A. L., Secrist, J., Braun, T., Casavant, T., Stone, E. M., and Sheffield, V. C. (2004). Comparative Genomic Analysis Identifies an ADP-Ribosylation Factor-like Gene as the Cause of Bardet-Biedl Syndrome (BBS3). Am J Hum Genet 75.

Ditzel, L., Lowe, J., Stock, D., Stetter, K. O., Huber, H., Huber, R., and Steinbacher, S. (1998). Crystal structure of the thermosome, the archaeal chaperonin and homolog of CCT. Cell 93, 125-138.

Gascuel, O. (1997). BIONJ: an improved version of the NJ algorithm based on a simple model of sequence data. Mol Biol Evol 14, 685-695.

Gutsche, I., Essen, L. O., and Baumeister, W. (1999). Group II chaperonins: new TRiC(k)s and turns of a protein folding machine. J Mol Biol 293, 295-312.

Hartl, F. U., and Hayer-Hartl, M. (2002). Molecular chaperones in the cytosol: from nascent chain to folded protein. Science 295, 1852-1858.

Horwich, A. L., and Willison, K. R. (1993). Protein folding in the cell: functions of two families of molecular chaperone, hsp 60 and TF55-TCP1. Philos Trans R Soc Lond B Biol Sci 339, 313-325; discussion 325-316.

Hynes, G., Kubota, H., and Willison, K. R. (1995). Antibody characterisation of two distinct conformations of the chaperonin-containing TCP-1 from mouse testis. FEBS Lett 358, 129-132.

Katsanis, N. (2004). The oligogenic properties of Bardet-Biedl syndrome. Hum Mol Genet 13 Spec No 1, R65-71.

Katsanis, N., Beales, P. L., Woods, M. O., Lewis, R. A., Green, J. S., Parfrey, P. S., Ansley, S. J., Davidson, W. S., and Lupski, J. R. (2000). Mutations in MKKS cause obesity, retinal dystrophy and renal malformations associated with Bardet-Biedl syndrome. Nat Genet 26, 67-70.

Kim, J. C., Badano, J. L., Sibold, S., Esmail, M. A., Hill, J., Hoskins, B. E., Leitch, C. C., Venner, K., Ansley, S. J., Ross, A. J., et al. (2004). The Bardet-Biedl protein BBS4 targets cargo to the pericentriolar region and is required for microtubule anchoring and cell cycle progression. Nat Genet 36, 462-470.

Kubota, H., Hynes, G., and Willison, K. (1995). The chaperonin containing t-complex polypeptide 1 (TCP-1). Multisubunit machinery assisting in protein folding and assembly in the eukaryotic cytosol. Eur J Biochem 230, 3-16.

Leroux, M. R., and Hartl, F. U. (2000). Protein folding: versatility of the cytosolic chaperonin TRiC/CCT. Curr Biol 10, R260-264.

Li, J. B., Gerdes, J. M., Haycraft, C. J., Fan, Y., Teslovich, T. M., May-Simera, H., Li, H., Blacque, O. E., Li, L., Leitch, C. C., et al. (2004). Comparative genomics identifies a flagellar and basal body proteome that includes the BBS5 human disease gene. Cell 117, 541-552.

Mack, G. J., Rees, J., Sandblom, O., Balczon, R., Fritzler, M. J., and Rattner, J. B. (1998). Autoantibodies to a group of centrosomal proteins in human autoimmune sera reactive with the centrosome. Arthritis Rheum 41, 551-558.

Meyer, A. S., Gillespie, J. R., Walther, D., Millet, I. S., Doniach, S., and Frydman, J. (2003). Closing the folding chamber of the eukaryotic chaperonin requires the transition state of ATP hydrolysis. Cell 113, 369-381.

Mykytyn, K., Braun, T., Carmi, R., Haider, N. B., Searby, C. C., Shastri, M., Beck, G., Wright, A. F., Iannaccone, A., Elbedour, K., et al. (2001). Identification of the gene that, when mutated, causes the human obesity syndrome BBS4. Nat Genet 28, 188-191.

Mykytyn, K., Mullins, R. F., Andrews, M., Chiang, A. P., Swiderski, R. E., Yang, B., Braun, T., Casavant, T., Stone, E. M., and Sheffield, V. C. (2004). Bardet-Biedl syndrome type 4 (BBS4)-null mice implicate Bbs4 in flagella formation but not global cilia assembly. Proc Natl Acad Sci U S A 101, 8664-8669.

Mykytyn, K., Nishimura, D. Y., Searby, C. C., Shastri, M., Yen, H. J., Beck, J. S., Braun, T., Streb, L. M., Cornier, A. S., Cox, G. F., et al. (2002). Identification of the gene

(BBS1) most commonly involved in Bardet-Biedl syndrome, a complex human obesity syndrome. Nat Genet 31, 435-438.

Nishimura, D. Y., Searby, C. C., Carmi, R., Elbedour, K., Van Maldergem, L., Fulton, A. B., Lam, B. L., Powell, B. R., Swiderski, R. E., Bugge, K. E., et al. (2001). Positional cloning of a novel gene on chromosome 16q causing Bardet-Biedl syndrome (BBS2). Hum Mol Genet 10, 865-874.

O'Halloran, T. J. (2000). Membrane traffic and cytokinesis. Traffic 1, 921-926.

Ou, Y., and Rattner, J. B. (2000). A subset of centrosomal proteins are arranged in a tubular conformation that is reproduced during centrosome duplication. Cell Motil Cytoskeleton 47, 13-24.

Ou, Y. Y., Zhang, M., Chi, S., Matyas, J. R., and Rattner, J. B. (2003). Higher order structure of the PCM adjacent to the centriole. Cell Motil Cytoskeleton 55, 125-133.

Pappenberger, G., Wilsher, J. A., Roe, S. M., Counsell, D. J., Willison, K. R., and Pearl, L. H. (2002). Crystal structure of the CCTgamma apical domain: implications for substrate binding to the eukaryotic cytosolic chaperonin. J Mol Biol 318, 1367-1379.

Piel, M., Nordberg, J., Euteneuer, U., and Bornens, M. (2001). Centrosome-dependent exit of cytokinesis in animal cells. Science 291, 1550-1553.

Siegers, K., Waldmann, T., Leroux, M. R., Grein, K., Shevchenko, A., Schiebel, E., and Hartl, F. U. (1999). Compartmentation of protein folding in vivo: sequestration of non- native polypeptide by the chaperonin-GimC system. EMBO J 18, 75-84.

Siegert, R., Leroux, M. R., Scheufler, C., Hartl, F. U., and Moarefi, I. (2000). Structure of the molecular chaperone prefoldin: unique interaction of multiple coiled coil tentacles with unfolded proteins. Cell 103, 621-632.

Slavotinek, A. M., Stone, E. M., Mykytyn, K., Heckenlively, J. R., Green, J. S., Heon, E., Musarella, M. A., Parfrey, P. S., Sheffield, V. C., and Biesecker, L. G. (2000). Mutations in MKKS cause bardet-biedl syndrome. Nat Genet 26, 15-16.

Stone, D. L., Slavotinek, A., Bouffard, G. G., Banerjee-Basu, S., Baxevanis, A. D., Barr, M., and Biesecker, L. G. (2000). Mutation of a gene encoding a putative chaperonin causes McKusick-Kaufman syndrome. Nat Genet 25, 79-82.

Strimmer, K., and von Haeseler, A. (1996). Quartet puzzling: a quartet maximum-likelihood method for reconstructing tree topologies. Mol Biol Evol 13, 964-969.

Tsvetkov, L., Xu, X., Li, J., and Stern, D. F. (2003). Polo-like kinase 1 and Chk2 interact and co-localize to centrosomes and the midbody. J Biol Chem 278, 8468-8475.

Vainberg, I. E., Lewis, S. A., Rommelaere, H., Ampe, C., Vandekerckhove, J., Klein, H. L., and Cowan, N. J. (1998). Prefoldin, a chaperone that delivers unfolded proteins to cytosolic chaperonin. Cell 93, 863-873.

Valpuesta, J. M., Martin-Benito, J., Gomez-Puertas, P., Carrascosa, J. L., and Willison, K. R. (2002). Structure and function of a protein folding machine: the eukaryotic cytosolic chaperonin CCT. FEBS Lett 529, 11-16.

Vaughan, K. T., and Vallee, R. B. (1995). Cytoplasmic dynein binds dynactin through a direct interaction between the intermediate chains and p150Glued. J Cell Biol 131, 1507-1516.

Weber, F., Keppel, F., Georgopoulos, C., Hayer-Hartl, M. K., and Hartl, F. U. (1998). The oligomeric structure of GroEL/GroES is required for biologically significant chaperonin function in protein folding. Nat Struct Biol 5, 977-985.

CHAPTER 4
TRANSCRIPTIONAL REGULATION OF BBS GENES THROUGH X-BOX ELEMENTS

Results of this chapter have been published in *Nature.* 2003, 425(6958): 628-33 with the following authors involved:

Stephen J. Ansley[1,*], Jose L. Badano[1,*], Oliver E. Blacque[3,*], Josephine Hill[4], Bethan E. Hoskins[1,4], Carmen C. Leitch[1], Jun Chul Kim[3], Alison J. Ross[4], Erica R. Eichers[5], Tanya M. Teslovich[1], Allan K. Mah[3], Robert C. Johnsen[3], John C. Cavender[7], Richard Alan Lewis[5,6], Michel R. Leroux[3], Philip L. Beales[4] and Nicholas Katsanis[1,2]

[1] Institute of Genetic Medicine, Johns Hopkins University, Baltimore, Maryland 21287, USA
[2] Wilmer Eye Institute, Johns Hopkins University, Baltimore, Maryland 21287, USA
[3] Department of Molecular Biology and Biochemistry, Simon Fraser University, Burnaby, British Columbia, V5A 1S6 Canada
[4] Molecular Medicine Unit, Institute of Child Health, University College London, London WC1N 1EH, UK
[5] Departments of Molecular and Human Genetics, Baylor College of Medicine, Houston, Texas 77030, USA
[6] Departments of Ophthalmology, Pediatrics, and Medicine, Baylor College of Medicine, Houston, Texas 77030, USA
[7] King Khaled Eye Hospital, Riyadh, 11462, Saudi Arabia
* These authors contributed equally to this work
Correspondence and requests for materials should be addressed to N.K. (katsanis@jhmi.edu).

Using *C.elegans* as a model organism, this study discovered that *bbs* genes are expressed only in ciliated cells. I made a significant discovery, which was that *bbs* genes are transcriptionally regulated by X-box transcription factor binding sites and that BBS8 protein localizes at the centrosome and basal body of the cilia in mammalian cells by immunocytochemistry. This chapter was written based on those two results.

4.1 Introduction

By October, 2003, eight *BBS* loci (*BBS1, 2, 3, 4, 5, 6, 7 and 8*) had been identified and six of them (*BBS1, 2, 4, 6, and 7*) had been positionally cloned. Bioinformatic approaches with these newly identified *BBS* genes provided several important clues to understand the cellular function of BBS proteins. Blast analysis against the NCBI database revealed that *BBS* genes do not exist in bacteria, fungi, and plant but are found in animal and flagellated lower eukaryotes such as *Chlamydomonas* and *Tetrahymena.* In addition, computational domain analysis showed that BBS4 contains multiple TPR domains involved in protein-protein interactions (see chapter 2), and that BBS6 has the same domain organization as the TCP-1 chaperonin family (see chapter 3).

Despite this additional information, it was not until *BBS8* gene was cloned and characterized that we began to understand the cellular function of BBS proteins. Ansley et al (2003) identified the *BBS8* gene by virtue of its domain similarity to BBS4 and showed that it contains two types of functional motif. Like BBS4, BBS8 was shown to have multiple TPR domains suggesting that BBS4 and 8 may bind each other and form a protein complex. The analysis also revealed that BBS8 contain a sequence similar to that of the pilF domain, which is involved in twitching mobility and type-IV pilus assembly in prokaryotes (Ansley et al, 2003). The meaning of this latter finding is unclear, however, given that the bacterial pilus is not homologous to eukaryotic cilia.

In this study, it was also demonstrated that BBS8 shows very specific spatial expression pattern in the adult body of mice and *C. elegans*. BBS8 was shown to localize at the centrosome and the basal body of the primary cilia in the cultured mammalian cell

(Figure 4-1), and immunohistochemistry experiment showed that BBS8 is exclusively expressed at ciliated structure in mice tissues including retina in eye, olfactory tissue in nose, and renal tubule in kidney.

Consistent with the expression pattern of *BBS8* in mice, studies with GFP-*bbs-8* promoter fusion construct demonstrated that *C.elegans bbs*-8 is exclusively expressed in ciliated neuronal cells (Ansley et al, 2003). The adult body of *C. elegans* consists of a total of 959 somatic cells and a variable number of germ cells. Out of 959 cells, only 302 are neuronal cells and of these, 60 are ciliated (Sloboda et al, 2002). The cilia of these neurons extend from the dendrites to outside of the worm's cuticle where they sample the chemical environment, therefore acting to sense chemical signals such as food or pheremone. Importantly, this specific spatial expression pattern of *bbs*-8 proved to be common for all *C. elegans bbs* genes. Specifically, experiments with GFP-*bbs* transcriptional fusion constructs revealed that all known C. elegans *bbs* orthologues are expressed in ciliated neuronal cells but not in non-ciliated cells (Ansley et al, 2003; Li et al, 2004; Blacque et al. 2004).

Given the fact that mutations in any of the known *BBS* genes causes symptoms that cannot distinguish which gene is abrogated in BBS patients, it had been a long held hypothesis that all BBS proteins are likely involved in the same cellular activity. Thus, the finding that multiple *BBS* genes are expressed exclusively in ciliated cells in both *C. elegans* and mouse obviously raised the hypothesis that BBS proteins should function in the cellular activities related to cilia and basal body, and therefore that the dysfunction of cilia or basal body is likely the cause of BBS.

Cilia and flagella are ubiquitous, hair-like organelles extending from the surfaces of many eukaryotic cell types, and they have evolved to play two very different roles, involving motility and sensory function (Scholey, 2003). Structurally, the cilium can be divided into two major parts; basal body and axoneme. Basal bodies are structurally identical to centrioles found in centrosomes, which are composed of nine triplet microtubule structures arranged in a barrel-like shape (Zimmerman et al., 1999). The axoneme of cilia, in contrast, consists of nine doublet microtubule structures surrounding two central, singular microtubules (9+2 structure). In addition, in motile cilia and flagella, axonemal dynein motors cross-link and slide adjacent microtubule doublets, therefore generating the force for the beating motion (Porter & Sale 2000). The membrane structure surrounding the ciliary axoneme is continuous with the plasma membrane of the cell surface, although its composition is assumed to be significantly different from that of plasma membrane (Rosenbaum and Witman, 2002).

Motile cilia found on protozoa and differentiated animal cells such as tracheal epithelia or spermatozoa have a characteristic 9+2 axoneme structure, and their rhythmic beating moves cells through fluid media or moves fluid media over stationary cell surfaces (Porter and Sale, 2000). Primary cilia found in many different types of animal cells have a 9+0 architecture (meaning the central microtubule pair is missing) and are not motile, except for those cilia found on the embryonic node which are motile (Scholey, 2003). The function of primary cilia is less clear than that of motile cilia, but it has been shown that the flow-induced bending of primary cilia on cultured kidney cells leads to an elevation of intracellular calcium ion, suggesting that the primary cilia play a mechanosensory role (Praetorius and Spring, 2001). It has been also demonstrated that

during early embryonic development, two different populations of primary cilia on the embryonic node determine the left-right axis of body plan by generating a fluid flow called nodal flow on the surface of embryo and sensing a resulting morphogen gradient. Centrally located, dynein-containing motile primary nodal cilia generate leftward nodal flow, and non-dynein containing immotile nodal primary cilia sense the morphogen gradient that are thought to be formed by a nodal flow (McGrath et al., 2003).

There is also a very specialized type of immotile cilia, namely the sensory cilia. The sensory cilia are found in vertebrate photoreceptors in the retina, epithelial layer in olfactory tissue, and at the tip of sensory neurons in *C. elegans*, for example (Perkins et al. 1986, Marszalek et al. 2000) where it serves as specialized structures that concentrates and organizes the sensory signaling machinery (Scholey, 2003).

The assembly of cilia involves the delivery of key components, including tubulins, dynein arms, and radial spokes to the tip of cilia where the actual assembly occurs (Scholey, 2003). Because these key components such as dynein arms and radial spokes are either synthesized or preassembled in the cell body, it had been proposed that there should be a certain type of transport process which can actively move cargos along the axoneme. Indeed, Kozminsky et al (1993) discovered by differential interference contrast (DIC) microscopy that granule-like 500nm particles (IFT particles) move bidirectionally along the ciliary axoneme in *Chlamydomonas reinhardtii*, at rates of 2.0 μm/s from base to tip and 3.5 μm/s from tip to base (Kozminski et al. 1993, 1995), and named it 'intraflagellar transport (IFT)'.

Since IFT was discovered in 1993, various biochemical and genetic studies with *Chlamydomonas* have identified the molecular machinery of IFT including IFT motors,

IFT particles, and cargo proteins. It was found that kinesin-II and cytoplasmic dynein (also known as IFT-dynein) motor complexes are responsible for anterograde and retrograde IFT, respectively. Two types of kinesin-II motor are thought to empower anterograde IFT, namely heterotrimeric kinesin-II (also known as FLA-10-kinesin-II or KIF3A/3B/KAP3) and homodimeric kinesin-II (also known as OSM-3-kinesin in *C. elegans* or KIF17 in mammals). In mouse, there are two heterotrimeric kinesin-II complexes, KIF3A/KIF3B/KAP and KIF3A/KIF3C/KAP; however, it is not understood whether they are functionally related each other (Yang et al. 2001).

Whereas the function of heterotrimeric kinesin-II as an anterograde IFT motor has been demonstrated in multiple organisms, including *Chlamydomonas* and *C. elegans*, and is therefore thought to be conserved throughout various organisms, the function of homodimeric kinesin-II in anterograde IFT has thus far only been observed in *C. elegans* (Signor et al. 1999). In *C. elegans*, loss of function mutation in *osm-3* gene encoding homodimeric kinesin-II lead to partially truncated sensory cilia (Starich et al. 1995).

The function of IFT dynein as retrograde motor was demonstrated by the findings that mutations in gene encoding the heavy chains (DHC-1b or CHE-3), light intermediate chains (D2LIC), and light chains (LC8) of IFT dynein motor complex in *Chlamydomonas or C. elegans* disrupt specifically the retrograde IFT movement without affecting anterograde IFT (Pazour et al. 1998, 1999; Porter et al. 1999; Wicks et al. 2000; Perrone et al. 2003; Schafer et al. 2003). As a result, in the retrograde IFT defective mutants, IFT particles accumulate at the tip of cilia.

Based on the observation that IFT particles are depleted from the flagella of the temperature sensitive *Chlamydomonas* kinesin mutant *fla10* (Kozminski et al. 1995), it

was hypothesized that one could purify the IFT particles by identifying proteins that disappear from the flagellar extract fractions when the *fla10* mutant is grown at non-permissive temperature. Following this idea, Cole et al. (1998) isolated two different type of protein complex (IFT complexes A and B) and found that the particles consist of approximately 15 polypeptides in total. It was demonstrated that mutations affecting homologs of two of the IFT particle polypeptides in *C. elegans* result in defects in the sensory cilia (Cole et al, 1998).

Interestingly, defects in intraflagellar transport (IFT) have been associated with various genetic diseases, including autosomal recessive polycystic kidney disease (ARPKD) and hereditary retinal degenerative disease. Mutations in *Tg737* gene, a mammalian homologue of *Chlamydomonas* IFT-88 or *C. elegans* OSM-5 cause ARPKD in mice (Moyer et al, 1994). Mice that have homozygous insertional mutations in *Tg737* fail to assemble the primary cilia on kidney collecting ducts and tubules owing to IFT defect, and develop polycystic kidney phenotypes (Pazour et al, 2000).

In an attempt to test the hypothesis that BBS proteins are involved in growth or maintenance of cilia, Blacque et al. (2004) demonstrated that loss of function mutations in *C. elegans bbs-7* and *bbs-8* genes result in structural and functional defects in cilia, including shortened/abnormal cilia and chemosensory abnormalities (Blacque et al., 2004). As shown in mice tissue and the cultured mammalian cells, the translational GFP-BBS fusion proteins are expressed exclusively in ciliated sensory neurons and localize predominantly at the base of cilia. Surprisingly, however, time-lapse fluorescence microscopy revealed that GFP-BBS fusion proteins show bidirectional movements along the ciliary axoneme, which is reminiscent of that of IFT particles (Blacque et al., 2004),

suggesting that BBS proteins may be associated with the IFT process. To test this hypothesis, the authors investigated the localization and movement of known IFT particle proteins (OSM-5, CHE-2, and CHE-11) in the *bbs-7* and *bbs-8* mutants. OSM-5, CHE-2, and CHE-11 in the wild-type animals are localized to the transition zones (basal bodies) and ciliary axonemes, where they show prominent IFT movements. However, when same IFT particle proteins were observed in the *bbs-7* and *bbs-8* mutants, OSM-5 and CHE-11 showed abnormal localization pattern and decreased IFT movements. Interestingly, the localization and IFT movement of CHE-2 was nearly normal, suggesting the function of BBS-7 and BBS-8 may not required for IFT process in general but more likely associated with specific sets of IFT proteins.

Given that there are no detectable differences in the expression pattern between different *bbs* genes in *C. elegans*, we hypothesized that there should be a common transcription factor that regulates the cilia-specific expression of all *bbs* genes. In order to find this regulatory factor, we computationally analyzed the promoter sequences of all available *C. elegans bbs* genes (*bbs-1, 2, 4, 7, and 8*) and obtained lists of transcription factors which can potentially bind to the promoter of *bbs* genes. Interestingly, we noticed that there are putative binding sites termed X-box which is the binding site for the RFX (Regulatory Factor X) type family of transcription factor, in the promoter regions of all *bbs* genes tested suggesting that RFX type transcription factor(s) are responsible for the cilia-specific expression of *bbs* genes.

An RFX type transcription factor was first identified as a protein binding to the loosely conserved, cis-acting element named X-box in major histocompatibility complex II (MHC II) promoter, regulating its expression during immune responses (Reith et al.,

1989). Since then, many homologues have been found in different organisms including human and mouse, and it is now known that RFX transcription factors exist in a broad range of eukaryotic organisms, including fungi, nematode, fruit fly, and vertebrates (Morotomi-Yano et al., 2002). For example, five different members (RFX1-5) have been identified in human and mice, and one member was identified in *C. elegans* (DAF-19) and yeast (ScRFX) (Emery et al., 1996; Swoboda et al., 2000).

RFX type transcription factors consist of two functional motifs; a DNA binding domain that is highly conserved within the RFX family, and a domain for dimerization required for its association with other RFX type transcription factors (Emery et al., 1996). Interestingly, despite the strong conservation in DNA binding domains among the members of RFX family, each member of RFX family has been shown to bind different X-box sequences (Emery et al., 1996), suggesting that the range of their downstream targets may be broader than was initially thought.

Swoboda et al. (2000) provided the first evidence that the RFX transcription factor DAF-19 plays a role in cilia formation and function in *C. elegans*. Through genetic mapping and transgenic rescue experiments, the study demonstrated that mutations in *daf-19*, the *C. elegans* orthologue of human *RFX*, are responsible for the constitutive dauer formation phenotype (Daf-c phenotype) of a *daf-19* mutant worm, a phenotype sometimes associated with ciliary mutants (Malone and Thomas, 1994; Swoboda et al., 2000). Dauer larva represent an arrested form of the nematode that is capable of enduring harsh environmental conditions. When conditions become favourable again, it can revert to a larval form that develops into an adult worm (Swoboda et al., 2000). Importantly, the

entry into and exit from the dauer stage requires functional amphid (ciliated) sensory neurons (Bargmann, 1997).

Swoboda et al. (2000) showed that X-box binding sites for DAF-19 exist in the promoter region of several known genes that are involved in cilia growth and function, including, *che-2, che-13, odr-4, osm-1, osm-5, osm-6, xbx-1,* and *daf-19* itself. Mutations in X-box sequences abolished the cilia-specific expression pattern of *che-2*, *osm-1*, and *osm-6* in a DAF-19 dependant manner, suggesting that binding of DAF-19 to X-box elements is required for the transcriptional activation of genes required for sensory cilia formation or function.

4.2 Materials and methods

MatInspector is a free, web-based software tool that utilizes a large library of matrix descriptions for transcription factor binding sites to locate matches in DNA sequences (http://www.genomatix.de/cgi-bin/eldorado/main.pl). The results output consist of a core and a matrix similarity and the position and sequence of the found matches. The core sequence of a matrix is defined as the highest conserved positions of the transcription factor binding sites. The maximum core similarity of 1.0 is only reached when the highest conserved bases of a matrix match exactly in the sequence. The matrix sequences are the core sequence and the sequences flanking the core sequence which cover the whole recognition sites and affect the DNA binding efficiency of transcription factors. The matrix similarity is calculated as previously described (Quandt et al., 1995). A perfect match to the matrix returns a score of 1.00 (each sequence position corresponds

to the highest conserved nucleotide at that position in the matrix) and a "good" match to the matrix usually has a similarity of > 0.80. 1000bp upstream region from first ATG of *C. elegans bbs-1, 2, 5, 7, and 8* genes were analyzed to predict the potential transcription factor binding sites in *bbs* genes. The analysis results were sorted by quality, and only matches that show the core similarity of 1.0 and the matrix similarity of higher than 0.90 were considered as potential transcription factor binding sites.

4.3 Results

The promoter regions of *C. elegans* genes tend to be short, usually less than 1kb. By fusing the promoter sequence of the gene to the reporter system such as GFP, the idea of how the gene is developmentally regulated can be obtained. Previous studies on *C. elegans bbs* genes using the GFP-promoter fusion showed that *bbs* genes are specifically expressed only in ciliated neuron, implying the existence of common transcription factor(s) among different *bbs* genes promoter which derives the ciliated-cell specific transcription (Ansley et al., 2003).

To identify the unknown transcription factor(s) responsible for the tissue specific expression of *bbs* genes in *C. elegans*, the putative promoter region (1kb of 5'-upstream regions of translation start) of *C. elegans bbs-1, 2, 7,* and *8* were computationally analyzed by the software called MatInspector (see materials and methods). The MatInspector analysis revealed multiple potential binding sites for transcription factors in *bbs* genes promoter (Figure 4-2). The first 50 hits in the results sorted by quality were listed, and based on the published literature database, an analysis of whether any of them

is involved in the ciliated-cell specific expression was carried out. Interestingly, we found that the binding sites, namely X-box, for the transcription factor called RFX1, one of five known human RFX type transcription factors, exist in the promoter region of all *bbs* genes tested (Figure 4-2). The X-box elements of *bbs* genes are located around approximately 100bp upstream region from the first ATG. Alignment of X-box sequences from different *bbs* genes showed that these cis-acting elements are very well conserved among all *C. elegans bbs* genes (Figure 4-2).

Of major interest is the finding by Swoboda et al (2000) that DAF-19, *C. elegans* orthologue of human RFX1 was previously shown to bind to X-box and drive the cilia specific expression of several important genes including *che-2, osm-1, osm-5, osm-6,* and *daf-19* itself. Sequence alignments revealed that the consensus X-box sequence found in these ciliary genes is very similar to that of *C. elegans bbs* genes, suggesting DAF-19 likely recognizes X-box element of *bbs* genes and induces ciliated cell-specific expression in a similar manner (Figure 4-3).

4.4 Discussion

4.4.1 Regulation of *bbs* genes by forkhead type transcription factor

Our bioinformatic analysis of the promoter sequences of *C. elegans bbs* genes suggests that binding of DAF-19 to the X-box in the promoter induces the ciliogenic expression of *bbs* genes. The hypothesis was confirmed by experiments showing that the expression of *bbs* genes are greatly reduced when the X-box is mutated or *daf-19* loses its function (Li et al., 2004; Blacque et al, unpublished data). Intriguingly, however, a low

level expression of *bbs* genes could still be detected in the ciliated neuron in *daf-19* mutant background. Swoboda et al. (2000) also reported in his study this low-level expression by X-box containing promoters such as those of *che-2*, *osm-1* and *osm-6* in the absence of the functional *daf-19* (Swoboda et al., 2000). Together, these data suggest that besides DAF-19, there may be other transcription factor involved in the minimal expression of *bbs* genes in ciliated sensory neuron.

The *C. elegans* transcription factor UNC-130, for example, may play such a role. UNC-130 is the *C. elegans* orthologue of mammalian FOXJ1, a member of the forkhead box (FOX) domain family of transcription factor characterized by the highly conserved 100 amino acids DNA binding domain called forkhead box (Kaufmann and Knochel, 1996). It was shown by Sarafi et al. (2000) that loss of function mutation in *unc-130* causes the ectopic expression of several regulatory proteins, including ODR-7, ODR-10, and GPA-5, that are specifically expressed in AWA neurons (Sarafi-Reinach and Sengupta, 2000). Because development of chemosensory neurons in *C. elegans* depends on asymmetrical cell divisions of neuronal precursor cells (Hawkins and Garriga, 1998), it was proposed that UNC-130 plays a role in the chemosensory neuron development by regulating the developmental fate of precursor cells (Sarafi-Reinach and Sengupta, 2000).

Consistent with the role of UNC-130 in the ciliary cell development in *C. elegans*, its mammalian orthologue, FOXJ1/HFH-4 has been shown to be involved in the development of ciliated tissues in mice (Chen et al., 1998). *FOXJ1* is expressed in all tissues containing ciliated cells, including the respiratory tract, oviduct, and ependyma in late development through adulthood (Hackett et al., 1995). Interestingly, *FOXJ1* null mice manifest phenotypes similar to BBS symptoms such as hydrocephalus and

randomized left-right asymmetry (*situs inversus*) (Chen et al., 1998). Microscopic examination on the null mice showed that the cilia on oviduct, brain, and lung epithelial layer are absent whereas the cilia on embryonic node and olfactory epithelia are still present, suggesting only motile cilia with 9+2 microtubule structure are affected. Although the target genes regulated by FOXJ1 in ciliated cells remains unknown, RT-PCR analysis in the study demonstrated that left-right dynein (lrd) expression are absent in the embryonic lungs of FOXJ1 null mice, suggesting that FOXJ1 may function in ciliogenesis by regulating expression of members of the dynein family of genes (Chen et al., 1998).

Based on overlapping phenotypes between FOXJ1 null mice and BBS patients, we hypothesized that forkhead transcription factors may regulate the transcription of *bbs* genes. Although we did not find the FOXJ1 binding sites, computational analysis on promoter regions of *C. elegans* and human *BBS* genes revealed potential binding sites for several different subtypes of forkhead transcription factors. Human *BBS* gene promoters (*BBS1, 2, 4, 6, and 7*) contain binding sites for FoxF2, FoxC1, FoxD1, and *C. elegans bbs* gene promoters (*bbs-1, 2, 3, 5, and 7*) contain binding sites for FoxD3, FoxL1, Foxa2a, Foxa4a, and FoxI1a (Figure 4-1). Because the forkhead DNA binding domains within each protein subfamily are highly conserved, each member would bind to very similar DNA sequences. For example, the consensus binding sites for FOXD and FOXJ are NNA(A/T)TGTTT(A/G)TTTNN and NNT(A/G)TTT(A/G)TTT(A/T)NN (TRANSFAC database, http://www.gene-regulation.com). It is possible that FOXJ1 may be able to bind to FOXD1 binding sites in human *BBS* genes promoter. Therefore it should be

experimentally tested whether any of forkhead transcription factor identified above, including FoxJ1 and UNC-130 regulate human or *C. elegans bbs* genes expression.

4.4.2 X-box in human *BBS* genes promoter

Consistent with the expression pattern of *C. elegans bbs* genes, immunohistochemistry experiments on the mice tissue using the antibody to BBS proteins (BBS4, 5, 6, and 8) showed that BBS proteins are expressed only in tissues containing cilia (Ansley et al., 2003; Li et al., 2004;, also see chapter 3 and 4). Such a similar expression pattern suggests that the regulatory machinery controlling the ciliogenic *bbs* expression would be conserved between mammals and *C. elegans*. Surprisingly, however, our computational analysis failed to identify X-box elements in human *BBS* genes promoter with an exception of *BBS1* promoter where a less conserved form of X-box for RFX1 is located at 1.5kb upstream from the translation start site. Do these data suggest the transcription of human *BBS* genes is regulated by other transcription factor than RFX? Considering that only upstream 2kb region from the translation start site were used for the analysis, it is still possible that X-box elements may exist at further upstream than 2kb or at other untranslated regions such as intron or 3'-UTR. Thus, more extensive bioinformatic approach should be carried out to test such a possibility.

4.5 Figures

Figure 4-1 BBS8 is a centrosomal and basal body protein.

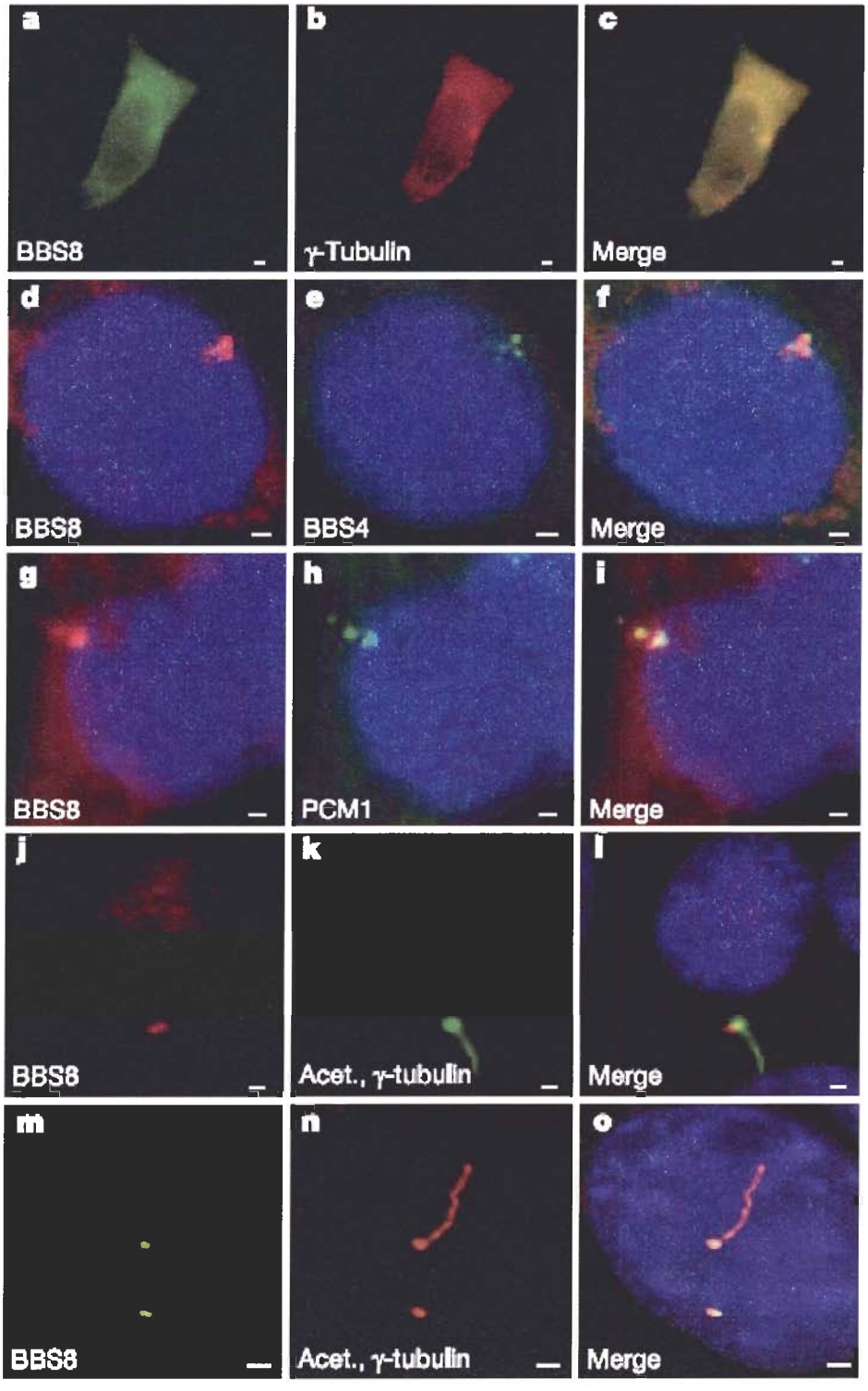

BBS8 is a centrosomal and basal body protein. **A-I**, BBS8 co-localizes with γ-tubulin (**A-C**; HEK293), BBS4 (**D-F**; HeLa) and PCM1 (**G-I**; HeLa). **J-O**, In ciliated cells BBS8 localizes to the basal body in NIH3T3 cells (**J-I**) and to both basal bodies and centrosomes in IMCD3 cells (**M-O**). Scale bar, 1μm. Acet., acetylated.

Figure 4-2 Computational analysis of the promoter region of *C. elegans bbs* genes

Putative promoter regions of *C. elegans bbs* genes (*bbs-1, 2, 3, 5, 7 and 8*) were computationally analyzed with the MatInspector. The list below shows only top 30 hits based on the MatInspector algorithm. A perfect match to the matrix gets a score of 1.00 (each sequence position corresponds to the highest conserved nucleotide at that position in the matrix) and a "good" match to the matrix usually has a similarity of > 0.80. Nucleotide numbers in the position column indicates the distance from the first ATG translation start codon. Core binding sites for each transcription factor are shown in upper case (e.g., gtGGGGa represents the MZF1 binding site).

(A) List of potential transcription binding sites found in *C. elegans bbs-1* promoter region (496bp)

Rank	Transcription factor	Position	Core similarity	Matrix similarity	Sequence
1	Myeloid zinc finger protein MZF1	250-244	1.000	1.000	gtGGGGa
2	GATA-binding factor 1	185-173	1.000	0.992	ttctGATAatcta
3	Sox-5	468-452	1.000	0.992	aaaaaCAATattttatc
4	Myeloid zinc finger protein MZF1	110-104	1.000	0.990	ggGGGGa
5	AREB6 (Atp1a1 regulatory element binding factor 6)	339-327	1.000	0.985	tcaccGTTTctaa
6	HNF-3/Fkh Homolog 2 (FOXD3)	473-457	1.000	0.974	aaaaaaaaAACAatatt
7	MEF2	77-55	1.000	0.971	tccccctctcTAAAcattcct cc
8	c-Myb	394-382	1.000	0.960	ttTAACtgctcac
9	CHRF (Cell cycle gene homology region)	162-150	1.000	0.957	gaatTTGAatata
10	Nuclear factor	97-79	1.000	0.956	gctTGGCaggttgctatgg
11	v-Myb, variant of AMV v-myb	339-329	1.000	0.951	agaAACGgtga
12	TEF-1 related muscle factor	69-53	1.000	0.951	tctaaaCATTcctccta
13	Zinc finger transcription factor ZBP	86-64	1.000	0.950	tgccaagcctCCCCctctcta aa
14	Homeodomain transcription factor HNF	139-123	1.000	0.947	ataacaaaTCAAtactt
15	X-box binding protein RFX1	103-85	1.000	0.945	gtgttcccataGCAAcctg
16	CCAAT/enhancer binding protein beta	336-322	0.985	0.942	catgtttaGAAAcgg
17	POU-factor Tst-1/Oct-6	161-147	1.000	0.940	ggggAATTtgaatat
18	Ikaros 1	104-92	1.000	0.934	ctatGGGAacacg
19	Basic transcription element (BTE) binding protein	247-233	1.000	0.934	aaggtGGAGtagtgg
20	Muscle-specific Mt binding site	156-148	1.000	0.931	gggaATTTg
21	Tumor suppressor p53	319-299	1.000	0.927	ctttcgaatgaaaCATGtttc

Rank	Transcription factor	Position	Core similarity	Matrix similarity	Sequence
22	Ets - family member ELF-2	128-112	1.000	0.927	accacaGGAAgaagtat
23	Octamer-binding factor 1	165-153	0.980	0.903	aattatATTCaaa
24	Xenopus fork head domain factor 2 (Foxl1a)	335-319	1.000	0.903	cgtttcTAAAcatgggc
25	Interferon regulatory factor 7 (IRF-7)	166-148	0.936	0.903	ggGAATttgaatataattt
26	Homeobox transcription factor Gsh-1	196-180	1.000	0.889	agcaaaATTAtttctga
27	Homeo domain factor Nkx-2.5	19-7	1.000	0.884	tgtTAATtttgga
28	E2F	306-292	1.000	0.849	ttcgagcGAAAcatg
29	Prostate-specific homeodomain protein NKX3.1	131-119	1.000	0.845	gaagAAGTattga
30	Hepatic nuclear factor	23-7	1.000	0.831	tGTTAattttggagcac

(B) List of potential transcription binding sites found in *C. elegans bbs-2* promoter region (477bp)

Rank	Transcription factor	Position	Core similarity	Matrix similarity	Sequence
1	Binding site for S8 type homeodomains	398-390	1.000	0.995	tttaATTAt
2	DLX-1, -2, and -5 binding sites	400-388	1.000	0.994	tgatAATTaaaat
3	GATA-binding factor	213-201	1.000	0.993	atctGATAagaaa
4	MEF2	364-342	1.000	0.990	ttgcaattttTAAAaacgttttt
5	Halfsite of PXR (pregnane X receptor)	453-443	1.000	0.988	ttTGAActttt
6	AREB6 (Atp1a1 regulatory element binding factor 6)	59-47	1.000	0.985	agtcgGTTTcgat
7	TCF/LEF-1	430-414	1.000	0.974	ttattttCAAAgaatat
8	X-box binding protein RFX1	98-80	1.000	0.961	cagtatccatgGCAAcatg
9	Bright, B cell regulator of IgH transcription	400-388	1.000	0.959	tgataATTAaaat
10	cellular and viral TATA box elements	312-296	1.000	0.955	tcttaTAAAatcaatgt
11	Intestine specific homeodomain factor CDX-1	25-7	1.000	0.949	atttagtTTTAttagaaat
12	STAT5: signal transducer and activator of transcription 5	432-414	1.000	0.948	ttataTTCTttgaaaataa
13	Mammalian C-type LTR TATA box	370-354	1.000	0.931	ttcaaTAAAaacgtttt
14	LIM-homeodomain transcription factor	402-388	1.000	0.924	gcatttTAATtatca
15	Myocyte enhancer factor	361-339	1.000	0.906	aacgttttTAAAaattgcaatgt
16	Growth factor independence 1 zinc finger protein Gfi-1B	307-293	1.000	0.903	taaAATCaatgtttt
17	Ecotropic viral integration site 1 encoded factor	210-194	1.000	0.895	tGATAagaaaacatata
18	MyT1 zinc finger transcription factor involved in primary neurogenesis	454-442	1.000	0.893	taaAAGTtcaaaa

Rank	Transcription factor	Position	Core similarity	Matrix similarity	Sequence
19	Related to serum response factor, C4	227-205	1.000	0.872	ttatcagatattaATAGaattat
20	Homeobox transcription factor Gsh-1	262-246	1.000	0.867	tcttatATTAttttacg
21	Interferon regulatory factor 7 (IRF-7)	45-27	1.000	0.863	aaGAAAatgaacaggttta
22	AT-binding transcription factor 1	398-382	1.000	0.863	cgagtttgatAATTaaa
23	PAR-type chicken vitellogenin promoter-binding protein	86-76	1.000	0.860	cTTACatgttg
24	Octamer-binding factor 1	398-384	1.000	0.855	agtttgatAATTaaa
25	Cdx-2 mammalian caudal related intestinal transcr. factor	258-240	1.000	0.843	atattatTTTAcggtaaag
26	Homeobox protein MEIS1 binding site	446-434	1.000	0.843	aTGATttttaaaa
27	Pancreatic and intestinal lim-homeodomain factor	425-405	1.000	0.828	ctttgaaaaTAATagttcgtc
28	Xenopus homeodomain factor Xvent-2	230-214	1.000	0.820	atTAATagaattatcac
29	Fork head related activator-4 (FOXD1)	209-193	1.000	0.808	gataagaaAACAtatat
30	Brn-3	265-247	1.000	0.785	ctgtcttatATTAttttac

(C) List of potential transcription binding sites found in *C. elegans bbs-3* promoter region (1503bp)

Rank	Transcription factor	Position	Core similarity	Matrix similarity	Sequence
1	Muscle segment homeo box 2, homologue of Drosophila (HOX 8)	1437-1425	1.000	1.000	gaCTAAttcaagt
2	TG-interacting factor belonging to TALE class of homeodomain factors	1307-1301	1.000	1.000	tGTCAaa
3	Binding site for S8 type homeodomains	1033-1025	1.000	1.000	atcaATTAa
4	AREB6 (Atp1a1 regulatory element binding factor 6)	639-627	1.000	0.997	aaactGTTTcatg
5	MEF2	189-167	1.000	0.995	aaaaacggttTAAAaatatatcc
6	GATA-binding factor 1	217-205	1.000	0.992	atttGATAagaat
7	Homeodomain transcription factor Otx2 (homolog of Drosophila orthodenticle)	882-866	1.000	0.990	agagggATTAataagga
8	Homeodomain proteins MSX-1 and MSX-2	234-222	1.000	0.989	tttTAATttatca
9	Pituitary Homeobox 1 (Ptx1, Pitx-1)	1495-1479	1.000	0.988	gaaaggaTTAGcgtttt
10	Nuclear hormone receptor TR2, half site	96-78	1.000	0.986	ccgaaaaGGTCattatgac
11	Myoblast determining factor	154-140	0.914	0.986	caacCATCtgtcaga
12	TCF/LEF-1, involved in the Wnt signal transduction pathway	34-18	1.000	0.986	ttaatttCAAAgtattt
13	Binding site for monomeric Meis1 homeodomain protein	941-933	1.000	0.985	gtGACAgtt
14	Ribonucleoprotein associated zinc finger protein MOK-2 (human)	900-880	1.000	0.983	atggatttcggtaCCTTttcc
15	Transcriptional repressor CDP	57-41	1.000	0.983	tgattaATCGattttgg

Rank	Transcription factor	Position	Core similarity	Matrix similarity	Sequence
16	DLX-1, -2, and -5 binding sites	341-329	1.000	0.982	tgatAATTacttt
17	Cdx-2 mammalian caudal related intestinal transcr. factor	940-922	1.000	0.978	tgacagtTTTAttaccaga
18	NMP4 (nuclear matrix protein 4) / CIZ (Cas-interacting zinc finger protein)	633-623	1.000	0.975	agAAAAactgt
19	PAR-type chicken vitellogenin promoter-binding protein	1214-1204	1.000	0.975	gTTACataaat
20	Interferon regulatory factor 3 (IRF-3)	1334-1316	1.000	0.974	aagaaaacGAAAcctccga
21	E4BP4, bZIP domain, transcriptional repressor	1218-1198	1.000	0.971	tttcatttatGTAAcgaatgt
22	cellular and viral TATA box elements	1400-1384	1.000	0.968	ctgtaTAAAacgtattt
23	Tal-1alpha/E47 heterodimer	156-140	1.000	0.968	tctgaCAGAtggttggg
24	complex of Lmo2 bound to Tal-1, E2A proteins, and GATA-1, half-site 2	1341-1329	1.000	0.967	ctccGATAatgat
25	Myelin transcription factor 1-like, neuronal C2HC zinc finger factor 1	755-743	1.000	0.967	ggaaAGTTaggat
26	Octamer-binding factor 1, POU-specific domain	1063-1051	0.980	0.966	cataatATTCaaa
27	CCAAT/enhancer binding protein beta	813-799	1.000	0.964	taaattacGCAAtac
28	Winged helix protein, involved in hair keratinization and thymus epithelium differentiation	922-912	1.000	0.958	acgACGCaaaa
29	Hepatocyte Nuclear Factor 3beta (FOXA2)	977-961	1.000	0.957	gaaaaggaAATAatgat
30	X-box binding protein RFX1	856-838	1.000	0.912	ctgtcgatttgGCAActaa

(D) List of potential transcription binding sites found in *C. elegans bbs-5* promoter region (1003bp)

Rank	Transcription factor	Position	Core similarity	Matrix similarity	Sequence
1	Myelin transcription factor 1-like, neuronal C2HC zinc finger factor 1	999-987	1.000	1.000	tgaaAGTTctaaa
2	MyT1 zinc finger transcription factor involved in primary neurogenesis	901-889	1.000	1.000	gaaAAGTttttgg
3	Amino acid response element, ATF4 binding site	691-683	1.000	1.000	gTTTCatca
4	Binding site for S8 type homeodomains	509-501	1.000	0.997	ttcaATTAt
5	Ikaros 2, potential regulator of lymphocyte differentiation	480-468	1.000	0.996	atttGGGAaaaat
6	Hepatocyte Nuclear Factor 3beta (FOXA2)	826-810	1.000	0.993	aaaaaataAACAtttat
7	Myeloid zinc finger protein MZF1	228-222	1.000	0.990	ggGGGGa
8	DLX-1, -2, and -5 binding sites	544-532	1.000	0.988	agttAATTaatca
9	cellular and viral TATA box elements	246-230	1.000	0.980	gtgtaTAAAagaaagtg
10	AREB6 (Atp1a1 regulatory element binding factor 6)	464-452	1.000	0.980	tccagGTTTctga
11	NMP4 (nuclear matrix protein 4) / CIZ (Cas-interacting zinc finger protein)	454-444	1.000	0.979	ggAAAAaaacg
12	Heat shock factor 1	113-103	1.000	0.977	AGAAgtttcga
13	Octamer-binding factor 1	527-513	0.944	0.976	aATATgaaattatgc
14	Homeodomain proteins MSX-1 and MSX-2	511-499	1.000	0.973	ataTAATtgaata

Rank	Transcription factor	Position	Core similarity	Matrix similarity	Sequence
15	Nuclear factor of activated T-cells	457-447	1.000	0.973	cctgGAAAaaa
16	Zinc finger / POZ domain transcription factor	584-574	1.000	0.972	gtggGCGCagg
17	NMP4 (nuclear matrix protein 4) / CIZ (Cas-interacting zinc finger protein)	369-359	1.000	0.971	gcAAAAagacg
18	complex of Lmo2 bound to Tal-1, E2A proteins, and GATA-1, half-site 2	261-249	1.000	0.971	gaaaGATAtcgta
19	cellular and viral TATA box elements	124-108	1.000	0.970	tattaTAAAaatcgaaa
20	Winged helix protein, involved in hair keratinization and thymus epithelium differentiation	374-364	1.000	0.968	aagACGCtcag
21	v-Myb	202-192	1.000	0.961	aaaAACGgaaa
22	CCAAT/enhancer binding protein beta	760-746	0.985	0.960	tacgtttcGAAAttt
23	Sex-determining region Y gene product	873-857	1.000	0.956	ttaaACAAaaaatttct
24	Mammalian transcriptional repressor RBP-Jkappa/CBF1	346-332	1.000	0.956	aattTGGGaaaattc
25	Erythroid krueppel like factor (EKLF)	561-549	1.000	0.955	actcgcaGGGTgt
26	X-box binding protein RFX1	69-51	1.000	0.952	cggtctccatgGCAActct
27	Elk-1	208-192	1.000	0.943	aaaaacGGAAatcatca
28	c-Ets-1 binding site	605-589	1.000	0.937	tcggcAGGAaatgcatt
29	Homeo domain factor Nkx-2.5/Csx, tinman homolog low affinity sites	527-515	1.000	0.936	gcaTAATttcata
30	Distal-less 3 homeodomain transcription factor	957-945	1.000	0.924	aaaTAATttcaaa

(E) List of potential transcription binding sites found in *C. elegans bbs-7* promoter region (1453bp)

Rank	Transcription factor	Position	Core similarity	Matrix similarity	Sequence
1	E2F	1210-1196	1.000	1.000	caagcgcGAAAgatt
2	Sox-5	1390-1374	1.000	0.997	gttaaCAATatataatc
3	Multifunctional c-Abl src type tyrosine kinase	1330-1320	1.000	0.997	aaAACAaaaat
4	HMGI(Y) high-mobility-group protein I (Y)	1171-1155	1.000	0.995	gtcggaAATTttcgatt
5	N-Myc	1223-1209	1.000	0.990	tgtccaCGTGtagta
6	Homeodomain proteins MSX-1 and MSX-2	1316-1304	1.000	0.989	atcTAATtttaaa
7	MyT1 zinc finger transcription factor involved in primary neurogenesis	1357-1345	1.000	0.988	aaaAAGTttgact
8	Elk-1	1069-1053	1.000	0.984	tttgccGGAAgttttca
9	Myoblast determining factor	136-122	1.000	0.984	gagcCACCtgacccc
10	Upstream stimulating factor	1222-1208	1.000	0.981	actaCACGtggacaa
11	X-box binding protein RFX1	112-94	1.000	0.979	gagttactatgGCAAcatg
12	NMP4 (nuclear matrix protein 4)	1359-1349	1.000	0.975	tgAAAAagttt
13	Nuclear factor of activated T-cells	980-970	1.000	0.970	atcgGAAAatt
14	MEF2	385-363	1.000	0.969	aaaaataattTAAAaaaacagga
15	Interferon regulatory factor 7 (IRF-7)	741-723	1.000	0.969	ccGAAAatgaaaatttccg
16	Nuclear factor 1	798-780	1.000	0.967	aatTGGCaagttgccggaa
17	Cone-rod homeobox-containing transcription factor	823-807	1.000	0.954	ttgctgATTAgccagaa
18	Tumor suppressor p53	626-606	0.921	0.951	caaaaatttccggCAAGtcgg
19	CCAAT/enhancer binding protein beta	1263-1249	1.000	0.950	gtgattttGCAAgtg
20	AhR nuclear translocator homodimers	1222-1208	1.000	0.947	ttgtccaCGTGtagt

21	Heat shock factor 1	685-675	0.916	0.945	GGAAttttcaa
22	Cell cycle gene homology region	367-355	1.000	0.942	ttttTTGAatttt
23	Pu.1 (Pu120) Ets-like transcription factor identified in lymphoid B-cells	393-377	1.000	0.940	aaaacaGGAAttgaaaa
24	Bright, B cell regulator of IgH transcription	1280-1268	1.000	0.939	caggaATTAaaaa
25	HNF-3/Fkh Homolog 2 (FOXD3)	1330-1314	1.000	0.938	aaaaaaaaAACAaaaat
26	Gut-enriched Krueppel-like factor	1407-1393	1.000	0.935	ttaaaaaaaaAGGGa
27	Growth factor independence 1 zinc finger protein Gfi-1B	1269-1255	1.000	0.931	caaAATCacctcttt
28	Mammalian C-type LTR TATA box	1372-1356	1.000	0.931	ttcaaTAAAatggaacg
29	Nuclear hormone receptor TR2, half site	135-117	1.000	0.927	ggagaggGGTCaggtggct
30	cAMP-responsive element binding protein	158-138	1.000	0.925	ttggggTGACgggtgagaagc

(F) List of potential transcription binding sites found in *C. elegans bbs-8* promoter region (513bp)

Rank	Transcription factor	Position	Core similarity	Matrix similarity	Sequence
1	Avian C-type LTR TATA box	478-462	1.000	1.000	tcgtattTAAGtattcc
2	TG-interacting factor belonging to TALE class of homeodomain factors	191-185	1.000	1.000	tGTCAat
3	MyT1 zinc finger transcription factor involved in primary neurogenesis	358-346	1.000	0.998	gaaAAGTtttcag
4	Binding site for S8 type homeodomains	247-239	1.000	0.995	attaATTAt
5	DLX-1, -2, and -5 binding sites	249-237	1.000	0.988	taatAATTaatcc
6	Intestine specific homeodomain factor CDX-1	236-218	1.000	0.987	aaattttTTTAttatccat
7	Winged helix protein, involved in hair keratinization and thymus epithelium differentiation	156-146	1.000	0.987	ctgACGCtatt
8	Homeodomain proteins MSX-1 and MSX-2	320-308	1.000	0.983	atcTAATtatatg
9	Homeodomain transcription factor Otx2 (homolog of Drosophila orthodenticle)	253-237	1.000	0.981	acgcggATTAattatta
10	Multifunctional c-Abl src type tyrosine kinase	490-480	1.000	0.972	aaAACAacacg
11	Hey-like bHLH-transcriptional repressor	101-87	1.000	0.970	agggCACGcggcaag
12	POU-factor Tst-1/Oct-6	502-488	1.000	0.969	acggAATTaaaataa
13	X-box binding protein RFX1	88-70	1.000	0.958	ctgtacccatgGCAAcgac

Rank	Transcription factor	Position	Core similarity	Matrix similarity	Sequence
14	Octamer-binding factor 1	143-129	1.000	0.956	agcATGCaaaagatt
15	STAT5: signal transducer and activator of transcription 5	431-413	0.945	0.952	gagtaTTCCaagaagctac
16	GATA-binding factor 3	148-136	1.000	0.950	aaaAGATtataat
17	CCAAT/enhancer binding protein beta	223-209	0.985	0.947	tgactttcGAAAttt
18	Aryl hydrocarbon receptor / Arnt heterodimers	105-83	1.000	0.947	ctctcttgccgCGTGccctgtac
19	Bright, B cell regulator of IgH transcription	249-237	1.000	0.944	taataATTAatcc
20	Prostate-specific homeodomain protein NKX3.1	474-462	1.000	0.944	atttAAGTattcc
21	MYC-MAX binding sites	101-87	1.000	0.941	agggCACGcggcaag
22	LIM-homeodomain transcription factor	251-237	1.000	0.937	gcggatTAATtatta
23	Pit1, GHF-1 pituitary specific pou domain transcription factor	273-263	1.000	0.927	agttATTCagt
24	TCF/LEF-1, involved in the Wnt signal transduction pathway	390-374	1.000	0.900	atatgaaCAAAgagcaa
25	Homeobox transcription factor Gsh-1	304-288	1.000	0.883	tccaaaATTAtaagtta
26	Ikaros 3, potential regulator of lymphocyte differentiation	426-414	1.000	0.883	ttcttGGAAtact
27	FAST-1 SMAD interacting protein	181-167	0.983	0.869	cattgtcGATTtttt
28	CUT-homeodomain transcription factor Onecut-2	181-165	1.000	0.848	tcaaaaAATCgacaatg

Rank	Transcription factor	Position	Core similarity	Matrix similarity	Sequence
29	Hox-1.3, vertebrate homeobox protein	245-229	1.000	0.844	ttatccATTAataatta
30	Binding site for a Pbx1/Meis1 heterodimer	195-179	1.000	0.788	atgagaatTGACatgat

Figure 4-3 X-box sequences of *C.elegans* ciliogenic genes promoter including *bbs genes*

Alignment of X-boxes from C. elegans genes expressed in ciliated neurons and all bbs genes. Distances after the X- boxes are from the translation start site (ATG) of each gene.

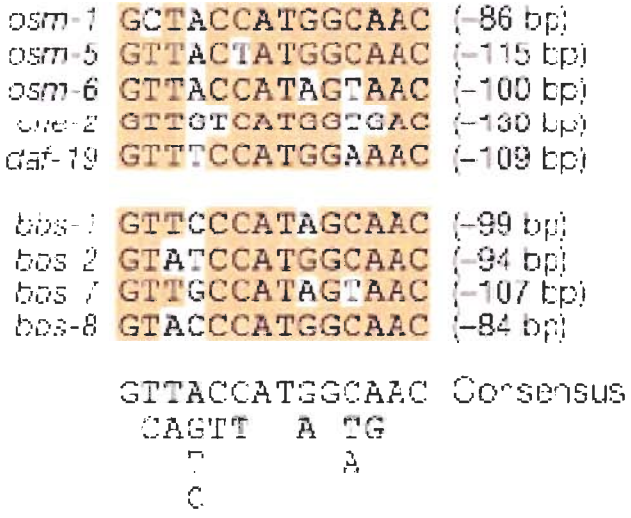

4.6 Reference list

Ansley, S. J., Badano, J. L., Blacque, O. E., Hill, J., Hoskins, B. E., Leitch, C. C., Kim, J. C., Ross, A. J., Eichers, E. R., Teslovich, T. M., et al. (2003). Basal body dysfunction is a likely cause of pleiotropic Bardet-Biedl syndrome. Nature 425, 628-633.

Bargmann, C. I. (1997). Olfactory receptors, vomeronasal receptors, and the organization of olfactory information. Cell 90, 585-587.

Chen, J., Knowles, H. J., Hebert, J. L., and Hackett, B. P. (1998). Mutation of the mouse hepatocyte nuclear factor/forkhead homologue 4 gene results in an absence of cilia and random left-right asymmetry. J Clin Invest 102, 1077-1082.

Cole, D. G., Diener, D. R., Himelblau, A. L., Beech, P. L., Fuster, J. C., and Rosenbaum, J. L. (1998). Chlamydomonas kinesin-II-dependent intraflagellar transport (IFT): IFT particles contain proteins required for ciliary assembly in Caenorhabditis elegans sensory neurons. J Cell Biol 141, 993-1008.

Emery, P., Durand, B., Mach, B., and Reith, W. (1996). RFX proteins, a novel family of DNA binding proteins conserved in the eukaryotic kingdom. Nucleic Acids Res 24, 803-807.

Hackett, B. P., Brody, S. L., Liang, M., Zeitz, I. D., Bruns, L. A., and Gitlin, J. D. (1995). Primary structure of hepatocyte nuclear factor/forkhead homologue 4 and characterization of gene expression in the developing respiratory and reproductive epithelium. Proc Natl Acad Sci U S A 92, 4249-4253.

Hawkins, N., and Garriga, G. (1998). Asymmetric cell division: from A to Z. Genes Dev 12, 3625-3638.

Kaufmann, E., and Knochel, W. (1996). Five years on the wings of fork head. Mech Dev 57, 3-20.

Kozminski, K. G., Beech, P. L., and Rosenbaum, J. L. (1995). The Chlamydomonas kinesin-like protein FLA10 is involved in motility associated with the flagellar membrane. J Cell Biol 131, 1517-1527.

Kozminski, K. G., Johnson, K. A., Forscher, P., and Rosenbaum, J. L. (1993). A motility in the eukaryotic flagellum unrelated to flagellar beating. Proc Natl Acad Sci USA 90, 5519-5523.

Li, J. B., Gerdes, J. M., Haycraft, C. J., Fan, Y., Teslovich, T. M., May-Simera, H., Li, H., Blacque, O. E., Li, L., Leitch, C. C., et al. (2004). Comparative genomics identifies a flagellar and basal body proteome that includes the *BBS5* human disease gene. Cell 117, 541-552.

Malone, E. A., and Thomas, J. H. (1994). A screen for nonconditional dauer-constitutive mutations in Caenorhabditis elegans. Genetics 136, 879-886.

Marszalek, J. R., Liu, X., Roberts, E. A., Chui, D., Marth, J. D., Williams, D. S., and Goldstein, L. S. (2000). Genetic evidence for selective transport of opsin and arrestin by kinesin-II in mammalian photoreceptors. Cell 102, 175-187.

Maurer, L., and Orndorff, P. E. (1987). Identification and characterization of genes determining receptor binding and pilus length of Escherichia coli type 1 pili. J Bacteriol 169, 640-645.

McGrath, J., Somlo, S., Makova, S., Tian, X., and Brueckner, M. (2003). Two populations of node monocilia initiate left-right asymmetry in the mouse. Cell 114, 61-73.

Merz, A. J., So, M., and Sheetz, M. P. (2000). Pilus retraction powers bacterial twitching motility. Nature 407, 98-102.

Morotomi-Yano, K., Yano, K., Saito, H., Sun, Z., Iwama, A., and Miki, Y. (2002). Human regulatory factor X 4 (RFX4) is a testis-specific dimeric DNA-binding protein that cooperates with other human RFX members. J Biol Chem 277, 836-842.

Moyer, J. H., Lee-Tischler, M. J., Kwon, H. Y., Schrick, J. J., Avner, E. D., Sweeney, W. E., Godfrey, V. L., Cacheiro, N. L., Wilkinson, J. E., and Woychik, R. P. (1994). Candidate gene associated with a mutation causing recessive polycystic kidney disease in mice. Science 264, 1329-1333.

Blacque, O. E., Reardon, M. J., Li, C., McCarthy, J., Mahjoub, M. R., Ansley, S. J., Badano, J. L., Mah, A. K., Beales, P. L., Davidson, W. S., et al. (2004). Loss of *C. elegans* BBS-7 and BBS-8 protein function results in cilia defects and compromised intraflagellar transport. Genes Dev 18, 1630-1642.

Pazour, G. J., Wilkerson, C. G., and Witman, G. B. (1998). A dynein light chain is essential for the retrograde particle movement of intraflagellar transport (IFT). J Cell Biol 141, 979-992.

Pazour, G. J., Dickert, B. L., and Witman, G. B. (1999). The DHC1b (DHC2) isoform of cytoplasmic dynein is required for flagellar assembly. J Cell Biol 144, 473-481.

Pazour, G. J., Dickert, B. L., Vucica, Y., Seeley, E. S., Rosenbaum, J. L., Witman, G. B., and Cole, D. G. (2000). Chlamydomonas IFT88 and its mouse homologue, polycystic kidney disease gene tg737, are required for assembly of cilia and flagella. J Cell Biol 151, 709-718.

Perkins, L. A., Hedgecock, E. M., Thomson, J. N., and Culotti, J. G. (1986). Mutant sensory cilia in the nematode Caenorhabditis elegans. Dev Biol 117, 456-487

Perrone, C. A., Tritschler, D., Taulman, P., Bower, R., Yoder, B. K., and Porter, M. E. (2003). A novel dynein light intermediate chain colocalizes with the retrograde motor for intraflagellar transport at sites of axoneme assembly in chlamydomonas and Mammalian cells. Mol Biol Cell 14, 2041-2056.

Porter, M. E., Bower, R., Knott, J. A., Byrd, P., and Dentler, W. (1999). Cytoplasmic dynein heavy chain 1b is required for flagellar assembly in Chlamydomonas. Mol Biol Cell 10, 693-712.

Porter, M. E., and Sale, W. S. (2000). The 9 + 2 axoneme anchors multiple inner arm dyneins and a network of kinases and phosphatases that control motility. J Cell Biol 151, F37-42.

Praetorius, H. A., and Spring, K. R. (2001). Bending the MDCK cell primary cilium increases intracellular calcium. J Membr Biol 184, 71-79.

Quandt, K., Frech, K., Karas, H., Wingender, E., and Werner, T. (1995). MatInd and MatInspector: new fast and versatile tools for detection of consensus matches in nucleotide sequence data. Nucleic Acids Res 23, 4878-4884.

Reith, W., Barras, E., Satola, S., Kobr, M., Reinhart, D., Sanchez, C. H., and Mach, B. (1989). Cloning of the major histocompatibility complex class II promoter binding protein affected in a hereditary defect in class II gene regulation. Proc Natl Acad Sci U S A 86, 4200-4204.

Rosenbaum, J. L., and Witman, G. B. (2002). Intraflagellar transport. Nat Rev Mol Cell Biol 3, 813-825.

Sarafi-Reinach, T. R., and Sengupta, P. (2000). The forkhead domain gene unc-130 generates chemosensory neuron diversity in *C. elegans*. Genes Dev 14, 2472-2485.

Schafer, J. C., Haycraft, C. J., Thomas, J. H., Yoder, B. K., and Swoboda, P. (2003). XBX-1 encodes a dynein light intermediate chain required for retrograde intraflagellar transport and cilia assembly in Caenorhabditis elegans. Mol Biol Cell 14, 2057-2070.

Scholey, J. M. (2003). Intraflagellar transport. Annu Rev Cell Dev Biol 19, 423-443.

Signor, D., Wedaman, K. P., Rose, L. S., and Scholey, J. M. (1999). Two heteromeric kinesin complexes in chemosensory neurons and sensory cilia of Caenorhabditis elegans. Mol Biol Cell 10, 345-360.

Sloboda, R. D. (2002). A healthy understanding of intraflagellar transport. Cell Motil Cytoskeleton 52, 1-8.

Starich, T. A., Herman, R. K., Kari, C. K., Yeh, W. H., Schackwitz, W. S., Schuyler, M. W., Collet, J., Thomas, J. H., and Riddle, D. L. (1995). Mutations affecting the chemosensory neurons of Caenorhabditis elegans. Genetics 139, 171-188.

Swoboda, P., Adler, H. T., and Thomas, J. H. (2000). The RFX-type transcription factor DAF-19 regulates sensory neuron cilium formation in *C. elegans*. Mol Cell 5, 411-421.

Wicks, S. R., de Vries, C. J., van Luenen, H. G., and Plasterk, R. H. (2000). CHE-3, a cytosolic dynein heavy chain, is required for sensory cilia structure and function in Caenorhabditis elegans. Dev Biol 221, 295-307.

Yang, Z., Roberts, E. A., and Goldstein, L. S. (2001). Functional analysis of mouse kinesin motor Kif3C. Mol Cell Biol 21, 5306-5311.

Zimmerman, W., Sparks, C. A., and Doxsey, S. J. (1999). Amorphous no longer: the centrosome comes into focus. Curr Opin Cell Biol 11, 122-128.

CHAPTER 5
CONCLUSIONS

The findings presented in this thesis provide very important clues regarding the pathological mechanism underlying Bardet-Biedl syndrome. Two different BBS proteins, BBS4 and 6 were shown to be localized at the centrosome: The centrosome is a key to understanding this complex disorder. As the primary microtubule-organizing centre of the animal cells, centrosomes are involved in almost all of the microtubule dependent processes including organelle transport, cell shape, polarity and motility (Meraldi and Nigg, 2002). Centrosomes in dividing cells, for example, play a critical role in controlling spindle bipolarity, spindle positioning and cytokinesis. In non-dividing, differentiated cells, however, centrosome plays a very distinct role. One centriole of the centrosome migrates to the plasma membrane and becomes a basal body to form a primary cilium in mammalian cells or a flagellum in the sperm (Beisson and Wright, 2003).

The idea that centrosomes play separate roles in the dividing cells and the differentiated cells raises the important question regarding the role of BBS proteins: do BBS proteins function in the centrosome or in the basal body of cilia? Recent studies including ours suggest that they likely function in both places.

Our results suggested that BBS4 play a role in the intracellular transport as an adaptor molecule that mediates bindings between the dynein motor and cargo proteins, which proved to be critical for maintaining the microtubule organization in the dividing mammalian cultured cell (chapter 2). These findings have been also verified in a study

with *BBS4* knockout mice by Kulaga et al (2004) where the mice showed the disorganization of the dendritic microtubule network in olfactory epithelia and the trapping of ciliary proteins in dendrites and cell bodies, which collectively led to severe reduction of the ciliated border in olfactory epithelia and an anosmic condition in mice (Kulaga et al., 2004).

Unlike BBS4, there is no experimental evidence that BBS6 is involved in the intracellular transport. Interestingly, however, our results show that *BBS6* silenced-mammalian cultured cells cannot complete the cytokinesis, likely due to defects in the abscission process at the midbody (chapter 3). Although the working mechanism is unknown, growing evidence suggests that the successful abscission during cytokinesis requires two sequential steps: 1) the delivery of Golgi-derived endosomal vesicles to the midbody and 2) the subsequent fusion between these vesicles and the midbody membrane. It is, therefore, conceivable that BBS6 may play a role in vesicle transport between the centrosome and the midbody during cytokinesis, although this possibility will need to be experimentally tested.

Whereas the function of BBS proteins at the centrosome has been studied primarily in cultured mammalian cells, their function at the basal body of cilia and within cilia has been mainly investigated in *C. elegans* (Ansley et al., 2003; Blacque et al., 2004). All known *C.elegans* orthologues of human *BBS* genes are expressed only in ciliated sensory neurons. Remarkably, the upstream regulatory regions of these nematode *bbs* genes all contain DNA-binding sites (X boxes) for DAF-19 (chapter 4), a transcription factor required for the expression of several cilia-specific genes in the nematode (Swoboda et al. 2000). In ciliated neuronal cells, GFP-BBS proteins localize

predominantly at the base of ciliated sensory cilia and show bidirectional movement along the ciliary axoneme, in a manner similar to that of IFT particles (Blacque et al., 2004; see also chaper 4. Introduction). *C.elegans* mutants with loss of function mutations in *bbs-7* and *bbs-8* genes manifest both structural and functional defects in their sensory cilia, including shortened/abnormal cilia and chemosensory abnormalities (Blacque et al., 2004).

It is intriguing that the results from the knockout mice model of BBS are not exactly identical to those from *C. elegans*. Loss of function mutant worm of *bbs-7* and *bbs-8* gene develop abnormal sensory cilia, however, *BBS2* and *BBS4* null mice show defects in only subsets of ciliated cells. *BBS2* and *BBS4* null mice develop normal motile cilia in the lung and normal primary cilia in the kidney where they are thought to play a mechanosensory function (Kulaga et al., 2004; Mykytyn et al., 2004; Nishimura et al., 2004), but the mice show defects in ciliated olfactory epithelial cells, ciliated retinal cells (rod and cone cells), and flagellated sperm cells. The finding that only subsets of cilia and ciliated cells are affected in *BBS* null mice indicates that BBS proteins may not be essential for the IFT process in general but rather play roles in specific types of ciliated cells, and also suggests that there may be significant differences in the intraflagellar transport process between the different types of cilia such as immotile sensory cilia, tracheal cilia and sperm flagella.

In summary, recent studies including this thesis suggest that BBS proteins function in the intracellular and intraflagellar transport process in specific types of ciliated cells, and dysfunction within these ciliated cells during development likely gives rise to specific and pleiotrophic symptoms in BBS patients.

5.1 References

Ansley, S. J., Badano, J. L., Blacque, O. E., Hill, J., Hoskins, B. E., Leitch, C. C., Kim, J. C., Ross, A. J., Eichers, E. R., Teslovich, T. M., et al. (2003). Basal body dysfunction is a likely cause of pleiotropic Bardet-Biedl syndrome. Nature 425, 628-633.

Beisson, J., and Wright, M. (2003). Basal body/centriole assembly and continuity. Curr Opin Cell Biol 15, 96-104.

Blacque, O. E., Reardon, M. J., Li, C., McCarthy, J., Mahjoub, M. R., Ansley, S. J., Badano, J. L., Mah, A. K., Beales, P. L., Davidson, W. S., et al. (2004). Loss of *C. elegans* BBS-7 and BBS-8 protein function results in cilia defects and compromised intraflagellar transport. Genes Dev 18, 1630-1642.

Kulaga, H. M., Leitch, C. C., Eichers, E. R., Badano, J. L., Lesemann, A., Hoskins, B. E., Lupski, J. R., Beales, P. L., Reed, R. R., and Katsanis, N. (2004). Loss of BBS proteins causes anosmia in humans and defects in olfactory cilia structure and function in the mouse. Nat Genet 36, 994-998.

Meraldi, P., and Nigg, E. A. (2002). The centrosome cycle. FEBS Lett 521, 9-13.

Mykytyn, K., Mullins, R. F., Andrews, M., Chiang, A. P., Swiderski, R. E., Yang, B., Braun, T., Casavant, T., Stone, E. M., and Sheffield, V. C. (2004). Bardet-Biedl syndrome type 4 (*BBS4*)-null mice implicate BBS4 in flagella formation but not global cilia assembly. Proc Natl Acad Sci U S A 101, 8664-8669.

Nishimura, D. Y., Fath, M., Mullins, R. F., Searby, C., Andrews, M., Davis, R., Andorf, J. L., Mykytyn, K., Swiderski, R. E., Yang, B., et al. (2004). *BBS2*-null mice have neurosensory deficits, a defect in social dominance, and retinopathy associated with mislocalization of rhodopsin. Proc Natl Acad Sci U S A.

Swoboda, P., Adler, H. T., and Thomas, J. H. (2000). The RFX-type transcription factor DAF-19 regulates sensory neuron cilium formation in *C. elegans*. Mol Cell 5, 411-421.